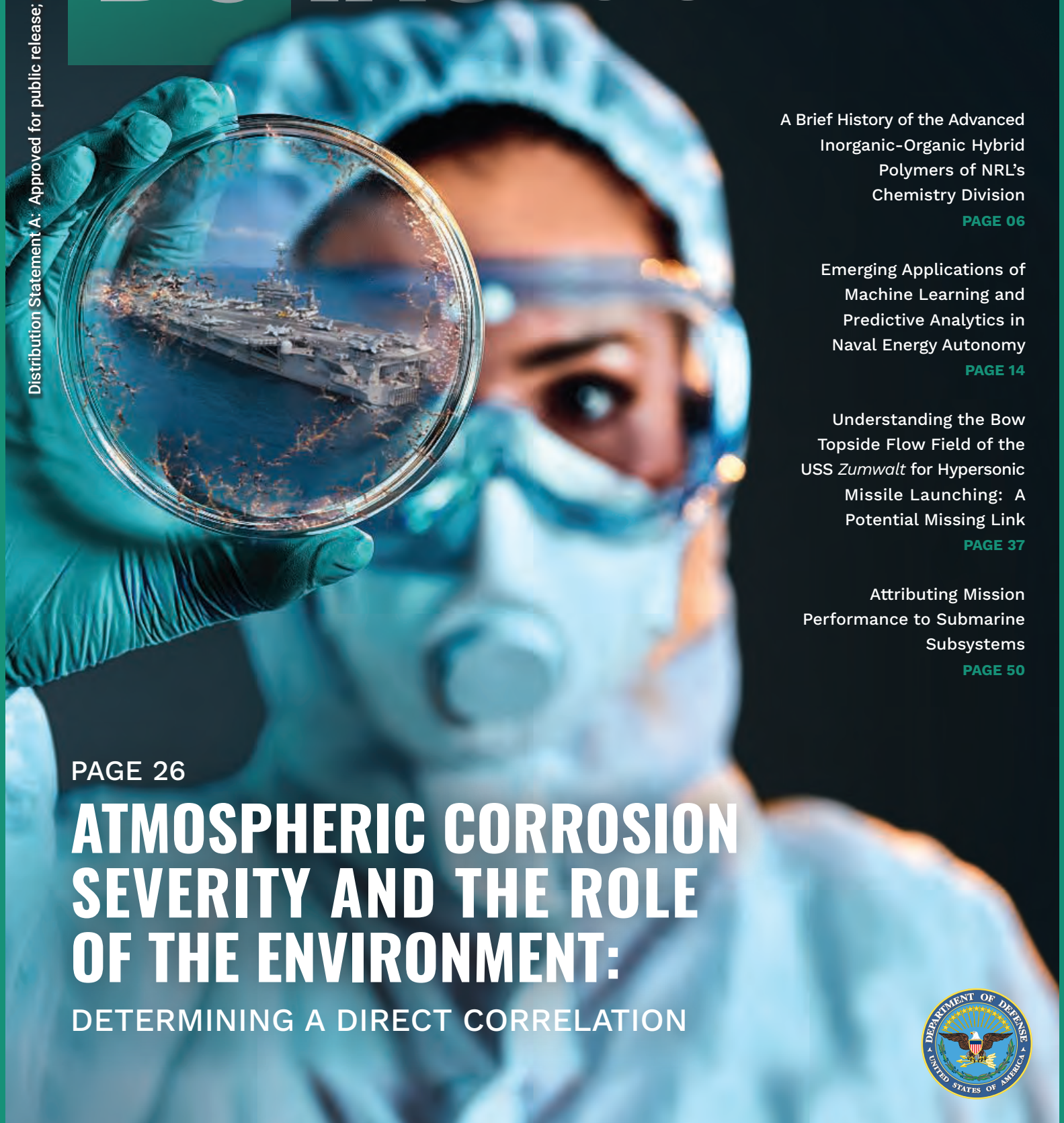


DS IAC JOURNAL

Distribution Statement A: Approved for public release; distribution is unlimited.



A Brief History of the Advanced Inorganic-Organic Hybrid Polymers of NRL's Chemistry Division
PAGE 06

Emerging Applications of Machine Learning and Predictive Analytics in Naval Energy Autonomy
PAGE 14

Understanding the Bow Topside Flow Field of the USS Zumwalt for Hypersonic Missile Launching: A Potential Missing Link
PAGE 37

Attributing Mission Performance to Submarine Subsystems
PAGE 50

PAGE 26

ATMOSPHERIC CORROSION SEVERITY AND THE ROLE OF THE ENVIRONMENT:

DETERMINING A DIRECT CORRELATION



SPECIAL NAVY EDITION

Special Edition // Navy // 2024

Editor-in-Chief:

Gregory Nichols

Sr. Technical Editor:

Maria Brady

Graphic Designers:

Melissa Gestido, Katie Ogorzalek

The DSIAC Journal is a publication of the Defense Systems Information Analysis Center (DSIAC). DSIAC is a DoD Information Analysis Center (IAC) sponsored by the Defense Technical Information Center (DTIC) with policy oversight provided by the Office of the Under Secretary of Defense (OUSD) for Research and Engineering (R&E). DSIAC is operated by the SURVICE Engineering Company.

Copyright © 2024 by the SURVICE Engineering Company.

This journal was developed by SURVICE under DSIAC contract FA8075-21-D-0001. The Government has unlimited free use of and access to this publication and its contents, in both print and electronic versions. Subject to the rights of the Government, this document (print and electronic versions) and the contents contained within it are protected by U.S. copyright law and may not be copied, automated, resold, or redistributed to multiple users without the written permission of DSIAC. If automation of the technical content for other than personal use, or for multiple simultaneous user access to the journal, is desired, please contact DSIAC at 443.360.4600 for written approval.

Reference herein to any specific commercial products, process, or service by trade name, trademark, manufacturer, or otherwise does not necessarily constitute or imply its endorsement, recommendation, or favoring by the United States Government or DSIAC.

The views and opinions of authors expressed herein do not necessarily state or reflect those of the United States Government or DSIAC and shall not be used for advertising or product endorsement purposes.

ISSN 2471-3392 (Print) // ISSN 2471-3406 (Online)

Distribution Statement A:

Approved for public release; distribution is unlimited.

On the Cover:

Digital Art Rendering (Source: Canva).



ABOUT DSIAC

Who We Are

A DoD Information Analysis Center comprised of scientists, engineers, researchers, analysts, and information specialists.

What We Do

Generate, collect, research, analyze, synthesize, and disseminate scientific and technical information (STI) to DoD and federal government users and industry contractors.

Why Our Services

To eliminate redundancy, foster collaboration, and stimulate innovation.

DSIAC SERVICES

Subject Matter Expert (SME) Connections

Access to a network of experts with expertise across our technical focus areas.

Technical Inquiries (TIs)

Up to 4 hours of FREE research using vast DoD information resources and our extensive network of SMEs.

Specialized Task Orders

Research and analysis services to solve our customer's toughest scientific and technical problems.

Webinars & Events

Our webinars feature a technical presentation from a SME in one of our focus areas. We also offer key technical conferences and forums for the science and technology community.

STI Collection

Our knowledge management team collects and uploads all pertinent STI into DTIC's Research & Engineering Gateway.

Information Research Products

The Defense Systems Digest, state-of-the-art reports, journals, TI response reports, and more available on our website.

CONTACT DSIAC

IAC Program Management Office

8725 John J. Kingman Road
Fort Belvoir, VA 22060
Office: 571.448.9753

DSIAC Headquarters

4695 Millennium Drive
Belcamp, MD 21017-1505
Office: 443.360.4600
Fax: 410.272.6763
Email: contact@dsiac.org

DSIAC Technical Project Lead

Brian Benesch
4695 Millennium Drive
Belcamp, MD 21017-1505
Office: 443.360.4600



FEATURED ARTICLE

ATMOSPHERIC CORROSION SEVERITY AND THE ROLE OF THE ENVIRONMENT: DETERMINING A DIRECT CORRELATION

By Douglas C. Hansen, Christine E. Sanders, Ronald A. Zeszut, Raymond J. Santucci, and Matthew J. Rothgeb

Corrosion costs the U.S. Department of Defense billions of dollars annually and heavily impacts the availability of DoD assets to carry out their missions. This article discusses the future of addressing this issue using condition-based maintenance utilizing artificial intelligence/machine-learning and cutting-edge exposure simulation chambers.

IN THIS ISSUE

SPECIAL NAVY EDITION

06 PERSPECTIVE: A Brief History of the Advanced Inorganic-Organic Hybrid Polymers of NRL's Chemistry Division

By Manoj Kolel-Veetil

14 Emerging Applications of Machine Learning and Predictive Analytics in Naval Energy Autonomy

By Zhenhua Jiang, Scott C. Miller, and David Dunn

37 Understanding the Bow Topside Flow Field of the USS *Zumwalt* for Hypersonic Missile Launching: A Potential Missing Link

By Peter J. Disimile and Syed Qasim Zaheer

50 Attributing Mission Performance to Submarine Subsystems

By Jonathan Proule

NOTE FROM THE EDITOR-IN-CHIEF

BY GREG NICHOLS



CELEBRATING NEARLY 250 YEARS OF U.S. NAVAL INNOVATION

On March 9, 1862, as the first sunlight of the day sparkled over the Chesapeake Bay, history was being made with the world's first clash of steam-powered, ironclad warships.¹ The U.S. Navy's newest and most advanced ship, the *USS Monitor*, engaged in an hours-long battle with the *CSS Virginia* (formerly the *USS Merrimack*). Though the resulting battle would end in a draw, naval

warfare was changed forever. Nearly 160 years later, the Navy launched Task Force 59—a one-of-a-kind and advanced concept to quickly combine unmanned systems and artificial intelligence with naval operations.

From its humble beginnings in 1775 with a schooner and a sloop, the Navy has since transformed into a formidable fighting force—perhaps the strongest and most capable naval force in world history. Apart from the courage and legacy of the sailors and marines who have fought and served gallantly for centuries, the Navy also owes its continued success and fierceness to a long-time tradition of embracing innovation. For nearly 250 years, they have been committed to pushing the boundaries of what is possible with the latest technology, thus enabling them to prepare for the future fight.

As we launch the renewed DSIAC Journal, we dedicate this first special edition to the Navy and its celebrated tradition of embracing innovation and technology, especially in the most pivotal and volatile of times. From the screw propeller to nuclear propulsion

“

As we launch the renewed DSIAC Journal, we dedicate this first special edition to the Navy and its celebrated tradition of embracing innovation and technology, especially in the most pivotal and volatile of times.

to nanotechnology and advanced materials to autonomy, hypersonic missiles, multidomain operations, and additive manufacturing, the Navy continuously pushes forward. We highlight some of these advancements here with a collection of five articles that embrace the spirit of current naval innovation and operational direction.

We begin this issue with a historical perspective from the Naval Research Laboratory's (NRL's) Chemistry Division on the development of inorganic-organic hybrid polymers. Then, we turn to an exploration of emerging applications of artificial

¹ Naval History and Heritage Command. “The Battle of Hampton Roads.” <https://www.history.navy.mil/our-collections/photography/wars-and-events/the-american-civil-war--1861-1865/css-virginia-destroys-uss-cumberland-and-uss-congress--8-march-1.html>, accessed on 5 July 2023.

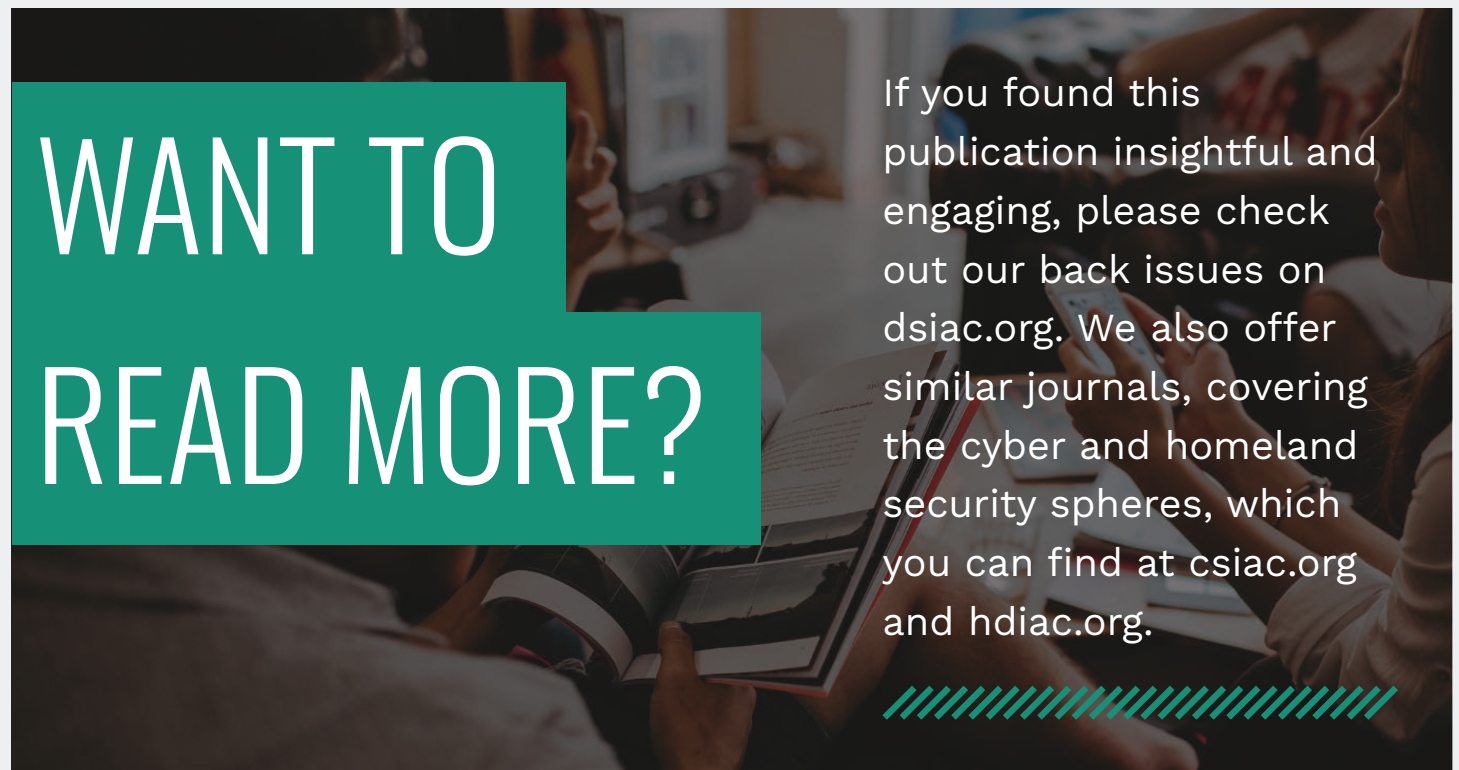
intelligence and machine learning in naval energy autonomy and digital transformation from a collaboration between the Naval Facility Engineering and Expeditionary Warfare Center and the University of Dayton Research Institute (UDRI). A team from NRL and UDRI present our feature article that covers new methods for understanding an old enemy of Navy steel that costs billions of dollars each year—corrosion. They describe research that seeks to improve upon the age-old Environmental Severity Index rankings used in corrosion maintenance by combining real-world corrosion measurements with advanced analytical techniques to better understand the relationship

between the environmental conditions and the reliability and maintainability of Navy assets.

We end this special issue with two articles focusing on naval weapons systems. One depicts the modeling and characterization of airwake needed to determine how to properly fit a Zumwalt class destroyer with hypersonic launch capabilities. The other discusses the Mission Effectiveness Dashboard, a browser-based tool that allows users to quantify the performance of a submarine across missions, thus allowing architects to visualize outputs as part of the process of making informed submarine design decisions.

Admiral Chester Nimitz famously said, “It is the function of the Navy to carry the war to the enemy so that it is not fought on U.S. soil.”² We hope this special edition offers an overview of how the Navy is doing that, mainly through shipbuilding (materials and design), maintenance, weaponry, and power. The work never ends. The information we present here is only a tiny fraction of the research the Navy is currently conducting but offers a glimpse into the large-scale, long-range planning needed to keep the fleet in fighting shape. ■

Sincerely,



**WANT TO
READ MORE?**

If you found this publication insightful and engaging, please check out our back issues on dsiac.org. We also offer similar journals, covering the cyber and homeland security spheres, which you can find at csiac.org and hdiac.org.



² Naval History and Heritage Command. “Employment of Naval Forces by Fleet Admiral Chester W. Nimitz, USN.” <https://www.history.navy.mil/research/library/online-reading-room/title-list-alphabetically/e/employment-of-naval-forces.html>, accessed on 5 July 2023.

PERSPECTIVE

A BRIEF HISTORY OF

THE ADVANCED INORGANIC-ORGANIC HYBRID POLYMERS

OF NRL'S CHEMISTRY DIVISION

BY MANOJ KOLEL-VEETIL (PHOTO SOURCE: CANVA AND M. KOLEL-VEETIL)

INTRODUCTION

In common language, the term “polymer” elicits references to many ordinary, practical items, including the phrase “*paper or plastic*” in checkout counters. “Polymer” is derived from Greek, with “poly” meaning many and “mer” meaning part. For example, in typical human-made polymers such as polyethylene, polyurethane, and polyvinyl chloride, there are many units of either ethylene, urethane, or vinyl chloride put together to form the ultimate polymer. In all commonly known polymers, the repeating units are made from mainly carbon-containing units. Hence, they all belong to the group of organic polymers. In addition to human-made organic polymers, nature is abundant with *organic* polymers such as wool, silk, proteins, starch, and cellulose. In contrast, any material that does not contain the element carbon can be considered “*inorganic*.”

Borates, silanes, and polyphosphazenes are inorganic polymers since they do not contain carbon. Typically, organic polymers are flexible and have an operating window with an upper bound of 400 °C. For example, the polyimide film Kapton has an operating window of -269 °C to 400 °C. Carbon-containing polymers with high thermal and

oxidative stabilities are stiffer materials, such as the rigid rod polymer poly(benzobisoxazole) (Zylon). In such polymers, the in-plane aromatic conjugation restricts the availability of functional groups that can be attacked by oxygen. More flexible polymers like polyethylene, polypropylene, and polystyrenes tend to be attacked by oxygen at much lower temperatures and have melting temperatures below 250 °C. In contrast, inorganic polymers are usually rigid and tend to have higher operating windows. To combine the properties of organic and inorganic polymers, a new group of polymers emerged that comprised both groups. Thus, *inorganic-organic hybrid polymers* are a rarified class of materials possessing combined properties of both inorganic main group element- and carbon-containing components.

The terms “inorganic-organic” or “organic-inorganic” were first coined in 1990 by Saegusa and Chujo, who reported the polymer poly(N-acetylenimine)(polyoxazoline) with terminal triethoxysilyl groups [1]. In addition to increasing the flexibility of polymers, a principal intent in forming an inorganic-organic hybrid polymer is to improve its thermal and oxidative properties. One way to circumvent the oxidation problem is by slowing down the

“

A principal intent in forming an inorganic-organic hybrid polymer is to improve its thermal and oxidative properties.

diffusion of oxygen into a polymer sample’s interior during oxidation, i.e., by diffusion-limited-oxidation (DLO) [2]. The most common polymers that can provide such a condition are silanes and siloxanes. In addition to the flexibility of their backbones, they tend to form inorganic silica (SiO₂, melting point [M.P.] = 1710 °C) during oxidation that significantly impedes the diffusion of oxygen. Other groups of inorganic polymeric entities that provide such DLO conditions contain the elements aluminum, boron, and phosphorous. During oxygen attack, these polymers produce alumina (Al₂O₃, M.P. = 2072 °C), boron oxide (B₂O₃, M.P. = 450 °C), and phosphorus pentoxide (P₂O₅, M.P. = 340 °C) during oxidation, which substantially slows the diffusion of oxygen. In general, inorganic-organic polymers are used in coatings, functional particles, bulk materials, fibers, and composites [3]. Such applications are crucial for the Navy.

SILOXANE POLYMER ORIGINS

The origins of siloxane chemistry can be attributed to the English chemist Frederic Kipping and his coworkers in the early 1900s. However, the discoverers of siloxanes did not deem this group of compounds to be of significant interest, as evident in the statement of Kipping during his 1936 Bakerian lecture that “the prospect of any immediate and important advance in this section of organic chemistry does not seem to be very hopeful” [4, 5]. Fortunately, Kipping was proven to be wrong by a renaissance in siloxane chemistry in the 1940s led by Hyde and Delong at the Corning Glass Works [6], McGregor and Warrick at the Mellon Institute [7], and Rochow at the General Electric Company [8].

During this time, the synthesis of polysiloxanes was perfected and led to other silarylene-siloxane polymers and silalkarylene-siloxane polymers in the 1950s. These were the original inorganic-organic hybrid polymers, although the term was not coined at the time of their conception. Even though they were high-performance elastomeric materials, a major development occurred in the 1960s and 1970s with the discovery of carborane-siloxane polymers [9, 10]. (Carboranes are three-dimensional compounds of boron, carbon, and hydrogen with polyhedral skeletons of the general formula $C_pB_qH_{p+q}$)

The carborane-siloxane polymers possessed exceptional thermal and oxidative stabilities. However, they were mainly inorganic polymers and thermoelastomeric materials like siloxane polymers.

INORGANIC-ORGANIC HYBRID POLYMERS' HISTORY AT THE NAVAL RESEARCH LABORATORY'S (NRL'S) CHEMISTRY DIVISION

NRL Chemistry Division's entry into this exciting area of polymeric materials occurred in the 1990s. To add to the suite of their promising high-performance phthalonitrile polymers with the intent to develop novel *inorganic-organic hybrid* and “*thermosetting*” polymeric versions of the existing carborane-siloxane polymers, Henderson and Keller

reported the original synthesis of poly(carborane-siloxane-acetylene)s (PCSA) with exceptional thermal and oxidative stabilities [11]. In Figure 1, the organic entity in this group of polymers was derived by the dechlorination of hexachlorobutadiene (2) using *n*-butyl lithium yielding the dilithiated diacetylene entity (3) which, upon reaction with the halogenated carborane-siloxane monomer (named DEXIL monomer[4]), produced PCSA (1). Containing about 10 inorganic repeat units linked by the organic diacetylene entities, these oligomers retained up to 85% and 92% weight upon pyrolysis to 1000 °C in a nonoxidizing and oxidizing environment. This polymer started to crosslink from around 250 °C, with an exotherm peaking around 350 °C (Figure 1), by either 1,2- or 1,4- polymerization of the diacetylene groups to yield thermosetted carbon domains.

Subsequently, the carboraneless version of this polymer was also produced

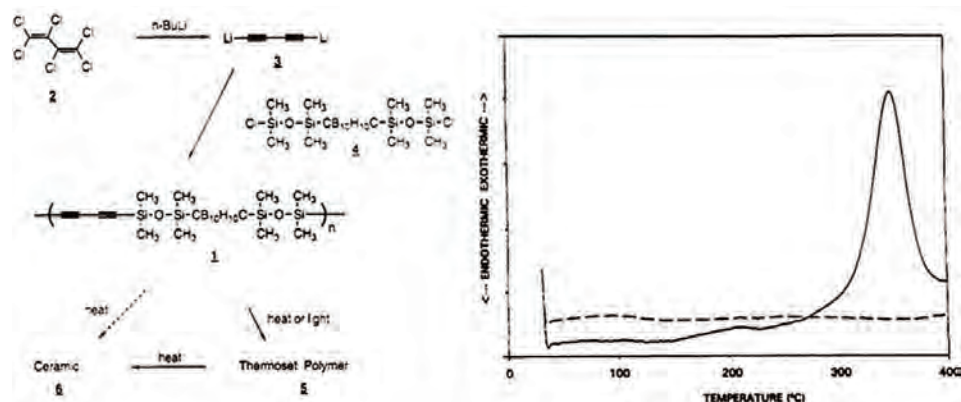


Figure 1. (Left) Reaction Scheme for the Synthesis of Poly(Carborane-Siloxane-Acetylene) (PCSA) and (Right) the Differential Scanning Calorimetry Thermogram of Neat PCSA (Solid) and Cured PCSA (Dashed) (Source: Reproduced With Permission From the American Chemical Society).

within the year by Son and Keller [12]. This was followed by the synthesis of a block copolymer wherein blocks of PCSA were alternated with siloxane-diacetylene monomers [13]. At this point, hydrosilylation was used as a reactive means to produce an acetylene-containing silicon (Si) monomer which could be further reacted with other aromatic organic entities to produce new versions of PCSA [14].

To fundamentally understand the thermo-oxidative stability of PCSA, surface analysis studies were carried out by Pehrsson et al. using scanning electron microscopy, X-ray photoelectron spectroscopy, scanning Auger microprobe scattering, and Raman microprobe scattering [15]. It was seen that PCSA samples heated to 400 °C in argon exhibited no inorganic segregation; however, treatment to the same temperature in air produced surface layers of boron and Si oxide. Furthermore, samples annealed in argon to 900 °C and then oxidized at 500 °C for up to 100 hr grew a continuous Si oxide surface layer with almost no underlying boron oxide. This layer retarded oxidation of the bulk sample at 500 °C. Thus, the thermo-oxidative stability was determined to be from the DLO of the polymer, with the formation of SiO_2 ,

B_2O_3 , and the possible formation of borosilicate-containing protective barriers at higher temperatures.

Further, in continuing inorganic-organic hybrid polymer research, a PCSA-like polymer wherein the carborane clusters were substituted by a clusterless B-Ph group was produced by Sundar and Keller [16]. The thermal stability of this polymer up to 1000 °C in nitrogen was found to be lower than PCSA (72.1% vs. 85%). However, the crosslinked versions exhibited similar oxidative stabilities as those obtained from PCSA. The main advantage of this polymer is substituting the expensive carborane with the inexpensive B-Ph group, thus reducing overall cost.

Subsequently, Bucca and Keller attempted to incorporate an aromatic group-like phenyl(benzene) in the backbone of the carborane-siloxane inorganic-organic hybrid polymer [17]. A 4-phenylethynylphenyl unit was used to introduce the aromatic group. However, the presence of a *labile phenyl group* after crosslinking caused the polymer to have low thermal stability. Further, the ligand 1,4-bis(dimethylchlorosilyl) benzene was used to incorporate a benzene(phenyl) group into a series of polymers with thermal stabilities between 79% and 86% [18].

An interesting development in the progress of inorganic-organic hybrid polymers occurred in 1998 when Houser and Keller introduced ferrocene in the PCSA polymer in the form of bridging groups between siloxane-carborane-siloxane-diacetylene entities [19]. This polymer, producing iron (Fe)-containing ceramic had a weight retention of 78% at 1000 °C in nitrogen compared to the typical ferrocenyl-siloxyl polymers with a weight retention of around 50% [20]. The DEXIL monomer was further used in hydrosilylation reaction with poly(methylhydrosiloxane) to produce crosslinked networks with high stability [21]. Oxidation-resistant thermosets were also formed from thermal copolymerization of acetylenic monomers containing boron and Si [22] and diacetylene-siloxane-carborane ceramic precursors [23].

In the early 2000s, a new set of high-temperature elastomers was synthesized at NRL from silarylene-siloxane-diacetylene linear polymers by Homrighausen and Keller [24, 25]. These differed from the silarylene-siloxane of the 1950s in that they contained the crosslinking unit diacetylene, which enabled conversion to a thermoset. Furthermore, both the diacetylene and phenyl groups were incorporated in the backbone of an inorganic-organic hybrid polymer using hydroxy-terminated, oligomeric poly(silarylene disiloxane)s via rhodium-catalyzed dehydrogenative coupling for their use in the



aminosilane-disilanol polymerization reaction [26].

In the meantime, the practical implications of PCSA and other produced inorganic-organic variants were becoming obvious as Keller in 2002 demonstrated that they could protect carbon fibers (CFs) from oxidation when applying PCSA as a protective coating [27]. While uncoated CFs were found to catastrophically degrade between 600 °C and 800 °C, PCSA-coated CFs retained up to 96 wt% when heated in air to 1000 °C. This was truly impressive! Around that time, Beckham and Keller synthesized diacetylene-terminated diacetylene containing polysiloxanes—a new addition to the class of polysiloxanes [28].

The research in the early 2000s on PCSA and its derivatives hinged on making these polymers elastomeric. Kolel-Veetil and Keller explored two ways of effecting this [29]. In the first method, the concentration of diacetylene units was diluted in PCSA to impart elasticity to the polymers. In the second method, different kinds of block polymers were incorporated in the PCSA and its variants, and their elastomeric properties as a function of the glass transition temperatures and corresponding thermal stabilities were evaluated [30].

Furthermore, Kolel-Veetil et al. expanded the utility of these polymers to produce transition metal (TM)-

derived nanoparticles (NPs) by reacting TM complexes with the diacetylene groups in PCSA to obtain *molecular-level* functionalization [31]. In reacting PCSA with the TM complex, $Cp_2Mo_2(CO)_6$, functionalization of the diacetylene occurred, and the TM-PCSA complexes on pyrolysis produced a superconducting mixture that contained β - Mo_2C NPs and carbon nanotubes. In a seminal paper that garnered the prestigious Berman Publication Award of NRL, Kolel-Veetil et al. demonstrated that by controlling the rate and temperature of pyrolysis, one could produce different phases of Mo_2C NPs and therefore different conductivity properties for the mixture

[32]. Thus, on pyrolysis only to 850 °C, smaller (~2–4 nm)-sized α - Mo_2C NPs were formed. Due to the sizes being below the Anderson criterion limit, these NPs were unable to sustain superconductivity in a typical BCS system since the coherence length of the Cooper pairs was larger than the particle sizes [33]. When pyrolysis was performed up to 1000 °C, β - Mo_2C of larger sizes was produced that sustained superconductivity with a T_c of ~5 °C (Figure 2).

In a similar vein, Kolel-Veetil et al. used a ferrocene-containing, siloxane-diacetylene polymer like the one developed in 1998 [34]. They showed

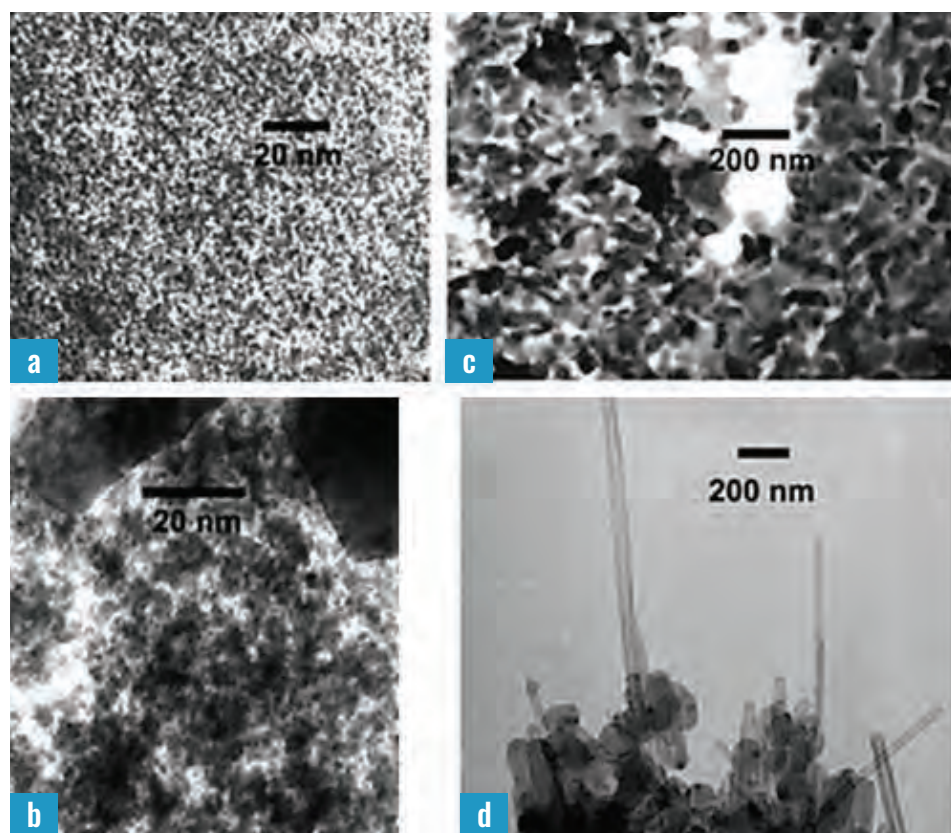


Figure 2. TEM Micrographs of the 850 °C Pyrolysis Product Containing Predominantly (a) α - Mo_2C NPs and (b) α - Mo_2C NPs With a Few β - Mo_2C NPs; and the 1000 °C Pyrolysis Product Containing (c) Larger β - Mo_2C NPs and (d) Larger β - Mo_2C NPs With MWCNTs (Source: Reproduced With Permission From the American Chemical Society).

that depending on the rate of thermal treatment, one could either form Fe NPs with CF and Si carbide or have carbon nanocapsules sequester both Fe and Si during reaction to produce the ferromagnetic Fe₅Si₃ NPs.

In 2009 and 2012, Kolel-Veetil et al. utilized the hydrosilation reactions to make new inorganic-organic hybrids of polyoctahedral silsesquioxanes (POSS), the smallest unit of silica [35, 36]. In the first example, crosslinked dendritic networks of POSS units with *diacetylene* crosslinkers were synthesized [35]. In the second instance, crosslinked dendritic networks of POSS units with *acetylene*

crosslinkers were synthesized [36]. The latter allowed the production of α -cristobalite in the converted ceramic. Finally, in 2013, Kolel-Veetil et al. were able to produce an inorganic-organic polymer variant of PCSA, known as *m*-poly(carborane-siloxane-arylacetylene) (*m*-PCSAA) and *p*-poly(carborane-siloxane-arylacetylene) (*p*-PCSAA) by incorporating *p*-diethynylbenzene and *m*-diethynylbenzene (Figure 3) [37]. These variants have slightly higher thermal and oxidative stabilities than PCSA. Impressively, they also protect high-performance organic fibers such as Kevlar, Zylon, and electrically

conducting wires during operation at high temperature and voltage. Furthermore, these polymers also have exceptional dielectric properties.

TODAY'S POLYMERS

From 2013 to the present, various materials properties of these polymers have been explored that have created some exciting applications. In 2020, PCSA, *m*-PCSAA, and *p*-PCSAA were licensed by the commercial entity Boron Specialties, Inc. in Ambridge, PA. Many more exciting future applications are also being created for these inorganic-organic hybrid polymers.

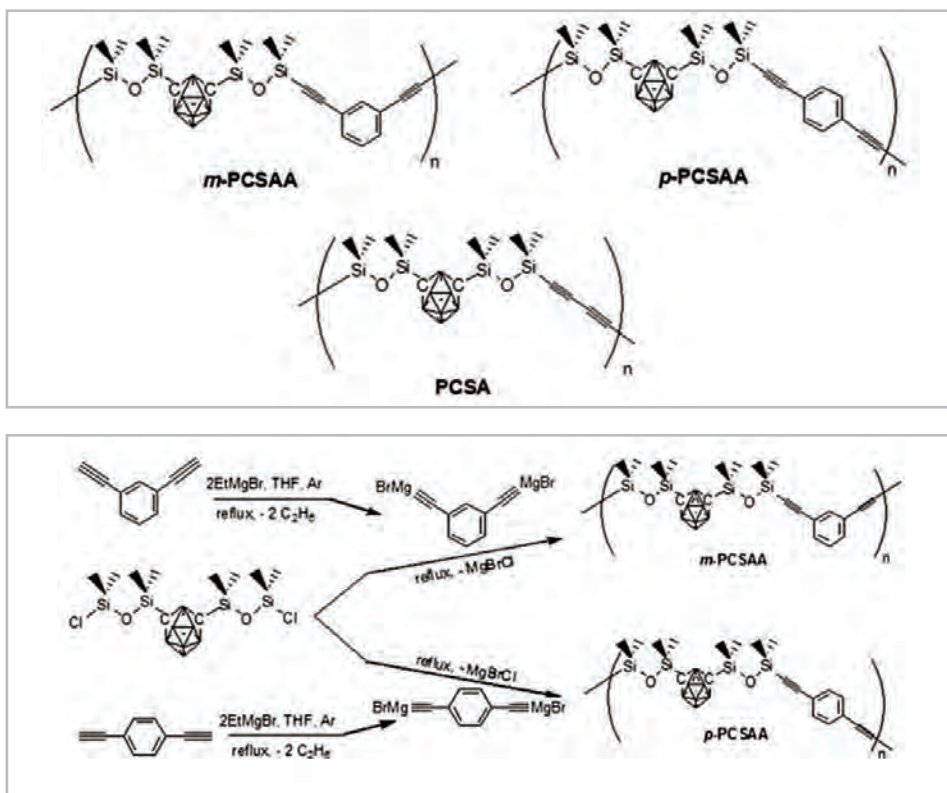


Figure 3. (Top Box) The In-Backbone Aromatic Group-Containing Carboranylesiloxanes *m*-PCSAA and *p*-PCSAA and Their Diacetylene Counterpart, PCSA. (Bottom Box) Synthetic Schemes for *m*-PCSAA and *p*-PCSAA (Source: Reproduced With Permission From the American Chemical Society).

CONCLUSIONS

While the science of siloxanes has come a long way since their discovery, the advent of inorganic-organic hybrid polymers has opened new possibilities for further evolution. The ultimate utility of the inorganic entities in the inorganic-organic hybrid siloxane polymers has been manufacturing DLO-producing oxide surfaces. The organic groups function as crosslinking sites enabling the creation of thermosets and sites for TM-functionalization and yielding a very impressive suite of TM-containing compositions with exceptional conducting and magnetic properties. Such developments have enabled the production of novel



While the science of siloxanes has come a long way since their discovery, the advent of inorganic-organic hybrid polymers has opened new possibilities for further evolution.

coatings, functional particles, bulk materials, fibers, and composites that are very important to the Navy. Thus, further growth in the science of these polymers, contrary to Kipping's trepidations, will only be limited by the imagination of the scientist. ■

ACKNOWLEDGMENT

The author gratefully acknowledges support by the NRL 6.1 Base program (FY23 Chemistry Division 6.1 Base Program; P.I.: M. K. Kolel-Veetil).

REFERENCES

- [1] Saegusa, T., and Y. Chujo. "An Organic/Inorganic Hybrid Polymer." *Journal of Macromolecular Science: Part A - Chemistry*, vol. 27, nos. 13-14, pp. 1603-1612, 1990.
- [2] Celina, M. C. "Review of Polymer Oxidation and Its Relationship With Materials Performance and Lifetime Prediction." *Polymer Degradation and Stability*, vol. 98, no. 18, pp. 2419-2429, 2013.
- [3] Haas, K.-H., and G. Schottner. "Hybrid Inorganic-Organic Polymers." *Encyclopedia of Glass Science, Technology, History, and Culture, Volume II, First Edition*, Pascal Richet, pp. 1057-1068, 2021.
- [4] Kipping, F. S. "The Bakerian Lecture: Organic Derivatives of Silicon." *Proceedings of the Royal Society of London A*, vol. 159, pp. 139-148, 1937.
- [5] Dvornic, P. R., and R. W. Lenz. *High Temperature Siloxane Elastomers*. Hüthig & Wepf Verlag Basel, Heidelberg, New York, 1990.
- [6] Hyde, J. F., and R. C. Delong. "Condensation Products of the Organo-Silane Diols." *Journal of the American Chemical Society*, vol. 63, pp. 1194-1196, 1941.
- [7] McGregor, R. R., and E. L. Warrick. U.S. Patent 2,380,057, 1945.
- [8] Rochow, E. G. "The Direct Synthesis of Organosilicon Compounds." *Journal of the American Chemical Society*, vol. 67, pp. 963-965, 1945.
- [9] Mayes, N., J. Green, and M. S. Cohen. *Journal of Polymer Science, Part A-1*, vol. 5, pp. 365-380, 1967.
- [10] Peters, E. N. *Journal of Macromolecular Science Review Macromolecular Chemistry*, vol. C17, no. 2, pp. 173-182, 1979.
- [11] Henderson, L. J., and T. M. Keller. "Synthesis and Characterization of Poly(Carborane-Siloxane-Acetylene)." *Macromolecules*, vol. 27, no. 6, pp. 1660-1661, 1994.
- [12] Son, D. Y., and T. M. Keller. "Synthesis and Characterization of Linear Siloxane-Diacetylene Polymers." *Macromolecules*, vol. 28, no. 61, pp. 399-400, 1995.
- [13] Son, D. Y., and T. M. Keller. "Oxidatively Stable Carborane-Siloxane-Diacetylene Polymers." *Journal of Polymer Science, Part A: Polymer Chemistry*, vol. 33, pp. 2969-2972, 1995.
- [14] Son, D. Y., D. Bucca, and T. M. Keller. "Hydrosilylation Reactions of Bis(Dimethylsilyl) Acetylenes: A Potential Route to Novel σ - and π -Conjugated Polymers." *Tetrahedron Letters*, vol. 37, no. 10, pp. 1579-1582, 1996.
- [15] Pehrsson, P. E., L. J. Henderson, and T. M. Keller. "High-Temperature Oxidation of Carborane-Siloxane-Acetylene-based Polymer." *Surface and Interface Analysis*, vol. 24, no. 3, pp. 145-151, 1996.
- [16] Sundar, R. A., and T. M. Keller. "Synthesis and Characterization of Linear Boron-Silicon-Diacetylene Copolymers." *Macromolecules*, vol. 29, no. 10, pp. 3647-3650, 1996.
- [17] Bucca, D., and T. M. Keller. "Thermally and Oxidatively Stable Thermosets Derived From Pre-ceramic Monomers." *Journal of Polymer Science, Part A: Polymer Chemistry*, vol. 35, no. 6, pp. 1033-1038, 1997.
- [18] Sundar, R. A., and T. M. Keller. "Linear Diacetylene Polymers Containing Bis(Dimethylsilyl) Phenyl and/or Bis(Tetramethyldisiloxane)Carborane Residues: Their Synthesis, Characterization and Thermal and Oxidative Properties." *Journal of Polymer Science, Part A: Polymer Chemistry*, vol. 35, no. 12, pp. 2387-2394, 1997.
- [19] Houser, E. J., and T. M. Keller. "Linear Ferrocenylene-Siloxyl-Diacetylene Polymers and Their Conversion to Ceramics With High Thermal and Oxidative Stabilities." *Macromolecules*, vol. 31, no. 12, pp. 4038-4040, 1998.
- [20] Patterson, W. J., S. P. McManus, and C. U. Pittman, Jr. *Journal of Polymer Science, Polymer Chemical Education*, vol. 12, pp. 837-848, 1974.
- [21] House, E. J., and T. M. Keller. "Hydrosilation Routes to Materials With High Thermal and Oxidative Stabilities." *Journal of Polymer Science, Part A: Polymer Chemistry*, vol. 36, no. 11, pp. 1969-1972, 1998.
- [22] Armistead, J. P., E. J. Houser, and T. M. Keller. "Diacetylene-Siloxane-Carborane Thermosets and Ceramic Precursors." *Applied Organometallic Chemistry*, vol. 14, no. 5, pp. 253-260, 2000.
- [23] Bucca, D., and T. M. Keller. "Oxidation-Resistant Thermosets Derived From Thermal Copolymerization of Acetylenic Monomers Containing Boron and Silicon." *Journal of Polymer Science, Part A: Polymer Chemistry*, vol. 37, no. 23, pp. 4356-4359, 1999.
- [24] Homrighausen, C. L., and T. M. Keller. "High-Temperature Elastomers From Silarylene-Siloxane-Diacetylene Linear Polymers." *Journal of Polymer Science, Part A: Polymer Chemistry*, vol. 40, pp. 88-94, 2002.
- [25] Homrighausen, C. L., and T. M. Keller. "Synthesis and Characterization of a Silarylene-Siloxane-Diacetylene Polymer and Its Conversion to a Thermosetting Plastic." *Polymer*, vol. 43, no. 9, pp. 2619-2623, 2002.
- [26] Homrighausen, C. L., and T. M. Keller. "Synthesis of Hydroxy-Terminated, Oligomeric Poly(Silarylene Disiloxane)s via Rhodium-Catalyzed Dehydrogenative Coupling and Their Use in the Aminosilane-Disilanol Polymerization Reaction." *Journal of Polymer Science, Part A: Polymer Chemistry*, vol. 40, no. 9, pp. 1334-1341, 2002.
- [27] Keller, T. M. "Oxidative Protection of Carbon Fibers With Poly(Carborane-Siloxane-Acetylene)." *Carbon*, vol. 40, no. 3, pp. 225-229, 2002.
- [28] Beckham, H. W., and T. M. Keller. "Diacetylene-Terminated Diacetylene-Containing Polysiloxanes." *Journal of Materials Chemistry*, vol. 12, no. 12, pp. 3363-3365, 2002.
- [29] Kolel-Veetil, M. K., and T. M. Keller. "The Effects of Concentration Dilution of Cross-Linkable Diacetylenes on the Plasticity of Poly(m-Carborane-Siloxane-Diacetylene)s." *Journal of Materials Chemistry*, vol. 13, no. 7, pp. 1652-1656, 2003.
- [30] Kolel-Veetil, M. K., H. W. Beckham, and T. M. Keller. "Dependence of Thermal Properties on the Copolymer Sequence in Diacetylene-Containing Polycarboranylenesiloxanes." *Chemistry of Materials*, vol. 16, no. 16, pp. 3162-3167, 2004.
- [31] Kolel-Veetil, M. K., S. B. Qadri, M. Osofsky, and T. M. Keller. "Formation of a Superconducting

Mixture of β - Mo_2C Nanoparticles and Carbon Nanotubes in an Amorphous Matrix of Molybdenum Compounds by the Pyrolysis of a Molybdenum Derivative of a Carboranylenesiloxane." *Chemistry of Materials*, vol. 17, no. 24, pp. 6101–6107, 2005.

[32] Kolel-Veetil, M. K., S. B. Qadri, M. Osofsky, T. M. Keller, R. Goswami, and S. A. Wolf. "Size-Induced Effects on the Superconducting Properties of Mo_2C Nanoparticles." *Journal of Physical Chemistry C*, vol. 111, no. 45, pp. 16878–16882, 2007.

[33] Anderson, P. W. "Theory of Dirty Superconductors." *Journal of Physics and Chemistry of Solids*, vol. 11, nos. 1–2, pp. 26–30, 1959.

[34] Kolel-Veetil, M. K., S. B. Qadri, M. Osofsky, R. Goswami, and T. M. Keller. "Carbon Nanocapsule-Mediated Formation of Ferromagnetic Fe_3Si_3 Nanoparticles." *Journal of Physical Chemistry C*, vol. 113, no. 33, pp. 14663–14671, 2009.

[35] Kolel-Veetil, M. K., D. D. Dominguez, C. A. Klug, and T. M. Keller. "Hydrosilated Dendritic Networks of POSS Cores and Diacetylene Linkers." *Macromolecules*, vol. 42, no. 12, pp. 3992–4001, 2009.

[36] Kolel-Veetil, M. K., K. P. Fears, S. B. Qadri, C. A. Klug, and T. M. Keller. "Formation of a Crosslinked POSS Network by an Unusual Hydrosilylation: Thermo-Oxidative Stabilization of the α -Cristobalite Phase in Its Amorphous Regions." *Journal of Polymer Science, Part A: Polymer Chemistry*, vol. 50, no. 15, pp. 3158–3170, 2012.

[37] Kolel-Veetil, M. K., D. D. Dominguez, C. A. Klug, K. P. Fears, S. B. Qadri, D. Fragiadakis, and T. M. Keller. "Hybrid Inorganic-Organic Poly(Carborane-Siloxane-Arylacetylene) Structural Isomers With In-Chain Aromatics: Synthesis and Properties." *Journal of Polymer Science, Part A: Polymer Chemistry*, vol. 51, no. 12, pp. 2638–2650, 2013.



BIOGRAPHY

DR. MANOJ KOLEL-VEETIL is a research chemist in the Chemistry Division at NRL, Washington, DC, where he started as an ASEE Postdoctoral Research Fellow and transitioned to federal employment. At NRL, he worked on several areas of chemistry, including hybrid inorganic-organic polymers, cyclic peptide nanotubular materials, boron carbide-based materials, ceramic materials, and the science of per- and polyfluoroalkyl substances. He holds a Ph.D. in chemistry from the University of Vermont and subsequently conducted postdoctoral research at Kansas State University and the University of Oklahoma.

DSIAC WEBINAR SERIES

EXPANDING RELEASE ENVELOPES INTO THE SUPERSONIC REGIME VIA CFD-DRIVEN ANALYSIS

FEBRUARY 28, 2024 12:00 PM

Register here:
bit.ly/48SU1DW



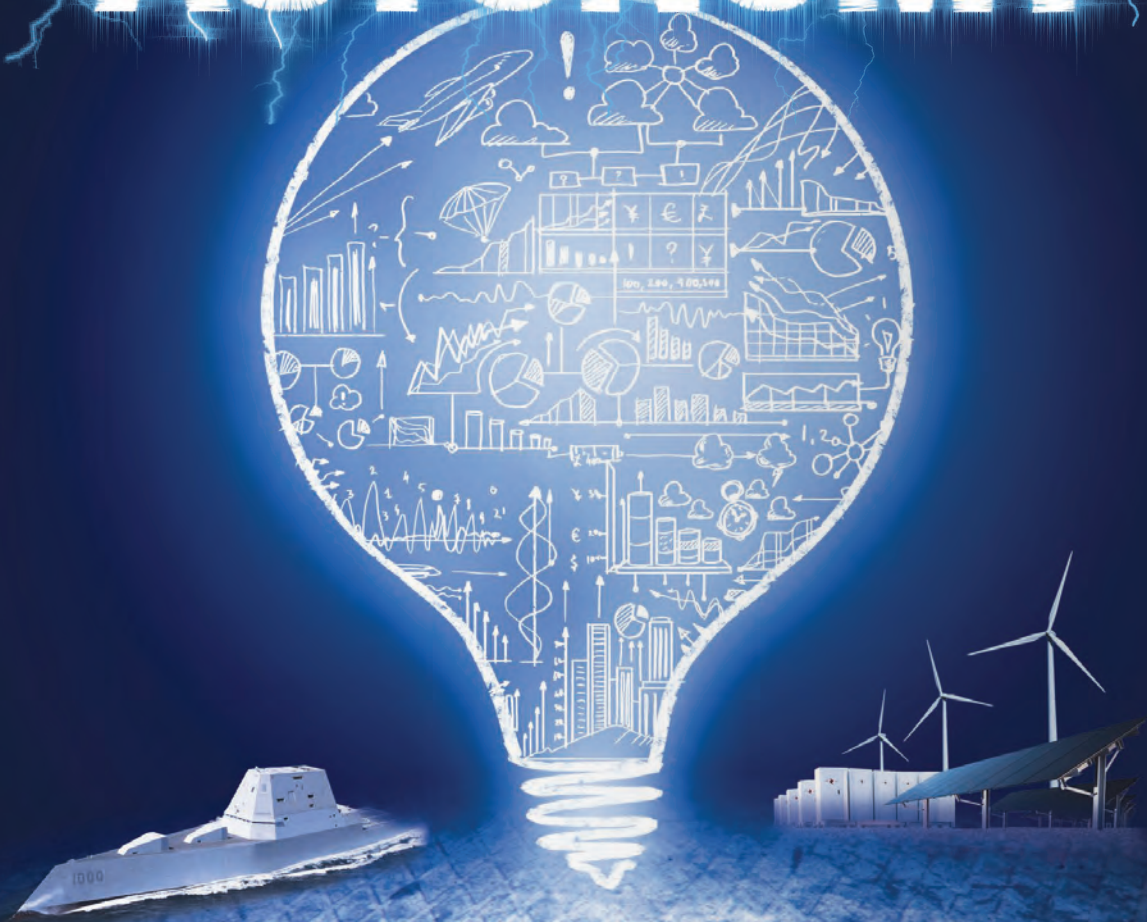
Photo Source: U.S. Air Force, Presenter-Supplied



CHRIS LIPFORD
& RAFAEL PEREZ

EMERGING APPLICATIONS OF MACHINE LEARNING AND PREDICTIVE ANALYTICS IN

NAVAL ENERGY AUTONOMY



**BY ZHENHUA JIANG, SCOTT C. MILLER,
AND DAVID DUNN**

(PHOTO SOURCE: CANVA, U.S. NAVY)

INTRODUCTION

This article explores several emerging applications of artificial intelligence (AI) and machine learning (ML) for U.S. Department of the Navy (DON) energy autonomy and digital transformation use. It also summarizes relevant research and development efforts carried out by the University of Dayton Research Institute (UDRI) in a contract with the Naval Facility Engineering and Expeditionary Warfare Center (NAVFAC EXWC).

BACKGROUND

U.S. Navy facilities have contributed a considerable fraction to the total energy consumption in the defense sector. To reduce energy costs at these facilities, a series of research, development, and demonstration programs related to distributed



U.S. Navy facilities have contributed a considerable fraction to the total energy consumption in the defense sector.

and renewable generation, energy storage, and energy efficiency technologies have been accomplished in the past decades [1–5].

Energy systems at installations typically contain a variety of components connected to power-critical missions or facilities. Traditionally, controls and optimization of energy systems at installations are addressed at the component levels (e.g., generator controllers, battery controllers, etc.). Solutions such as microgrids can provide improved resilience and performance [3–5], but challenges still exist in a highly autonomous operation condition. For example, it is challenging to achieve real-time, system-wide energy optimization that can consider a look-ahead time horizon and prediction of different factors like load profiles, renewable energy availability, fuel/electricity prices, etc.

Even in cases of parallel operation, multiple generators can operate at their full or partial capacities, leading to varying fuel efficiencies. For instance, the generators will need to adapt to different scenarios supporting the voltage or sharing active power or reactive power, particularly when the mobile generators are being rapidly deployed and connected in unknown situations [5]. Also, load shedding is

expected to be based upon a dynamic priority level, which depends on the operation data, scenarios, or user preference. Therefore, the enhanced situational awareness about generator fuel efficiency, load patterns, and the entire microgrid is essential to more efficient utilization of all generation and storage assets. However, traditional control solutions do not capture or address all these factors effectively and may result in inefficiency and other issues (e.g., adaptability or resilience) in real-time operation.

With the advances in sensor technologies, it is possible to install many cost-effective sensors in distributed power plants and load centers and collect and visualize the big data for hundreds or even thousands of parameters and variables [6, 7]. But a question remains on how we could use these large data sets to help improve energy generation/utilization efficiency and reduce energy costs. Since multiple complex energy conversion and flow processes exist in these energy systems, it is necessary to first figure out what data sets are most important and effective in generating energy savings and how they can be utilized to optimize operations before real benefits can be obtained. Therefore, modeling the variety of energy flow processes, understanding the options

and impact of potential energy-saving technologies, and even automating energy saving processes are very important for facility managers to determine action plans for strategical facility upgrade and achieve improved autonomous operation practice.

To address these challenges, the UDRI team recently proposed a unique solution that combines the benefits of data-driven Bayesian neural networks with a physics-guided learning framework where probabilistic weights are considered for learnable parameters [8–10]. This novel learning capability has been developed to enhance the predictive analytics and control system for microgrid operation (as shown in Figure 1) in a contract with NAVFAC EXWC. Specifically,

“

This solution may help improve the energy forecasting accuracy, reduce energy costs across the Navy shore establishment, and reduce redundant equipment and DON new equipment orders.

the system under development aims to optimize the operation of generators of different types, energy storage, and controllable loads at the system level in a resilient manner by leveraging the latest advances in ML, data

analytics, predictive control, and real-time computing. This solution may help improve the energy forecasting accuracy, reduce energy costs across the Navy shore establishment, and reduce redundant equipment and DON new equipment orders.

FEATURES OF ML ANALYTICS

In the general field of AI, the current practice of ML aims to search nonlinear functions between the input and output variables to fit training data samples and update the weights and biases iteratively by using the gradients calculated from the errors between the predicted and labelled values [11–18].

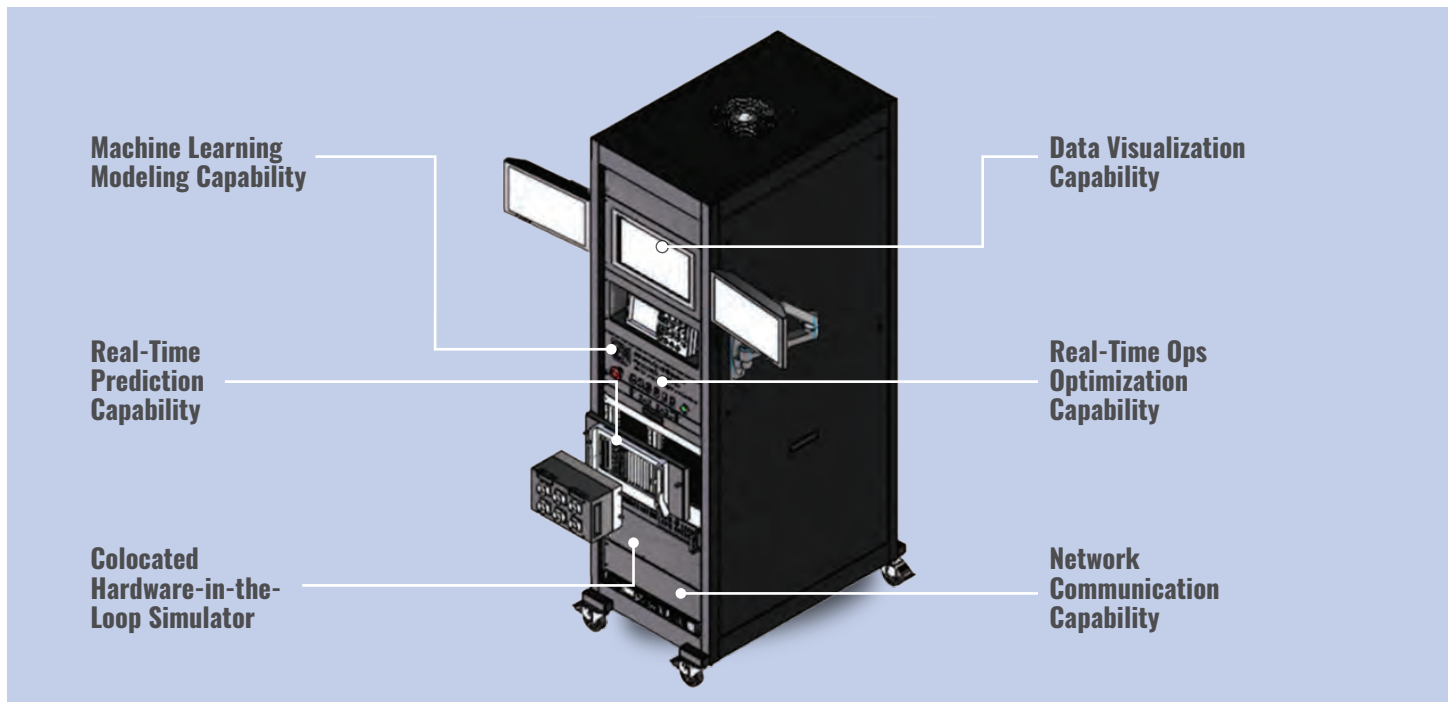


Figure 1. Capabilities of an ML-Driven Energy Optimizer Under Development (Source: Z. Jiang, S. C. Miller, and D. Dunn, Adapted From a Concept Design Art Image Codedigned by Advint LLC).

This process targets seeking unknown or hidden correlations and patterns from training data in an implicit manner. Because of this, the current ML paradigm has many limitations [14–18]. For instance, the iterative updating of weights/biases is fragile, relies on the gradients, and may not accurately reflect general correlations [14]. The classical training process is time-consuming and may sometimes result in overfitting or poor performance [15]. Typical point-to-point predictions based on fixed values of the learned weights may not sufficiently capture the variations or

uncertainty in the model parameters [16]. Slight variations in the input may also lead to large deviations in the predictions or wrong output results [17]. Probabilistic solutions exist, but they typically assume Gaussian distributions [18].

The unique solution recently developed at UDRI is a unified, data-driven, predictive modeling and control method for energy systems. This solution is a physics-guided, Bayesian neural-learning framework with probabilistic weights for learnable parameters in the networks. This

approach can account for our prior physical knowledge, operational data, and uncertainty in the model altogether to gain insight into the energy systems' behavior. Basically, this learning framework can (1) model the causal relationships between cause/effect factors (i.e., input/output variables) in energy systems, (2) learn the system dynamics or temporal dependence from operational data, and/or (3) characterize the uncertainty or variability in the dynamic trends or parameters, as illustrated in Figure 2. To facilitate digital transformation, our three-pronged approach is a physical-

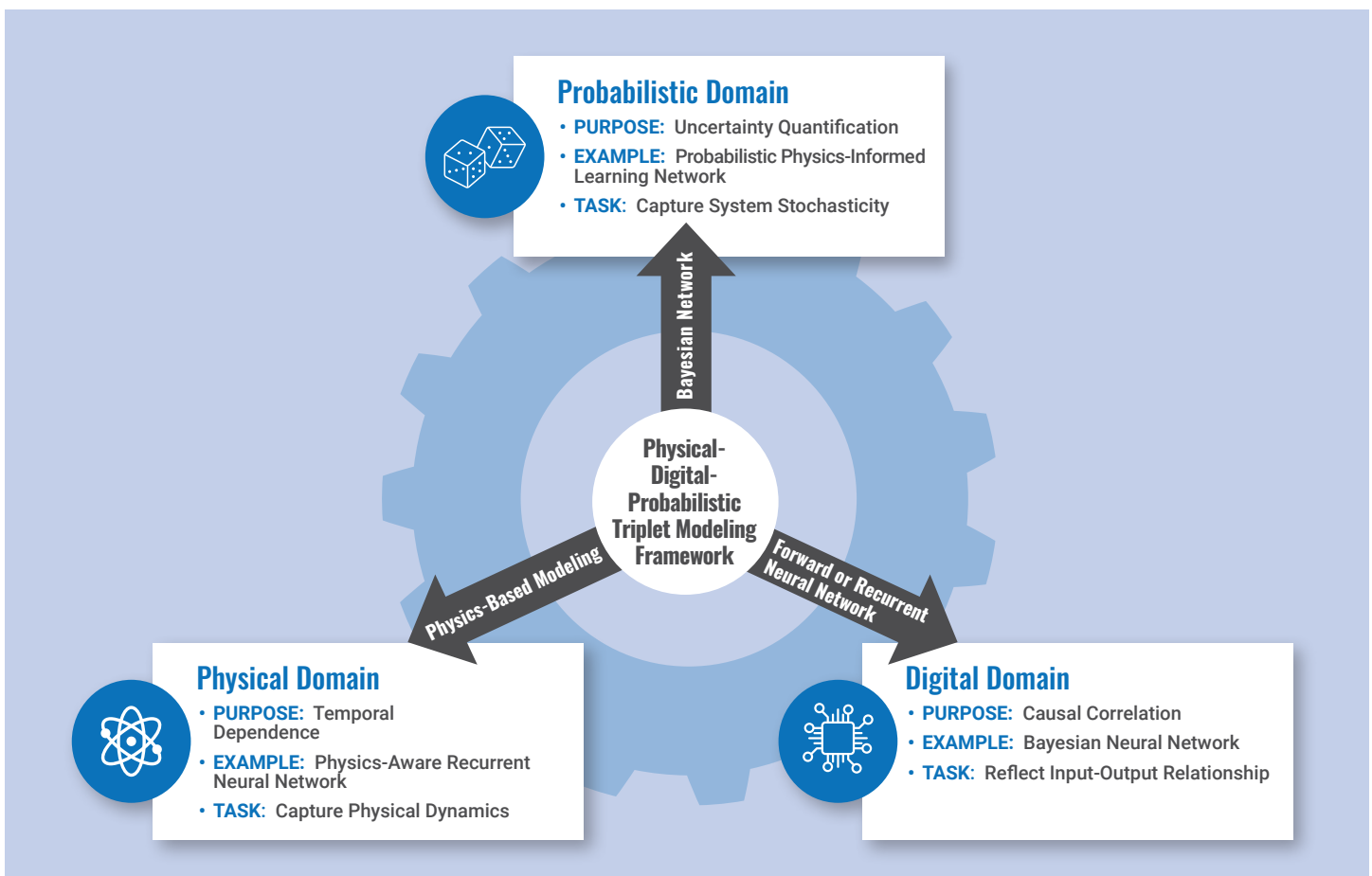


Figure 2. Three-Pronged Approach to the Physical-Digital-Probabilistic Triplet Modeling Framework for Industrial Processes and Dynamic Systems (Source: Z. Jiang, S. C. Miller, and D. Dunn).



The unique solution recently developed at UDRI is a unified, data-driven, predictive modeling and control method for energy systems.

digital-probabilistic triplet modeling framework for industrial processes and dynamic systems. This learning capability can thus be leveraged to enhance predictive analytics and optimal control strategies in planning, operating, and maintaining autonomous energy systems. Generally, application scenarios of this capability may include (1) predicting renewable power generation, load profiles, and cost/price trends; (2) dynamic model learning and calibrating the energy system; (3) quantifying uncertainty in stochastic energy production/consumption for asset planning or scheduling; and (4) real-time optimizing autonomous energy system operations for improved energy efficiency, quality, and resiliency.

The effort in the NAVFAC EXWC-UDRI partnership includes designing, developing, testing, and evaluating a suite of data-driven, ML-based models for energy prediction and an open-architecture, ML-enabled predictive control system. The outcomes from this work can be used to predict

and optimize energy production/consumption in microgrids or facility energy systems in real-time. Such energy systems may typically contain distributed or renewable generation (e.g., solar or wind power), energy storage (e.g., batteries), and controllable load. Key capabilities developed in this effort include the following, as also illustrated in Figure 1:

- Data-driven, ML-based modeling ability for energy systems with varying temporal, probabilistic, and categorical characteristics.
- Real-time energy prediction capability considering time-domain dynamics, uncertainty quantification, and causal relationships.
- Real-time operation optimization functionality.
- Real-time hardware-in-the-loop (HIL) simulation with hybrid physics/learning-based models.

The capabilities developed in this effort can be leveraged to apply the digital engineering and model-based systems engineering approaches to other technology projects that involve complex systems of systems [19]. For instance, these technologies can be transitioned to the U.S. Navy's installation energy infrastructure (such as naval base facilities and microgrids), shipboard power systems, naval aviation operational energy systems, naval logistics, and/or naval enterprise systems. Further, as options for future

development and applications, those developed ML methods can be used in multiple stages of modeling and real-time HIL simulation to achieve the following:

- Learn and validate a compact representation (e.g., a recurrent neural network-based model) of complex components or systems from offline operational data.
- Update and calibrate the model with online operational data (i.e., online learning capability).
- Learn the uncertainty in the model parameters/dynamics and consider the probabilistic variations and contingencies in the prediction.
- Accelerate the real-time simulation and HIL testing with compact learning-based models (rather than complicated, compute-intensive, physics-based models) for some components.

ML-ENABLED ENERGY OPTIMIZER

The effort performed by UDRI for a NAVFAC research, development, test, and evaluation contract laid out a foundation for system design, hardware prototype, software architecture, algorithms for model learning and predictive optimization, and HIL simulation models, as highlighted in Figure 1. The energy optimizer's "learning from operational

data” capability and look-ahead prediction mechanisms, designed for considering opportunistic optimization options to reduce costs, are what make it innovative. This solution also improves data security and privacy by aggregating and embedding actionable intelligence about operation data into the learned models and only communicating the model structures and parameters over the network to a microgrid controller.

The control system, based on ML and model predictive control (MPC), can dynamically integrate appropriate asset models (including generators and loads) into a real-time energy optimizer and generate optimized

control actions for each individual asset, as shown in Figure 3. This system consists of three closed loops for model calibration, equipment-level power optimization, and system-level energy optimization. The controller is scalable and adaptive, building on open-architecture communication, and can be implemented on real-time processors and field programmable gate arrays [20]. The proposed solution considers different asset configurations and types and uses real-time operational data to learn and model various energy phenomena. More importantly, these models will be used in a real-time, learning-enabled energy optimizer (through a model predictive control method) and

incorporated into the online operation to optimize the configurations and operational settings. To achieve this, the control system has multiple novel components connected in closed loops: (1) a learning-based modeling engine coupled with (2) a real-time predictor with scenario analysis for model calibration and (3) a real-time two-layer model predictive controller for optimization. It takes model data (e.g., model structure/parameters) as input and generates optimal control actions or setpoints for multiple generators or loads as output.

The control system has a hierarchical MPC structure (the outer two loops), with a higher-level MPC generating

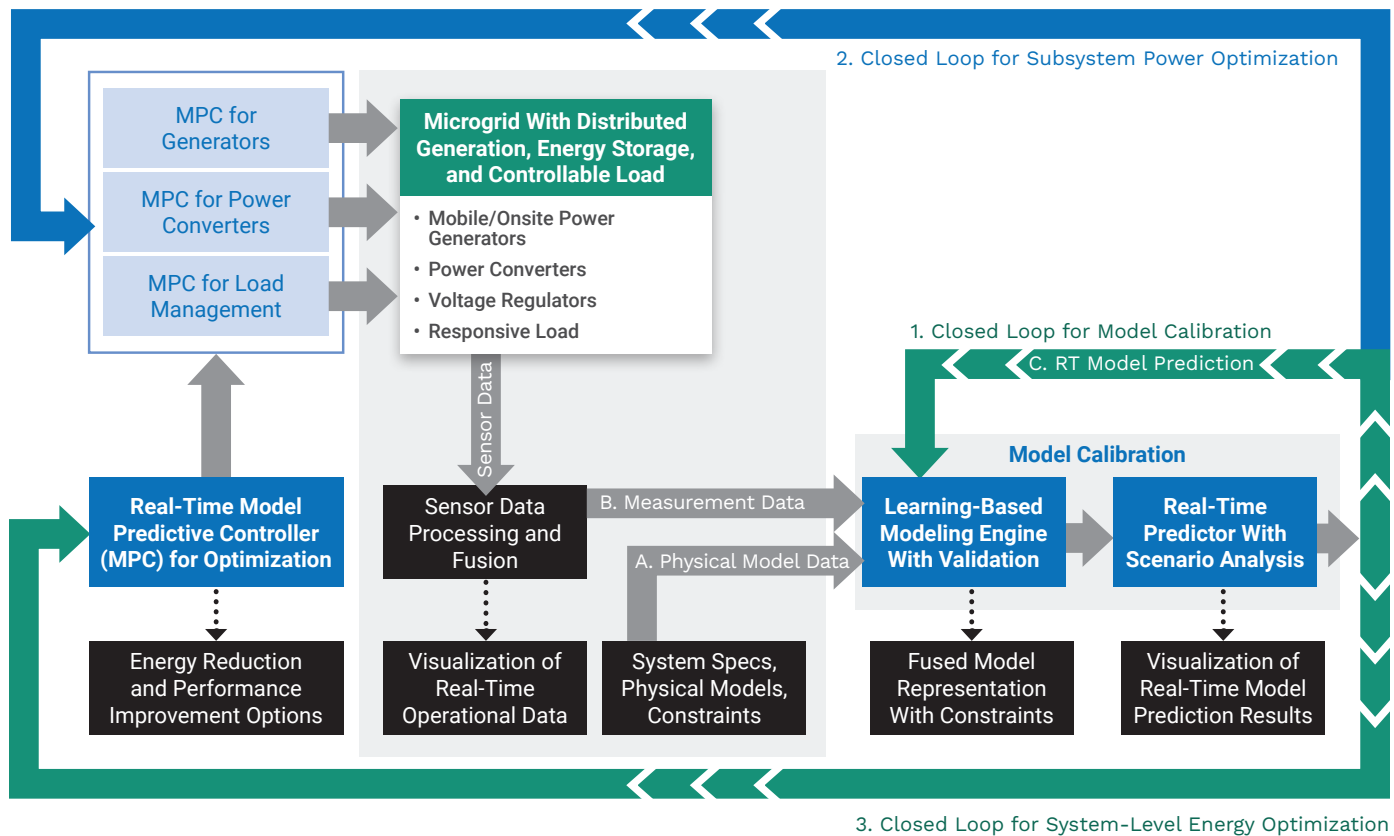


Figure 3. Block Diagram of the Learning-Driven MPC System (Source: Z. Jiang, S. C. Miller, and D. Dunn).

commands for multiple assets and a lower-level MPC managing each individual resource. The multilayer framework can decompose the control of the entire power system into layers or pieces of control territories that can be easily and efficiently managed and coordinated. In this control framework, the higher-level MPC optimizes the energy losses and costs subject to dynamic load profiles and also maintains a dynamic level of reserved energy in storage to meet future power changes. The lower-level MPC optimizes power management, i.e., regulating the currents while controlling the bus voltage. This way, the power generators are not necessarily configured to meet peak power demand but just average demand.

For example, an initial configuration of a small-scale microgrid

might consist of a fuel-based, distributed generation system (e.g., diesel engine or gas turbine-driven generator), a battery energy storage system, renewable power sources (e.g., a solar generation farm), and controllable load banks. These assets can connect with the utility grid and operate subject to time-of-use pricing signals. The solar power generation may be operating at a maximum power point tracking mode, where the output power varies and depends upon the solar irradiance. The generation costs (or energy conversion efficiency) of the fuel-fired generator may change with its output power. The energy storage system can be charged and discharged with constraints, and power losses may vary at different rates. The energy losses in both the power generation and storage processes can be learned from historical and real-time operational data through ML approaches. The load can be categorized into critical load and

noncritical load, the latter of which can be temporarily reduced or turned off.

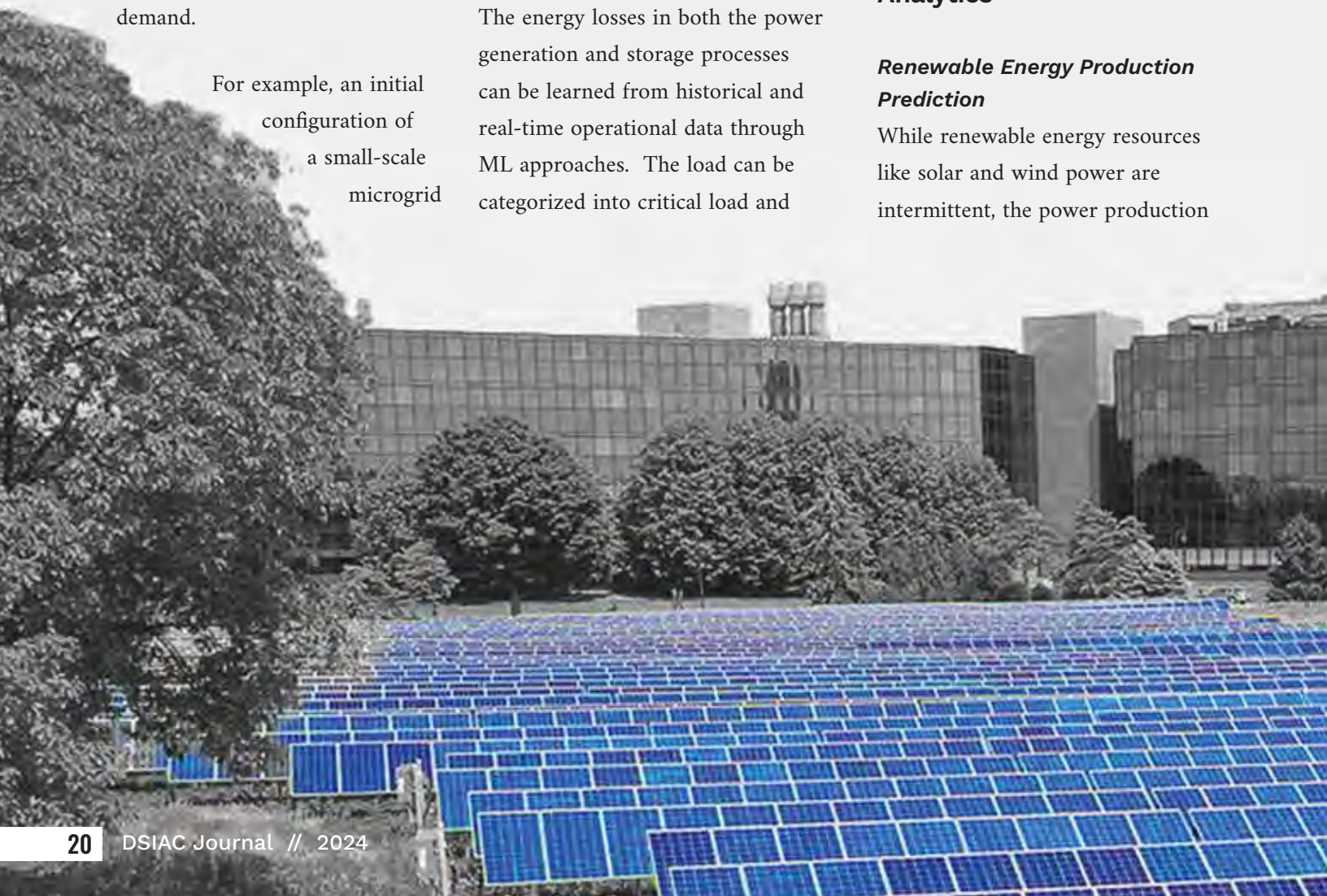
APPLICATIONS OF ML METHODS

The ML methods can be widely used in a model-based, systems-engineering approach. These powerful enabling techniques can serve as a driving force for the general trend of the latest digital engineering transformation [19] and require the digital interconnectedness of tools, models, and data necessary for mission success. Several examples are outlined next.

Utility Planning – Predictive Analytics

Renewable Energy Production Prediction

While renewable energy resources like solar and wind power are intermittent, the power production



from these assets correlates with the physical dynamics of solar or wind resources. By leveraging the historical weather data or measurement data, it is possible to generate more insight about the varying trends in energy production [10]. Sample results are shown in Figure 4. This prediction can be helpful in the utility's planning and scheduling tasks.

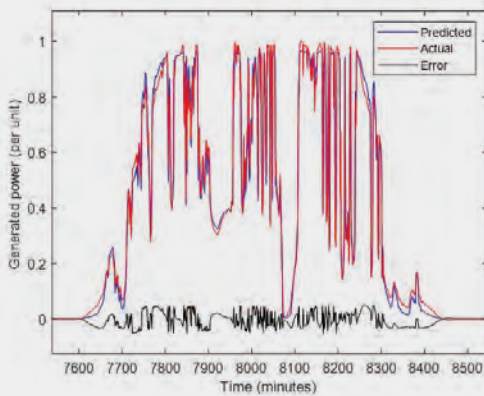


Figure 4. (Top) Results From the ML-Based Model for Solar Power Production Prediction [10] and (Bottom Main Image) Solar Power Installation on UDRI Campus (Source: University of Dayton).

Load Profile Forecasting

Public utilities typically give highest priority to load centers such as military bases. Load profile prediction is important for energy resource scheduling and planning. Load profiles can be predicted from historical data and operational conditions [21]. One application for load profile prediction is smart load shedding. During grid outage/microgrid isolation events, ML methods could be used to predict future circuit loads and then used for shedding loads from a prioritized list of circuits. A recent NAVFAC EXWC project involves testing and evaluating smart load shedding.

Energy Efficiency Prediction

ML can play an effective role in learning and predicting the fuel consumption of distributed generators or energy efficiency in data centers [22]. It is also important to apply ML-driven control for energy efficiency

improvement in electronics; computing; data centers; lighting; heating, venting, and air conditioning; etc.

Facility Management

Energy Management for Buildings or Vehicles

The functions of renewable energy production prediction, load profile forecasting, and energy efficiency prediction also apply to energy management for naval facilities and buildings and various vehicles such as hybrid trucks [23, 24]. The anticipated benefits can be leveraged to produce a reusable, adaptive, real-time energy system optimizer for Navy use that can address the issues of increasing power/energy needs and truly enable energy savings while not sacrificing performance or mission capabilities.

Digital Twin for Test Facilities

The developed capabilities, including



the digital engineering tools and model-based systems engineering approaches, can be extended to develop digital twins for naval test facilities [25, 26]. A current EXWC Digital Twin project involves the use of grid-forming inverters with AI computer technology to establish a well-defined and accurate Digital Twin energy system to manage the energy resources.

Predictive Maintenance

Similar techniques can be developed and leveraged to perform predictive maintenance, even considering the operational conditions and life-cycle use of the equipment and resources

[27, 28]. The proposed control platform, which is modular and reconfigurable, will greatly reduce installation and maintenance costs and provide expeditionary power when speed, range, agility, and flexibility are critical to mission success.

Microgrid Applications

Military Microgrids

Although a simple microgrid power system was modeled and tested in an HIL environment during a recent NAVFAC effort, the general approach applies to a wide range of military microgrid systems, such as based-wide microgrids [29, 30], expeditionary

microgrids, or mobile microgrids [5], as shown in Figure 5.

Microgrid Test Bed

The techniques developed for microgrids can be easily transitioned to a microgrid test bed to facilitate testing activities, particularly with digital engineering tools and a model-based systems engineering approach [31].

Shipboard Power Systems

The developed technologies can be widely applied in shipboard power systems, especially those onboard electrified warships, due to their versatile energy flows and flexible

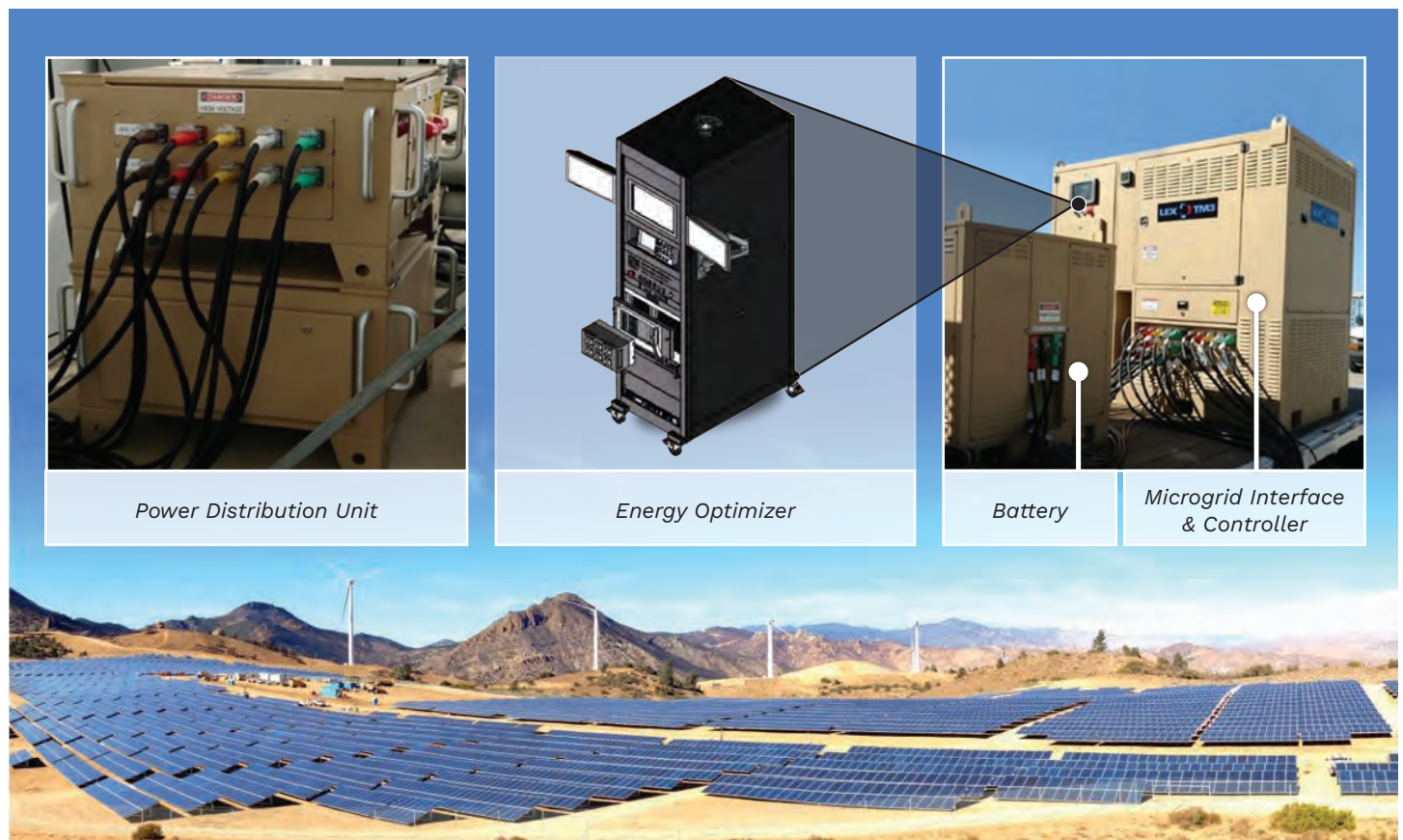


Figure 5. A Typical Application Scenario of an ML-Driven Energy Optimizer on a Military Base (Source: NAVFAC EXWC).

control opportunities. These systems may involve complex energy components, such as prime movers, generators, energy storage, distribution circuits, and sophisticated loads like high-power radar or directed energy, with operational constraints. Optimized operation of propulsion/power systems will reduce the system weight/size and improve the fuel consumption and operation costs of the military systems where power is used [32–34]. AI-driven digital engineering methods and tools can help reduce the development, acquisition, sustainment, or total ownership costs of fielded systems.

Naval Aviation Operational Energy

The Naval Aviation Operational Energy system, where safety, weight, size, maneuverability, and agility are high-priority features, can also benefit from the learning-enabled, model-predictive control scheme. The desired advantages may include



Optimized operation of propulsion/power systems will reduce the system weight/size and improve the fuel consumption and operation costs of the military systems where power is used.

predictive optimization in real-time, proactive actions prior to operational changes, and meeting economic, operational, or safety constraints in such systems. The total operation costs can be considerably reduced by optimal dynamic energy reserve, decreasing energy losses, optimizing mission profiles, and benefiting from automated operation [35, 36].

ANTICIPATED BENEFITS/RECOMMENDATIONS FOR FUTURE DEVELOPMENT

Previous efforts have laid out a systemic framework for energy modeling and developed a suite of ML-driven models and methods for energy prediction and control. The developed solution can significantly improve military capabilities due to enhanced power and energy performances enabled by AI technologies, even based upon existing commercial off-the-shelf power and energy sources only. This solution will have great impact on U.S. Department of Defense (DoD) capabilities because it (1) captures the energy system dynamics, degradation, and uncertainty into the model in a data-driven manner, which would be difficult to capture or otherwise unavailable in the energy system models; (2) provides mechanisms for online continuous model learning/validation; (3) enables fast (real-time) HIL simulation to gain insights into the system behaviors, greatly reducing

the design and development time/cost of military energy systems; and (4) empowers an integrated control platform to proactively manage the energy flows among the propulsion, power, and thermal subsystems to achieve higher efficiency and better performance and improve autonomy.

The anticipated advantages of these methods must be validated in realistic application systems and may include energy savings, cost savings, and power quality and resilience improvements [37, 38]. Future efforts are expected to demonstrate prototypes of an AI-driven predictive energy optimizer in improving energy resiliency on military installations and validate their advantages. Specifically, the anticipated objectives of future demonstration and validation efforts may include the following:

- Validate the effectiveness and accuracy of ML algorithms and models for forecasting generator fuel efficiency and load profiles based on operational data.
- Conduct power HIL testing of a prototype AI-driven, predictive optimizer to evaluate the effectiveness of learning-based prediction and model-based predictive optimization functionalities in a realistic microgrid.
- Perform field demonstration at a DoD installation site and validate the performance of the ML-driven

predictive optimizer prototype so the technology can be transitioned to the field faster.

As a recommendation for future development, ML can also be used in the test and evaluation stage to (1) screen and downselect test scenarios faster, (2) automatically analyze test data to determine correlations in system parameters or conditions, and (3) generate candidates of best design options. In addition, ML can be leveraged for diagnosis/prognosis and preventive maintenance. All these functions are closely related to digital engineering practice, with tangible benefits to the design, development, and testing of complex engineering systems.

CONCLUSIONS

The benefits and advantages of AI and ML can be expanded across the DoD's power and energy ecosystems. This article has briefly discussed several emerging applications of AI and ML technologies in naval energy autonomy and digital transformation. As these applications are widely transitioned and deployed, the potential impact on operational autonomy will be more clearly understood and realized. While digital engineering tools such as AI and ML techniques improve the effectiveness and resiliency of autonomous systems and workflow efficiency, their impact will be

multiplied and amplified when combined with other emerging digital technologies. These may include sensor fusion through universal learning, predictive analytics by deep-learning and data science methods, computational cognitive science, optimization techniques, quantum computing, and other technologies that can enable a deeper understanding of complex, integrated engineering system operations. ■

ACKNOWLEDGMENT

Funding provided by the NAVFAC EXWC is acknowledged.

REFERENCES

- [1] U.S. DON. "Department of the Navy Strategy for Renewable Energy." <https://www.secnav.navy.mil/eie/Documents/DoNStrategyforRenewableEnergy.pdf>, accessed on 15 May 2023.
- [2] NAVFAC P-602. "3 Pillars of Energy Security (Reliability, Resiliency, & Efficiency)." Washington, DC, June 2017.
- [3] U.S. DON. "Department of the Navy Climate Action 2030." <https://www.navy.mil/Portals/1/Documents/Department%20of%20the%20Navy%20Climate%20Action%202030%20220531.pdf>, accessed on 5 June 2023.
- [4] Stamp, J. "The SPIDERS project - Smart Power Infrastructure Demonstration for Energy Reliability and Security at US Military Facilities." 2012 IEEE PES Innovative Smart Grid Technologies, Washington, DC, 2012.
- [5] U.S. DoD. "DOD Demonstrates Mobile Microgrid Technology." <https://www.defense.gov/News/News-Stories/Article/Article/2677877/dod-demonstrates-mobile-microgrid-technology/>, accessed on 5 June 2023.
- [6] Shumway, R. H., and D. S. Stoffer. *Time Series Analysis and Its Applications*. Third edition, Springer: USA, 2011.

- [7] Karpatne, A., G. Atluri, J. Faghmous, M. Steinbach, A. Banerjee, A. Ganguly, S. Shekhar, N. Samatova, and V. Kumar. "Theory-Guided Data Science: A New Paradigm for Scientific Discovery from Data." In *IEEE Transactions on Knowledge and Data Engineering*, vol. 29, no. 10, pp. 2318–2331, 1 October 2017.
- [8] Jiang, Z., and J. Saurine. "Data-Driven, Physics-Guided Learning of Dynamic System Models." AIAA Science & Technology Forum, January 2023.
- [9] Jiang, Z., and K. Beigh. "Bayesian Learning of Dynamic Physical System Uncertainty." AIAA Aviation Symposium, June 2022.
- [10] Jiang, Z., and K. Beigh. "Data-Driven Modeling of Dynamic Systems Based on Online Learning." In AIAA Propulsion and Energy 2021 Forum, p. 3284, 2021.
- [11] LeCun, Y., Y. Bengio, and G. Hinton. "Deep Learning." *Nature*, vol. 521, pp. 436–444, <https://doi.org/10.1038/nature14539>, 2015.
- [12] Pan, J. "Machine Learning Proved Efficient." *Nature Computational Science*, vol. 2, p. 619, <https://doi.org/10.1038/s43588-022-00344-8>, 2022.
- [13] Caro, M., H. Huang, M. Cerezo, et al. "Generalization in Quantum Machine Learning From Few Training Data." *Nature Communications*, vol. 13, p. 4919, <https://doi.org/10.1038/s41467-022-32550-3>, 2022.
- [14] Rudin, C. "Stop Explaining Black Box Machine Learning Models for High Stakes Decisions and Use Interpretable Models Instead." *Nat. Mach. Intell.*, vol. 1, pp. 206–215, <https://doi.org/10.1038/s42256-019-0048-x>, 2019.
- [15] Takahashi, Y., M. Ueki, G. Tamiya, et al. "Machine Learning for Effectively Avoiding Overfitting Is a Crucial Strategy for the Genetic Prediction of Polygenic Psychiatric Phenotypes." *Transl. Psychiatry*, vol. 10, p. 294, <https://doi.org/10.1038/s41398-020-00957-5>, 2020.
- [16] Ghahramani Z. "Probabilistic Machine Learning and Artificial Intelligence." *Nature*, vol. 521, no. 7553, pp. 452–459, doi: 10.1038/nature14541, 28 May 2015.
- [17] Schramowski, P., W. Stammer, S. Teso, et al. "Making Deep Neural Networks Right for the Right Scientific Reasons by Interacting With Their Explanations." *Nat. Mach. Intell.*, vol. 2, pp. 476–486, <https://doi.org/10.1038/s42256-020-0212-3>, 2020.
- [18] Sebastian, A., A. Pannone, S. Subbulakshmi Radhakrishnan, et al. "Gaussian Synapses for Probabilistic Neural Networks." *Nat. Commun.*, vol. 10, p. 4199, <https://doi.org/10.1038/s41467-019-12035-6>, 2019.
- [19] U.S. Navy and Marine Corps. "United States Navy and Marine Corps Digital Systems Engineering Transformation Strategy." <https://nps.edu/documents/112507827/0/2020+Dist+A+DON+Digital+Sys>

+Eng+Transformation+Strategy+2+Jun+2020.pdf/, accessed on 15 May 2023.

[20] Jiang, Z., and A. Raziei. "Reconfigurable Hardware-Accelerated Model Predictive Controller." U.S. Patent 10,915,075, filed on 2 October 2017.

[21] Zhang, L., J. Wen, Y. Li, J. Chen, Y. Ye, Y. Fu, and W. Livingood. "A Review of Machine Learning in Building Load Prediction." *Applied Energy*, vol. 285, 1 March 2021.

[22] Haghshenas, K., A. Pahlevan, M. Zapater, S. Mohammadi, and D. Atienza. "MAGNETIC: Multi-Agent Machine Learning-Based Approach for Energy Efficient Dynamic Consolidation in Data Centers." In *IEEE Transactions on Services Computing*, vol. 15, no. 1, pp. 30–44, doi: 10.1109/TSC.2019.2919555, May 2019.

[23] Ngo, N. T., A. D. Pham, T. T. H. Truong, et al. "Developing a Hybrid Time-Series Artificial Intelligence Model to Forecast Energy Use in Buildings." *Sci. Rep.*, vol. 12, p. 15775, <https://doi.org/10.1038/s41598-022-19935-6>, 2022.

[24] Lee, W., H. Jeoung, D. Park, T. Kim, H. Lee, and N. Kim. "A Real-Time Intelligent Energy Management Strategy for Hybrid Electric Vehicles Using Reinforcement Learning." In *IEEE Access*, vol. 9, pp. 72759–72768, doi: 10.1109/ACCESS.2021.3079903, 2021.

[25] Lv, Z., Lv. Haibin, and M. Fridenfolk. "Digital Twins in the Marine Industry." *Electronics*, vol. 12, no. 9, <https://doi.org/10.3390/electronics12092025>, 2025.

[26] Sri Madusanka, N., Y. Fan, S. Yang, and X. Xiang. "Digital Twin in the Maritime Domain: A Review and Emerging Trends." *Journal of Marine Science and Engineering*, vol. 11, no. 5, p. 1021, 2023.

[27] RealClear Defense. "Navy to Deploy New Tech to Prevent Maintenance Problems." <https://www.nationaldefensemagazine.org/articles/2022/3/11/navy-to-deploy-new-tech-to-prevent-maintenance-problems>, accessed on 5 June 2023.

[28] Kimera, D., and F. Nduvu Nangolo. "Predictive Maintenance for Ballast Pumps on Ship Repair Yards via Machine Learning." *Transportation Engineering*, vol. 2, p. 100020, 2020.

[29] Association of Defense Communities. "NAVFAC EXWC Begins Testing Transportable Microgrid Project." <https://defensecommunities.org/2020/11/navfac-exwc-begins-testing-transportable-microgrid-project/>, accessed on 5 June 2023.

[30] Anderson, W., et al. "Growing Energy Resiliency Through Research." *Naval Science and Technology Future Force*, vol. 9, no. 1, p. 6, <https://www.nre.navy.mil/media/document/future-force-vol-9-no-1-2023>, accessed on 5 June 2023.

[31] U.S. DoD. "Department of Defense Annual Energy Management Report, Fiscal Year 2015." <https://www.acq.osd.mil/eie/downloads/ie/fy%20>

2015%20aemr.pdf, accessed on 5 June 2023.

[32] Jin, Z., L. Meng, J. M. Guerrero, and R. Han. "Hierarchical and Control Design for a Shipboard Power System With DC Distribution and Energy Storage Aboard Future More-Electric Ships." *IEEE Transactions on Industrial Informatics*, vol. 14, no. 2, pp. 709–720, 2018.

[33] Haseltalab, A., and R. R. Negenborn. "Model Predictive Maneuvering Control and Energy Management for All-Electric Autonomous Ships." *Applied Energy*, vol. 251, pp. 113308–113334, 2014.

[34] Islam, M. M. "Ship Smart System Design (S3D) and Digital Twin." In *VFD Challenges for Shipboard Electrical Power System Design*, IEEE, pp. 117–127, doi: 10.1002/9781119463474.ch9, 2019.

[35] U.S. Naval Aviation Enterprise. "Navy Aviation Vision 2030-2035." NAVY AVIATION VISION 2030-2035-FNL.PDF (defense.gov), accessed on 5 June 2023.

[36] Barnhill, D. "Analyzing U.S. Navy F/A-18 Fuel Consumption for Purposes of Energy Conservation." M.S. thesis, Naval Postgraduate School, <https://apps.dtic.mil/sti/trecms/pdf/AD1150419.pdf>, accessed on 5 June 2023.

[37] Li, P., D. Li, D. Vrabie, S. Benghea, and S. Mijanovic. "Experimental Demonstration of Model Predictive Control in a Medium-Sized Commercial Building." The 3rd International High Performance Buildings Conference at Purdue, 14–17 July 2014, <https://docs.lib.purdue.edu/cgi/viewcontent.cgi?article=1152&context=ihpbc>, accessed on 5 June 2023.

[38] Piette, M. A. "Hierarchical Occupancy Responsive Model Predictive Control at Room, Building, and Campus Levels." DOE/EERE 2017 Building Technologies Office Peer Review, Lawrence Berkeley National Lab, https://www.energy.gov/sites/prod/files/2017/04/f34/3_94150b_Piette_031517-1200.pdf, accessed on 5 June 2023.



BIOGRAPHIES

ZHENHUA JIANG is a principal research engineer at UDRI. His research interests include machine learning, autonomy, predictive analytics and control, microgrids, probabilistic modeling, and quantum computing. He has developed a data-driven physics-guided Bayesian neural learning method that is well suited to modeling, controlling, and optimizing various energy systems, autonomous air/space/ground/underwater vehicles, and quantum systems. He has over 100 publications and several patents on subjects such as distribution automation, model predictive control, probabilistic decision engines, and quantum probabilistic solvers. Dr. Jiang holds a Ph.D. in electrical engineering from the University of South Carolina.

SCOTT C. MILLER is an electrical engineer and project manager at the Energy Management Division of the NAVFAC Engineering and Expeditionary Warfare Center. His research, development, test, and evaluation interests include artificial intelligence and machine learning, data analytics and analysis, microgrids, utility and energy modeling, and cybersecurity communications. Mr. Miller holds an M.S. in electrical engineering from California State University, Northridge, California, and is a Professional Engineer (PE) of electrical engineering.

DAVID DUNN is the Power and Energy Division head at the University of Dayton Research Institute, where he oversees hundreds of power generation, storage, and use research projects for customers across the DoD, Department of Energy, and the National Aeronautics and Space Administration as well as commercial partners looking to improve their product efficiencies and innovation. He is a retired U.S. Air Force (USAF) officer and USAF Test Pilot School graduate. Mr. Dunn holds an M.S. in electrical engineering from the Air Force Institute of Technology and a B.S. in electrical engineering from the U.S. Air Force Academy.



ATMOSPHERIC CORROSION SEVERITY

AND THE ROLE OF THE ENVIRONMENT:
DETERMINING A DIRECT CORRELATION

BY DOUGLAS C. HANSEN, CHRISTINE E. SANDERS, RONALD A. ZESZUT,
RAYMOND J. SANTUCCI, AND MATTHEW J. ROTHGEB (PHOTO SOURCE: CANVA)

INTRODUCTION

Corrosion costs the U.S. Department of Defense (DoD) billions of dollars annually and heavily impacts the availability of DoD assets to carry out their missions [1]. The U.S. Navy is the hardest hit branch of the DoD, as it operates in the harshest environments with its assets exposed to seawater for extensive time. In the 2021 “DoD Corrosion Prevention and Control Strategy” [2], corrosion maintenance and repair were estimated to cost the Navy \$7 billion annually and led to 11 million hours of maintainer repair time and lost flight time (as exemplified in Figure 1a). In the time it took to read the previous sentence, corrosion cost the Navy \$2,219.68. Not only are ships and submarines constantly in direct contact with seawater, but Naval aircraft also operate primarily in the marine boundary layer containing high levels of aerosolized salts. These sea salt aerosols contribute to aircraft corrosion while on a ship’s flight deck, during normal flight operations, and at land-based Navy installations. Naval Air bases are typically near seawater but can vary from a few miles up to hundreds of miles. Sea-spray aerosols can remain in the air for at least 25 km, contributing heavily to the amount of corrosion observed near coastal areas [3].

Recently, there have been discussions about moving from a fixed maintenance schedule to one driven

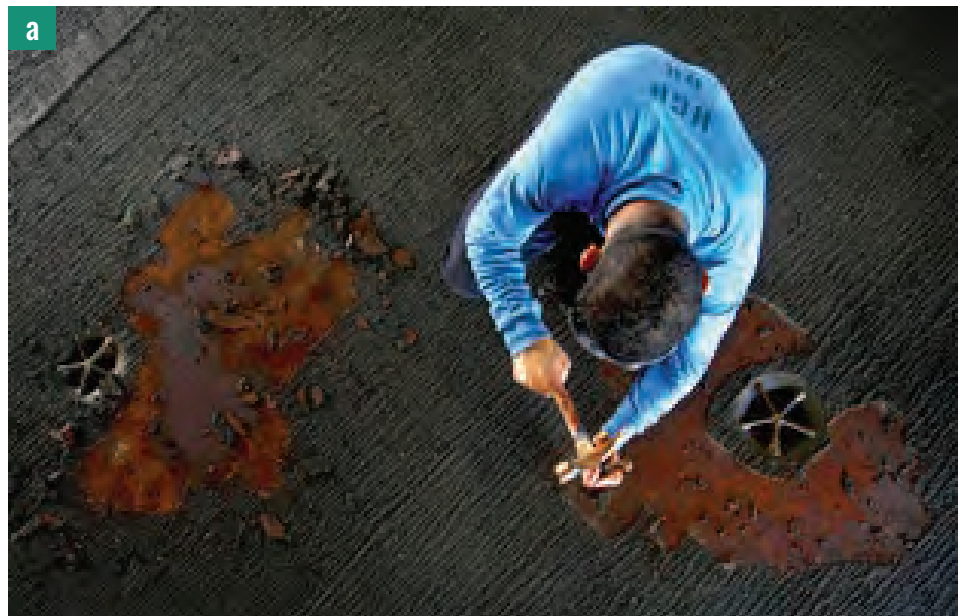


Figure 1. (a) Corrective Maintenance of Nonskid Coating on a Ship Deck (Source: U.S. DoD) and (b) Preventative Maintenance via Aircraft Rinsing (Source: U.S. Air Force).

by condition-based maintenance (CBM or CBM+). Under this new paradigm, assets would be inspected, washed, and serviced based on the actual condition. Specifically, this type of maintenance strategy would alter wash frequencies of aircraft to higher or lower frequencies, depending on the corrosion risk at the operational site (Figure 1b). One of the simplest

ways to do this is to differentiate sites by their proximity to a saltwater source. However, this may not always be the best practice. Ongoing work by DoD partners is examining this assumption by categorizing corrosion risk on a smaller scale and at individual locations rather than only using a map. The local environment plays a large role in salt deposition,

from wind direction and intensity to local vegetation, and moving just half a mile away can sometimes reduce the corrosion risk by an order of magnitude. It is imperative that these local impacts are considered when categorizing a site and determining maintenance intervals.

CORROSION SEVERITY IN THE ENVIRONMENT

Corrosion processes are affected by environmental conditions, which can change the rate, chemistry, and morphology of the corrosion attack [4, 5]. Many climate types have been categorized in corrosion literature—rural, suburban, urban, forest, highway, coastal/marine, industrial, alpine, tropical, volcanic, agricultural, and dry [6–8]. These sites are characterized by weather parameters and the chemistry of the atmosphere, which result in differences in corrosion across the different climate types, with marine and industrial sites often showing the highest levels of corrosion. Commonly measured weather parameters in corrosion studies include temperature, relative humidity, precipitation, solar radiation, and wind speed and direction. Because corrosion is an electrochemical process, a conductive moisture layer (very thin at times) is required on a metallic surface for corrosion reactions to occur, and the presence and characteristics of this layer are affected by these

meteorological factors [9]. Thus, environments that are very hot and dry (which prevent the formation of these moisture layers on samples) tend to show low corrosion rates [4, 5].

The atmospheric chemistry also plays a role in the corrosion processes. One of the most important environmental species is chloride ion, which is a major driver of the high corrosivity seen in many coastal and marine environments [7]. Other industrial pollutants such as sulfur and nitrogen oxide species and the ozone have also been shown to accelerate corrosion [10]. The proximity to the source of these corrosion-accelerating compounds will determine their concentration and effect at any given site. Other parameters like wind strength and direction, surrounding vegetation, and other structures will also play a role.

An interesting example of the effect of climate on corrosion processes is a study that was done in Hawaii [3, 8]. Across the main Hawaiian island and the island of Oahu, eight different corrosion test sites were chosen to characterize the corrosion severity of the seven climatological environments across the state—marine, industrial, tropical, volcanic, alpine, agricultural, and dry. A wide range of environmental conditions (temperature, humidity, rainfall, solar radiation, chloride ion deposition rates, and other environmental chemistry factors) was observed across the test



One of the most important environmental species is chloride ion, which is a major driver of the high corrosivity seen in many coastal and marine environments.

sites. These environmental differences resulted in corrosion rates that varied by up to a factor of 40.

ACCELERATED CORROSION TESTING AND MODELING

Although there are American Society for Testing and Materials (ASTM) test methods for exposing bare and coated metals in a controlled, corrosive environment to determine relative corrosion resistance and coating behavior, the prediction and correlation of corrosion performance of “accelerated exposure tests” in environmental chambers like salt spray (B117) to field environments are not always straightforward [11]. Existing test methods do not address the simultaneous exposure of various atmospheric and environmental conditions that can affect corrosion performance of a bare or coated metal. They also do not address the need to correlate results of exposure chamber tests with exposure to outdoor atmospheres and end-user

performance. Many investigations have been performed in recent years to clarify the role of environmental and climatic factors in the atmospheric corrosion of commonly used structural metals and coatings as well as simulate their observed corrosion behavior in the laboratory [12–16]. It is well documented that corrosion behavior of metal substrates in accelerated laboratory tests does not correlate with the observed performance in an outdoor exposure environment [17–19].

The first step toward developing better accelerated test methods is to analyze and accurately reproduce these environments in a laboratory setting. A successful, accelerated test method would therefore be environmentally “tunable” and provide accurate, predictable results for any substrate with any type of protective barrier layer or coating present. To achieve this goal, a new state-of-the-art accelerated combined effects simulation (ACES) exposure chamber is currently undergoing testing by the U.S. Air Force (USAF) Research Laboratory in collaboration with the U.S. Naval Research Laboratory (NRL) to replicate field conditions and corrosion behavior of various alloys, coating systems, and corrosion/environmental sensors. This chamber was built to include more environmental effects than any previous exposure chamber to accurately mimic a field environment that includes temperature and humidity control, ultraviolet (UV),

mixed gasses, and actuators to simulate mechanical stresses.

BACKGROUND OF ENVIRONMENTAL SEVERITY INDICES

Early attempts to correlate the environment with corrosion of DoD assets goes as far back as the 1960s under the U.S. Air Force Logistics Command, where the focus was to develop a corrosion severity classification for each operational airbase as part of the Corrosion Prevention and Control program (redesignated as Project RIVET BRIGHT in 1971) [20]. The program was redesignated as PACER LIME in 1972 and was a two-phase effort—develop a mathematical algorithm to calculate a corrosion factor that combined weather and other environmental factors and measure corrosion severity at selected locations through atmospheric tests, allowing for the calibration of the corrosion factor calculated from the algorithm.

“

Early attempts to correlate the environment with corrosion of DoD assets goes as far back as the 1960s under the U.S. Air Force Logistics Command.

This corrosion factor had a range of values: 1.00–2.00 (severe), 2.01–2.85 (moderate), and 2.85–3.75 (mild). As a result of that study, a system was developed for rating the corrosivity of aircraft operational environments, considering environmental variables such as weather, atmospheric pollutants, and geographical factors by Summitt and Fink [20]. The purpose was to compute a corrosion severity index for three aspects of corrosion maintenance—aircraft washing, repainting, and maintenance repairs. These indices were derived from the corrosion factor ranges and were thus labeled as mild, moderate, and severe. The corrosion severity index for each airbase location was then used to schedule the frequency of aircraft wash cycles. It was reported that the computed severity ratings agreed with aircraft maintainers’ experience and atmospheric testing programs at several DoD locations. These indices were incorporated into Technical Order (TO) 1-1-691 in 1996 [21].

Meanwhile, the Naval Air Systems Command (NAVAIR) 01-1A-509 [22] and 16-1-540 [23] Technical Manuals (TMs) were combined in 2005 into NAVAIR TMs 01-1A-509 Volumes I (Corrosion Program and Corrosion Theory) [24], Volume II (Aircraft) [25], and Volume III (Avionics and Electronics) [26], which superseded NAVAIR TO 1-1-689 [27] from 2000.

In 2008, Battelle Columbus published “A Decade of Corrosion Monitoring

in the World's Military Operating Environments: A Summary of Results" [28]. It describes an effort (1998–2008) to quantify and refine categories in the USAF TO 1-1-691 [21] in 2009 for aircraft wash cycles and maintenance actions. This attempt was based upon Battelle's program of placing "corrosion monitoring packages" consisting of well-defined corrosion cards containing bare metal coupons (i.e., similar sized, cleaned, and initial mass values recorded) at military bases worldwide for predetermined periods. Upon return from the field, the coupons were cleaned and the resulting mass loss per unit area for each coupon was measured and recorded, thus yielding a corrosion rate for the exposure period at a particular site.

One of the results of this study was an algorithm for corrosion prediction based upon the corrosion card mass loss and silver chloride film measurements, which only considered environments at greater than 70% relative humidity (RH), excluding the effect of temperature and sulfur dioxide in the statistical analysis [28]. The resulting Environmental Severity Index (ESI) classifications were based upon the corrosion rate of AA2024-T3 aluminum and also described as mild, moderate, or severe. International Organization for Standardization (ISO) Standard 9223:2012(E) [29] lists six different corrosivity categories (low to extreme) and uses the percentage exposure time above 80% RH. Overall,

more than 40 years of modeling attempts have been made to predict the rate of atmospheric corrosion and/or severity for a given metal substrate [30]. While numerous models have been developed, they all require inputs of environmental data as well as corrosion mass change data; obviously, a model is only as good as the data used for its calibration and development. It is apparent that very few, if any, of the models developed were ever independently validated [30].

RECENT NAVY EFFORTS

Strategic Environmental Research and Development Program – Environmental Security Technology Certification Program (SERDP-ESTCP) Projects

Current work funded by SERDP-ESTCP is examining the link between corrosion risk and environmental implications. The environmental and mechanical loading conditions govern the overall lifetime survivability and maintenance cycles of protective coatings. A model that can better predict maintenance based on accumulated damage will enable maintenance cycles to be performed only when necessary, as opposed to overly conservative, periodic time-based maintenance intervals based on worst-case scenarios. Using a CBM+ approach reduces the exposure of both personnel and the environment

to hazardous paint strippers and hexavalent chromium used in many primers. By evaluating each asset based on service history and expected future exposure, maintenance will be done when required based on usage/exposure history. To achieve the desired state, better modeling of coating and material lifetime performance need to be developed.

Furthermore, a combined model of real-world fatigue and corrosion damage for DoD assets does not exist. By generating data that simulates a real-world environment and inputting this information into a predictive model, better decisions can be made to the service intervals and reducing the number of man-hours spent on systems with potentially hazardous materials to refurbish the asset. The objective of this project is to generate a Bayesian network model to predict coating and lifetime performance based on a CBM+ approach. The resulting model could be used to



Using a CBM+ approach reduces the exposure of both personnel and the environment to hazardous paint strippers and hexavalent chromium used in many primers.

better inform life-cycle maintenance costs and adjust the schedules for planned maintenance. Successful implementation will reduce inspection costs and unnecessary repainting and better prioritize key asset maintenance. Model inputs should reflect what the real-world experience of the asset is in terms of environment, loading, and maintenance. Figure 2 shows what some of the considerations are for studying DoD aircraft (Figure 2a). Tailored for tackling DoD needs, the NRL-Key West facility implements rinsing and covering modifications (Figure 2b) to mimic what aircraft

experience. Fasteners (Figure 2c) are places where protective coatings are often breached and material incompatibility leads to corrosive attack, so modeling efforts are concentrated at these hot spots. Dynamic loading of simulated aircraft structures (panels, fasteners, coatings, etc.) in outdoor environments provides a higher level of testing fidelity (Figure 2d).

Field Exposure Testing

Current efforts to improve ESI research and development include standardizing how ESI work is

conducted. The Association for Materials Protection and Performance (AMPP) SC-07 Ad Hoc Group is developing a standard titled “Environmental Spectra for Severity Classification,” which brings together the atmospheric corrosion community to codify best practices and state-of-the-art understanding of the current problem. Three focus areas include sample design (what samples will be exposed and how), data acquisition (how data are collected), and data analysis (how data are interpreted and what the significance is for ESI). Critically, this standard will

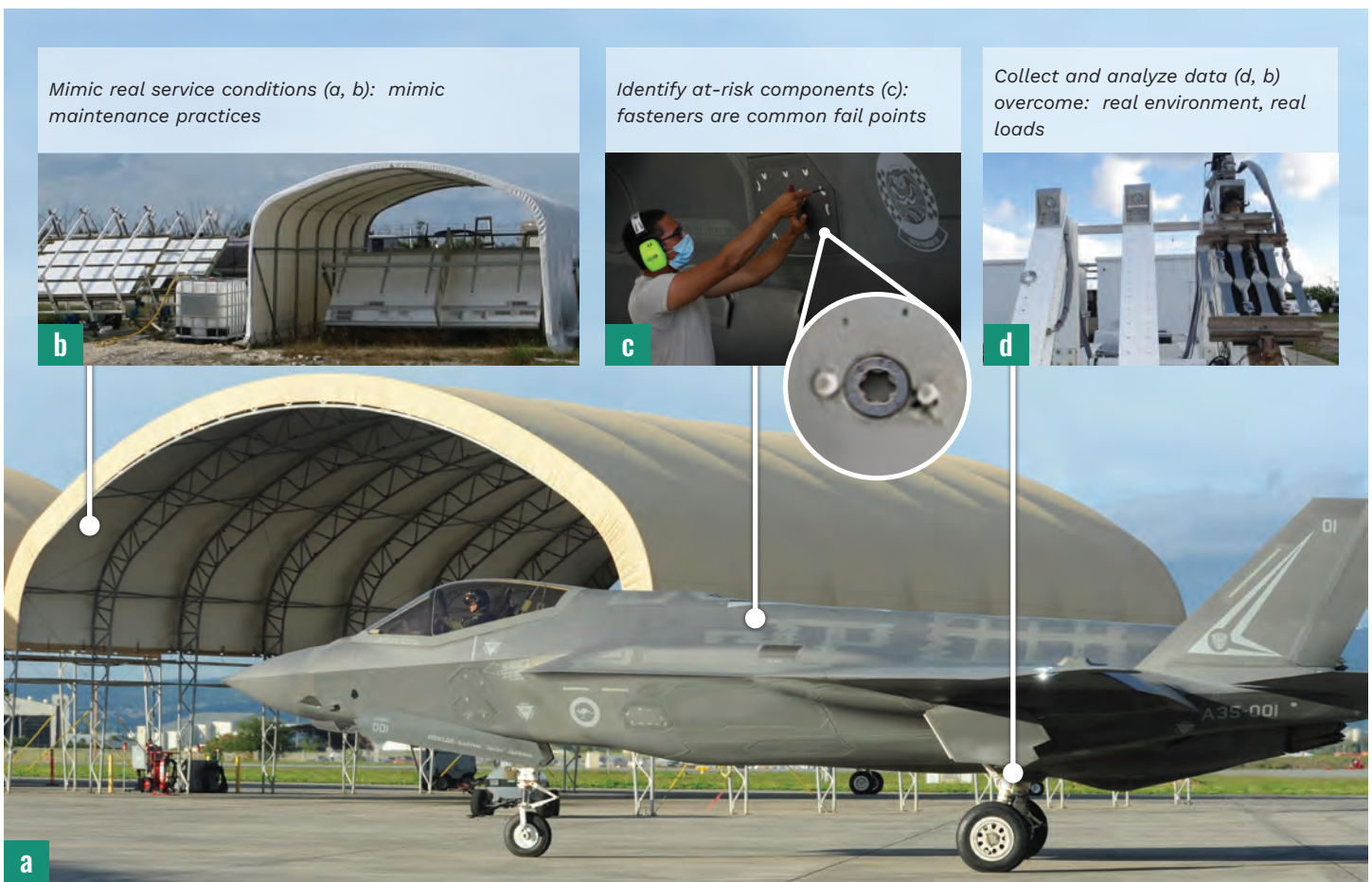


Figure 2. One Strategic Outlook on How the DoD Invests Research Into Atmospheric Corrosion to Counteract Its Effect on Mission Readiness (Sources for a and c Are U.S. Air Force; b and d Are S. Stanke, Excet).

consolidate a common vocabulary across the field, allow data sharing and encourage collaborations, enable a data network for long-term and large-area assessments, increase measurement accuracy and precision, and provide well-defined inputs for modeling efforts. Examples of what this standard addresses based on currently agreed-upon best practices include sample size and classification, data acquisition through coulometric reduction and surface profilometry, and core environmental variables to collect during exposure. The samples on the rack in Figure 3 show sample size and classification, and the large vertical box behind the rack collects the core environmental variables.

Corrosion Modeling

Several DoD-funded corrosion modeling efforts are currently underway that involve various forms of data collected from different locations. Atmospheric corrosion proceeds via several processes in sequence and/or parallel across multiple classes of matter—the atmosphere, condensed aqueous solution, polymer coatings, oxide scales, precipitated salts, and microstructurally heterogeneous metal alloys (see Figure 4). Multiple physical and chemical phenomena contribute to the corrosion process, including mass transport, electrochemical effects, metal dissolution, grain-boundary transport, etc. For this reason, using fundamental physics or chemical principles makes it difficult to directly predict the corrosion rate of a metal

“

Using fundamental physics or chemical principles makes it difficult to directly predict the corrosion rate of a metal in its environment.

in its environment. Likewise, it is difficult to directly extrapolate the results of short-term tests to long-term tests solely from physical principles. A data-driven modeling approach can assist in identifying the key environmental factors driving atmospheric corrosion.

One example is the use of machine learning (ML) and artificial neural network (ANN) modeling to identify leading meteorological factors that quantitatively control the extent of corrosion [24]. The systematic collection of atmospheric corrosion data has enabled the application of ML techniques to understand the most critical elements (Figure 4) impacting the differences in the amounts of corrosion observed in AA2024-T3 samples placed at three locations on the Florida coastline. The data were processed according to the three metrics of mass loss per unit area, linear corrosion rate, and a parabolic corrosion constant, as well as generating additional data by sample differencing that considers cumulative corrosion occurring between time periods. An



Figure 3. Instrumented Exposure Rack With Corrosion Test Coupons at NRL-Key West (Source: D. Hansen).

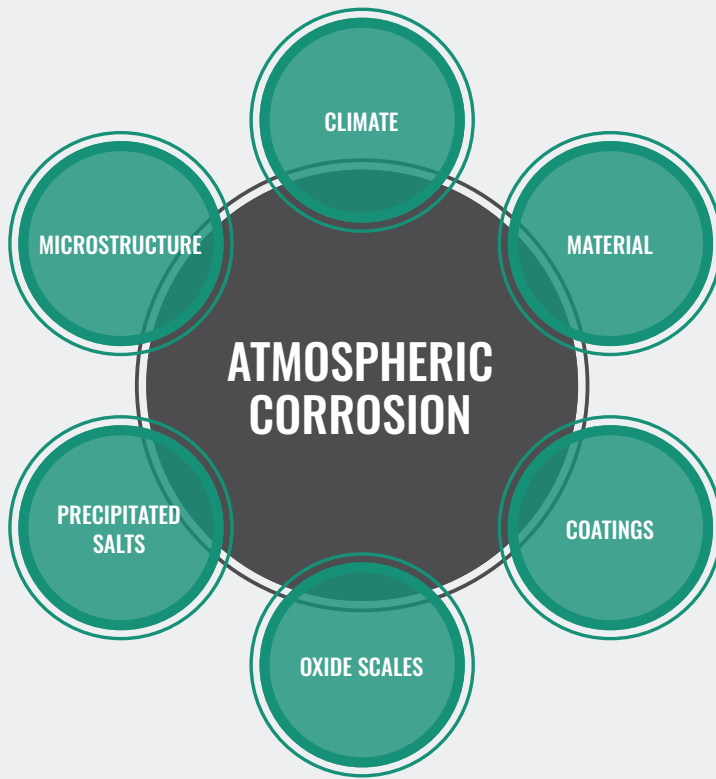


Figure 4. Components Needing Consideration in Modeling of Atmospheric Corrosion—Types of Material, Surface Types, Deposits, and Time-Dependent Processes [24].

automated approach was developed that can query public and/or pay-to-access websites for environmental data to construct an exposure profile for a sample placed at a known location (specified by latitude/longitude) and over a given range of dates. ML algorithms (feature selection and ANNs) were used to determine the most significant environmental features impacting the extent of atmospheric corrosion through sensitivity analysis. Five key variables were determined to have a quantitative effect on the corrosion rate and mass loss per unit area collected over 18 months of exposure—mean precipitation, the range of temperatures, the minimum

wind speed, the variability of ozone exposure, and the maximum solar irradiance [31]. This systematic approach could be applied to other materials of interest, different locations, and other metrics of corrosion (e.g., localized corrosion depth and pitting volume) to advance the understanding of how the environmental conditions can directly influence the corrosion behavior of materials.

CHALLENGES AHEAD

Transitioning from a schedule-based maintenance program to a condition-based maintenance program within

the DoD requires several issues to consider—how to categorize the corrosion severity occurring on the assets in the field and how to use the classifications to make informed decisions relating to weapon system maintenance, as well as DoD infrastructure (construction, storage, etc.). Another issue is how many classifications are appropriate. Are three categories enough (TO 1-1-691 as mild, moderate, or severe), six (ISO 9223 as C1-CX), or possibly 10? Studies have shown that it is possible to get significantly different levels of corrosion for different materials; so which should be used for the severity ranking? If the goal is to determine a corrosion severity for each DoD location, is it possible to rank a facility with more than one category, or do we use an average for multiple locations at the facility? Ultimately, can corrosion and environmental sensors reliably provide real-time information so that the corrosion severity of a location can be determined, allowing maintenance cycles to be adapted for season-season or year-year variability or even longer-term effects like climate change?

CONCLUSIONS

Collaborative efforts continue among the research arms of the Navy and Air Force to standardize the field exposure tests yielding data that will be used to categorize the corrosion severity rankings for DoD locations. In addition to field exposure testing,

a new state-of-the-art ACES exposure chamber is currently undergoing testing to replicate field conditions and corrosion behavior of various alloys, coating systems, and corrosion/environmental sensors. The combination of real-world corrosion data from depot and field exposure test sites, advanced modeling techniques utilizing artificial intelligence and ML, and cutting-edge exposure simulation chambers will ultimately provide a basis for a more accurate characterization of the corrosion severity for DoD locations around the world. Realization of a condition-based maintenance program across the services is not as far away as once thought. ■



REFERENCES

[1] Herzberg, E. F., T. K. Chan, S. Guo, A. K. Morris, A. Stevenson, and R. F. Stroh. "Estimated Impact of Corrosion on Cost and Availability of DoD Weapon Systems – FY18 Update." LMI, Tysons, VA, 2018.

[2] U.S. DoD. "DoD Corrosion Prevention and Control Strategy." Office of the Under Secretary of Defense for Acquisition and Sustainment, Washington, DC, 2021.

[3] de Leeum, G., F. P. Neele, M. H. Smith, and E. Vignati. "Production of Sea Spray Aerosol in the Surf Zone." *Journal of Geophysical Research*, vol. 105, no. D24, pp. 29397–29409, 2000.

[4] Yoon, Y., J. D. Angel, and D. C. Hansen. "Atmospheric Corrosion of Silver in Outdoor Environments and Modified Accelerated Corrosion Chambers." *Corrosion*, vol. 72, no. 11, pp. 1424–1432, 2016.

[5] Petry, L., and D. C. Hansen. "A Comparative Study of Two Coating Systems Exposed for Two Years in the Field and in Accelerated Atmospheric Corrosion Chamber Environments." *Corrosion*, vol. 72, no. 11, pp. 1385–1395, 2016.

[6] Oesch, S., and P. Heimgartner. "Environmental Effects on Metallic Materials – Results of an Outdoor Exposure Programme Running in Switzerland." *Materials and Corrosion*, vol. 47, pp. 425–438, 1996.

[7] Sun, S., Q. Zheng, D. Li, and J. Wen. "Long-Term Atmospheric Corrosion Behaviour of Aluminum Alloys 2024 and 7075 in Urban, Coastal, and Industrial Environments." *Corrosion Science*, vol. 51, pp. 719–727, 2009.

[8] Srinivasan, R., and L. H. Hihara. "Correlation Studies Between Outdoor Exposure and Accelerated Laboratory Corrosion Tests for Galvanic and Non-Galvanic Ceramic-Aluminum Couples." *ECS Transactions*, vol. 16, pp. 101–113, 2009.

[9] Saberi, L., and M. Amiri. "Modeling Atmospheric Corrosion Under Dynamic Thin Film Electrolyte." *Journal of The Electrochemical Society*, vol. 168, p. 081506, 2021.

[10] Oesch, S., and M. Faller. "Environmental Effects on Materials: The Effect of the Air Pollutants SO₂, NO₂, NO, and O₃ on the Corrosion of Copper, Zinc, and Aluminum. A Short Literature Survey and Results of Laboratory Exposures." *Corrosion Science*, vol. 39, no. 9, pp. 1505–1530, 1997.

[11] ASTM International. "B117 Standard Practice for Operating Salt Spray (Fog) Apparatus." West Conshohocken, PA, 2019.

[12] Chen, Z., D. Liang, G. Ma, G. Frankel, H. Allen, and R. Kelly. "Influence of UV Irradiation and Ozone on Atmospheric Corrosion of Bare Silver." *Corrosion Engineering Science and Technology*, vol. 45, pp. 2169–2180, 2010.

[13] Wan, Y., E. Macha, and R. Kelly. "Modification of ASTM B117 Salt Spray Corrosion Test and Its Correlation to Field Measurements of Silver Corrosion." *Corrosion*, vol. 68, no. 3, pp. 036001-1–036001-10, 2012.

[14] Feng, Z., G. Frankel, W. Abbott, and C. Matzdorf. "Galvanic Attack of Coated Al Alloy Panels in Laboratory and Field Exposure." *Corrosion*, vol. 72, no. 3, pp. 342–355, 2016.

[15] Tayler, M., M. Blanton, C. Konecki, J. Rawlins, and J. Scully. "Scribe Creep and Underpaint Corrosion on Ultra-High Molecular Weight Epoxy Resin Coated 1018 Steel Part 1." *Corrosion*, vol. 71, no. 1, pp. 71–91, 2015.

[16] Tayler, M., M. Blanton, C. Konecki, J. Rawlins, and J. Scully. "Scribe Creep and Underpaint Corrosion on Ultra-High Molecular Weight Epoxy Resin Coated 1018 Steel Part 2." *Corrosion*, vol. 71, no. 3, pp. 326–342, 2014.

[17] King, A., B. Kannan, and J. Scully. "Environmental Degradation of a Mg Rich Primer in Selected Field and Laboratory Environments: Part 1 – Without a Topcoat." *Corrosion*, vol. 70, no. 5, pp. 512–535, 2014.

[18] Liang, D., H. C. Allen, G. S. Frankel, Z. Y. Chen, R. G. Kelly, Y. Wu, and B. E. Wyslouzil. "Effects of Sodium Chloride Particles, Ozone, UV and Relative Humidity on Atmospheric Corrosion of Silver." *Journal of the Electrochemical Society*, vol. 157, no. 4, pp. C146–C156, 2010.

[19] Deflorian, F., S. Rossi, L. Fedrizzi, and C. Zanella. "Comparison of Organic Coating Accelerated Tests and Natural Weathering Considering Meteorological Data." *Progress in Organic Coatings*, vol. 59, no. 3, pp. 244–250, 2007.

[20] Summitt, R., and F. T. Fink. "AFWAL-TR-80-4102 PACER LIME: Part I – An Environmental Corrosion Severity Classification System." USAF, Dayton, OH, 1980.

[21] USAF TO 1-1-691. "Cleaning and Corrosion Prevention and Control, Aerospace and Non-Aerospace Equipment." Dayton, OH, 1996.

[22] NAVAIR TM 01-1A-509. "Avionics Cleaning and Corrosion Prevention/Control." Patuxent River, MD: Naval Air Systems Command, 2001.

[23] NAVAIR TM 16-1-540. "Avionics Cleaning and Corrosion Prevention/Control." Patuxent River, MD: Naval Air Systems Command, 2000.

[24] NAVAIR TM 01-1A-509-1. "Cleaning and Corrosion Control Volume I Corrosion Program and Corrosion Theory." Patuxent River, MD: Naval Air Systems Command, 2005.

[25] NAVAIR TM 01-A-1A-509-2. "Cleaning and Corrosion Control Volume II Aircraft." Patuxent River, MD: Naval Air Systems Command, 2005.

[26] NAVAIR TM 01-1A-509-3. "Cleaning and Corrosion Control Volume III Avionics and Electronics." Patuxent River, MD: Naval Air Systems Command, 2005.

[27] NAVAIR TM 1-1-689. "Avionics Cleaning and Corrosion Prevention/Control." Patuxent River, MD: Naval Air Systems Command, 2000.

[28] Abbott, W. "A Decade of Corrosion Monitoring in the World's Military Operating Environments: A Summary of Results." Battelle Memorial Institute, Columbus, OH, 2008.

[29] ISO Standard 9223:2012(E). "Corrosion of Metals and Alloys – Corrosivity of Atmospheres – Classification, Determination and Estimation," 2012.

[30] Rose, D. H. "A Cumulative Damage Approach to Modeling Atmospheric Corrosion of Steel." Dayton, OH: University of Dayton, 2014.

[31] Taylor, C. D., D. Borth, and D. C. Hansen. "Environmental Exposure Profiles for Atmospheric Corrosion." In AMPP Annual Conference + Expo, Denver, CO, 2023.



BIOGRAPHIES

DOUGLAS C. HANSEN is a distinguished research scientist at the University of Dayton Research Institute (UDRI) and professor (joint appointment) in the Department of Chemical and Materials Engineering in the School of Engineering at the

University of Dayton. He has more than 30 years of experience in protein biochemistry and corrosion electrochemistry, primarily in the development of environmentally friendly coatings and corrosion inhibitors. Dr. Hansen holds a Ph.D. in marine biochemistry from the University of Delaware studying marine biopolymers as corrosion inhibitors.

CHRISTINE E. SANDERS is the lead principal investigator for airframe corrosion efforts at NRL. Her current research includes atmospheric corrosion mechanisms and modeling, environmental exposure to simulate operational conditions, and maintenance cycle optimization. Dr. Sanders holds a Ph.D. in physical chemistry from The Ohio State University studying the atmospheric corrosion processes of silver.

RONALD A. ZESZUT is a senior researcher for UDRI. His research includes atmospheric corrosion, silver corrosion, nondestructive surface characterization techniques, biomaterials, and engine lubricants. Dr. Zeszut holds a Ph.D. in chemical engineering from Case Western Reserve University studying electroless deposition of copper for semiconductor applications.

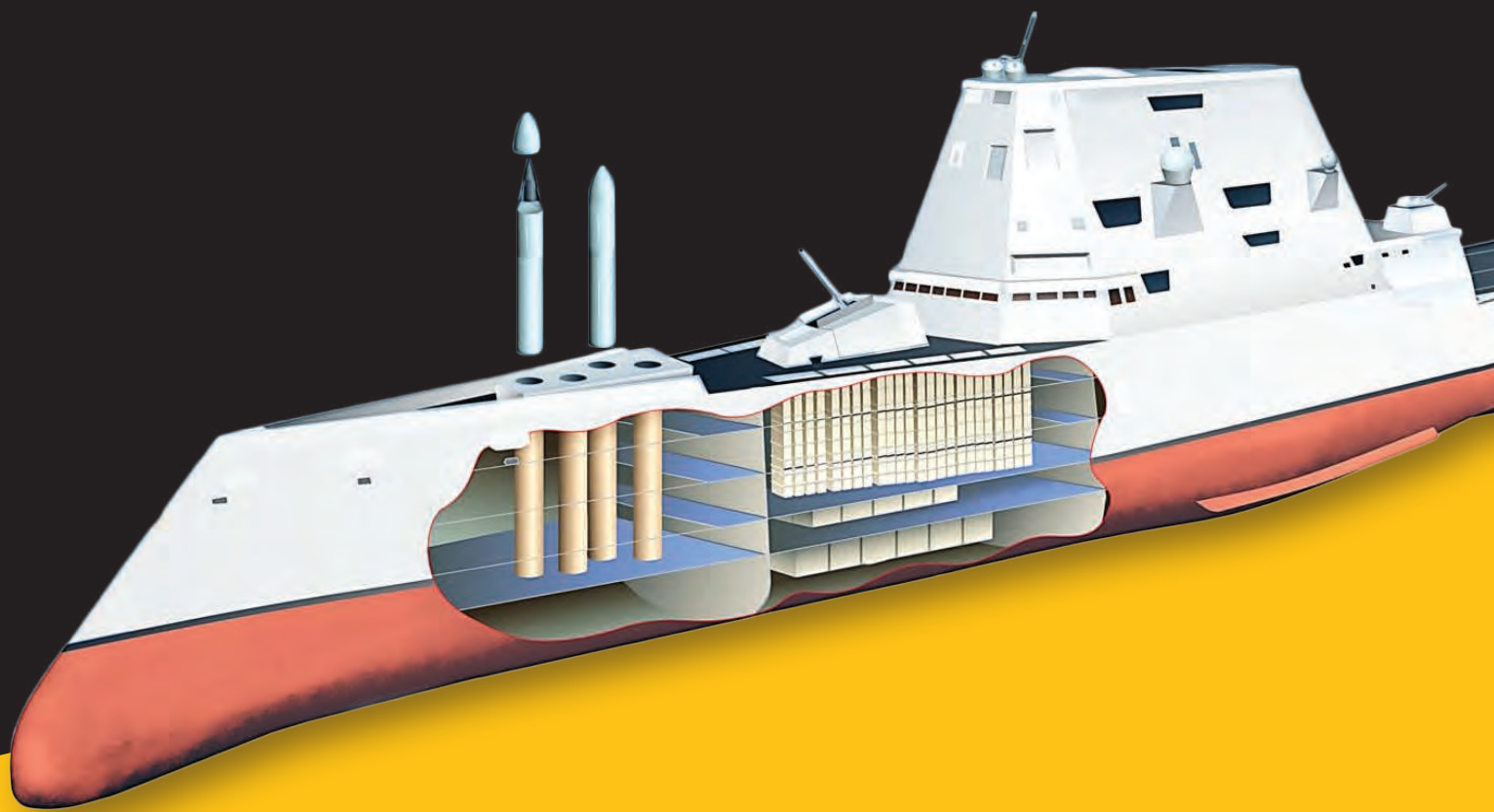
RAYMOND J. SANTUCCI is a materials engineer conducting research on atmospheric corrosion for the DoD at NRL. His research includes environmental severity prediction and monitoring techniques, machine learning, and additive manufacturing. Dr. Santucci holds a Ph.D. from the University of Virginia upon completing his research on sacrificial aerospace coatings.

MATTHEW J. ROTHGEB is a principal research scientist and group leader at UDRI. He manages the Coatings, Corrosion, and Erosion Laboratory at Wright-Patterson Air Force Base. His research includes studying the corrosive effects of multivariate environmental exposures on metals and corrosion preventative materials, coatings development, testing, and subsequent qualification of coatings to international and military specifications. Mr. Rothgeb holds an M.S. in engineering management sciences from the University of Dayton.

HAVE AN IDEA FOR AN ARTICLE?

If you would like to publish with DSIAC or have an idea for an article, we would love to hear from you. To learn more, visit www.dsiac.org/publish

Photo Source: 123rf.com



Understanding the Bow Topside Flow Field of the
USS *Zumwalt* for Hypersonic Missile Launching:

A POTENTIAL MISSING LINK

BY PETER J. DISIMILE AND SYED QASIM ZAHEER

(PHOTO SOURCE: H I SUTTON - COVERT SHORES)

INTRODUCTION

What happens when a hypersonic missile is launched from a Navy destroyer? Aside from the forthcoming damage effects and political fallout, there are a million complex physical interactions that take place right at the moment and place of the launch. One area of important study is the flow field around the launch system on the Navy destroyer to which it is integrated. Full-scale testing is an unrealistic method to understand such an environment for various reasons (e.g., cost, safety, resources, etc.). Therefore, we have conducted computational fluid dynamic (CFD) simulations to better characterize the flow field at the bow topside of a simplified model destroyer for the intended safe launch of conventional prompt strike (CPS) hypersonic missiles.

Recently, a numerical study characterizing the turbulent flow field of a simplified model having geometry and a Reynolds number resembling the USS *Zumwalt* was performed and revealed the existence of leading-edge vortical structures and a superstructure base vortical structure. The turbulent, integral-length scales of these vortical structures are of the order of the geometric diameter of a CPS missile and would interact with the missile during their initial launch phase, generating unfavorable aerodynamic

side forces. These forces would potentially cause a perturbation in the initial trajectory of the missile as well as introduce excessive vibration and rubbing of the missile within its canister. An understanding of the turbulent flow and vortical structures in the bow region of the Zumwalt class destroyer will help identify regions of lowest disturbance where the multiple all-up canisters (MACs) tubes may be safely installed and launched. For this purpose, the influence of superstructure shape modification, depicting the Zumwalt class destroyer, on the bow flow field is also investigated.

BACKGROUND

Research studies related to the flow field analysis of frigates and destroyers, including both realistic and simplified models like the SFS2 (simplified wind tunnel model for frigates) and ONRT (simplified wind tunnel model for the USS *Zumwalt*), have been directed toward turbulence characterization over the flight deck region [1–4]. Analysis of airwake turbulence over the flight deck is important to quantify pilot workload and handling qualities of helicopters while performing seaboard operations, including hovering, landing, and takeoff maneuvers. Active and passive control strategies have also been studied to reduce the impact of turbulence motions on handling qualities of the helicopters over the

“

Analysis of airwake turbulence over the flight deck is important to quantify pilot workload and handling qualities of helicopters while performing seaboard operations.

flight deck, significantly influencing the pilot workload [5].

CFD efforts have also focused on the flight deck region where the turbulence models have been validated against the wind tunnel results, performed at a reduced flow Reynolds number (Re), and compared to the full-scale prototype. Although geometric similarity is maintained, generally 1:200, 1:100, and or 1:60 in the wind tunnel tests, the dynamic similarity between the model and prototype was not achieved due to the limitation of experimental facility. This means that the flow Re_H (based on free stream velocity and superstructure height) of the wind tunnel model differs from the prototype by approximately 2 to 3 orders of magnitude. However, to overcome this limitation, it has been observed that beyond Re_H of 2×10^4 , the airwake characteristics over the flight deck region of frigates/destroyers are found to be Re_H independent [6]. However, these scaling factors need to be incorporated on the prototype when

using wind tunnel results. Currently, the experimental and numerical results of scaled down model are restricted to the flight deck region. Little or no attention has been given to the flow field in the ship's Bow region, hence becoming the focus of the current research.

Characterizing the turbulent flow field of a full-scale unmodified, simplified model (SFS2) using CFD revealed the existence of the bow leading-edge vortical structures and vortical structure at the superstructure base

(Figure 1). Since the geometric ratios, bow shape, and Re number of the simplified frigate model are very similar to the Zumwalt class destroyer, turbulent vortical structures are also expected in the bow region of the USS *Zumwalt* (or ONRT). As shown in Figure 1, the Navy has intended to integrate CPS hypersonic weapons on the Zumwalt class destroyer by replacing one or both gun mounts with the MACs [7]. These gun mounts are currently installed in the bow region. Research efforts addressing the bow region flow field are becoming more

relevant for the intended safe launch of CPS hypersonic missiles. Therefore, it is necessary to estimate scales of turbulence, intensity, and turbulent kinetic energy (TKE) as well as the orientation of the vortical structures at the probable CPS missile locations on the bow of the USS *Zumwalt*. Understanding of these turbulent vortical structures will highlight potential interactions with the missiles during the initial launch phase by generating unfavorable aerodynamic forces and causing disturbances in the initial missile trajectory. The simulation results can help decision-makers select a favorable location for MAC installation.

To bridge this research gap, preliminary research is carried out to critically investigate the bow topside flow field without launching the missile. The idea is to understand the undisturbed or unmodified bow flow field first to help identify regions of least disturbance for installation and safe launch of CPS missiles. As a continuation of this research, the initial launch trajectory of the CPS missile under the influence of bow turbulence will be simulated at a later stage. For this purpose, the full-scale, simplified frigate model (SFS2) is analyzed numerically and validated with available experimental data. Since the bow geometric dimensions and configuration of SFS2 are like the ONRT, dynamic flow similarity is expected between these simplified wind tunnel models of frigates and

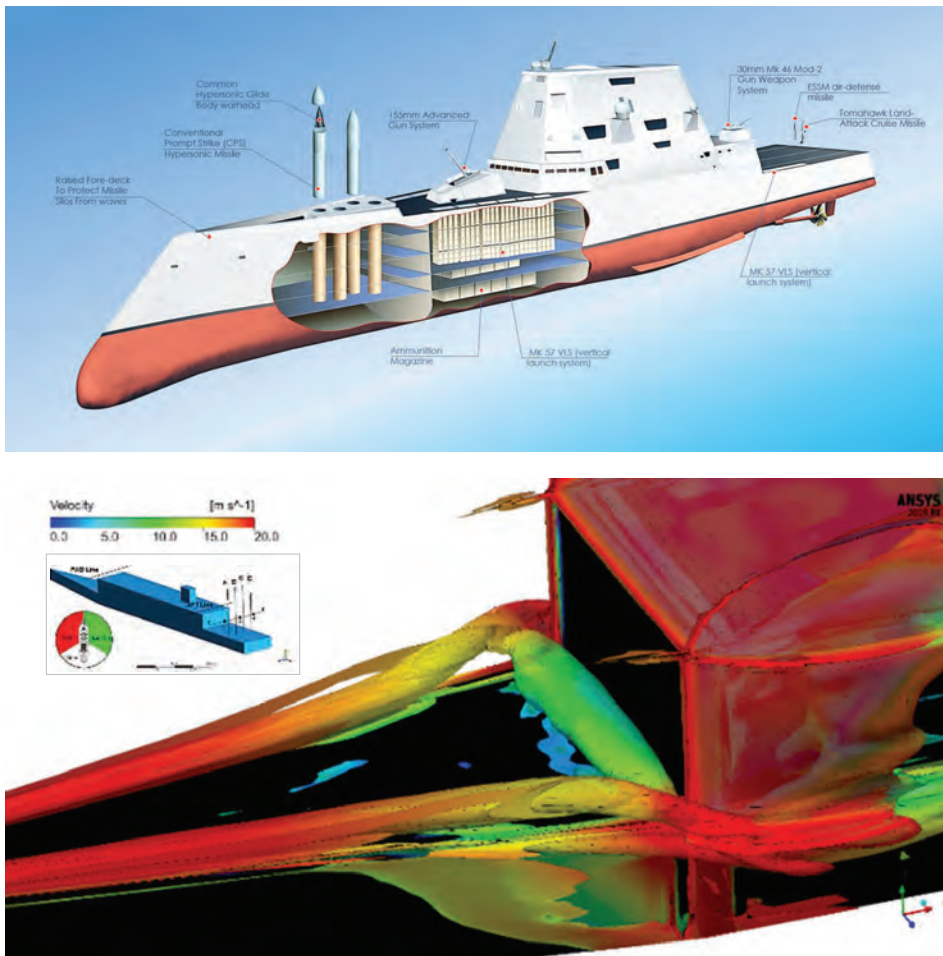


Figure 1. (Top) Proposed Location of the MAC Tubes on the USS *Zumwalt* [7], (Bottom) Identification of Bow Leading Edge and Base Vortices of the SFS2 [7], and (Insert) SFS2 Model Sketch [8].

the Zumwalt class destroyer. The geometric shape of the superstructures of the SFS2 and ONRT are different. Therefore, the forward face of the superstructure on top of the bow region of the SFS2 is modified to resemble the ONRT, and its impact on the bow flow is examined. (The unmodified SFS2 will be referred as the “Clean SFS2,” whereas modified superstructure geometry to resemble ONRT will be referred to as “Mod SS.”) Carrying almost 80% of the total TKE, the integral scales of turbulence at the probable CPS missile integration location are quantified, along with the distribution of turbulence intensity, kinetic energy, and vorticity at different streamwise locations along the bow. A comparative dynamic flow analysis between the Clean and Mod SS geometries of the simplified frigate model (SFS2) is also presented.

NUMERICAL SETUP

Methodology

The emerging trends in the literature suggest that scale-resolving turbulence models like the large eddy simulation (LES) and the detached eddy simulation and their variants perform better for the numerical simulation of unsteady and bistable airwake of SFS2 than the Reynolds-Averaged Navier-Stokes (RANS) turbulence models. Capturing the wake bimodality (i.e., switching the stable states of the bistable airwake) using a well-

resolved LES turbulence model is computationally expensive but viable, as found in the relevant CFD studies of similar domains of airwake bistability concerning the Ahmed body (simplified model for car aerodynamics). The high computational cost for an LES simulation is a restrictive factor. Therefore, in this research, the embedded LES (ELES) turbulence model is used, which is a hybrid RANS/LES turbulence model based on a zonal approach in which the RANS and LES turbulence models are used in predefined zones. In most cases, the LES zone is declared as the region of interest, and this zone is placed inside a global RANS zone. Such a technique bridges the gap between the high computational cost requirement of the full LES approach and inadequacy of the RANS models for such unsteady flow simulations.

To perform the ELES simulation, an a priori simulation using the standard k - ϵ RANS model is performed. Using this precursor solution, the integral length scales ($l_o \sim k^{3/2}/\epsilon$) of the turbulent structures in the flow field of SFS2 are estimated. Based on the minimum accepted value of the integral length scales, the mesh inside the LES zone is refined. The most important step in performing an accurate ELES simulation is designating the LES fluid zone inside a global RANS domain. In the ELES turbulence model, the LES turbulence model is used during the simulation only within the declared or predefined

“

The most important step in performing an accurate ELES simulation is designating the LES fluid zone inside a global RANS domain.

LES fluid zone, whereas the standard k - ϵ RANS turbulence model is used to simulate the flow field, thereby reducing the computational cost compared to performing an LES turbulence model in a complete fluid zone. As detailed in previous research [8, 9], four different cases were simulated wherein the RANS-LES interface was defined at a different streamwise location along the length of SFS2 geometry. This analysis [9] revealed that once the complete geometry of the SFS2 was placed inside the predefined LES fluid zone, the numerical results agreed with the experimental data set. The flowchart in Figure 2 indicates the steps performed in an accurate simulation of the SFS2 flow field using the embedded ELES turbulence model.

Setting

To numerically simulate the flow field of the geometric version of the SFS2, a fluid domain is created around the vessel whose boundaries extend to 5L (L = length of SFS2) on both the

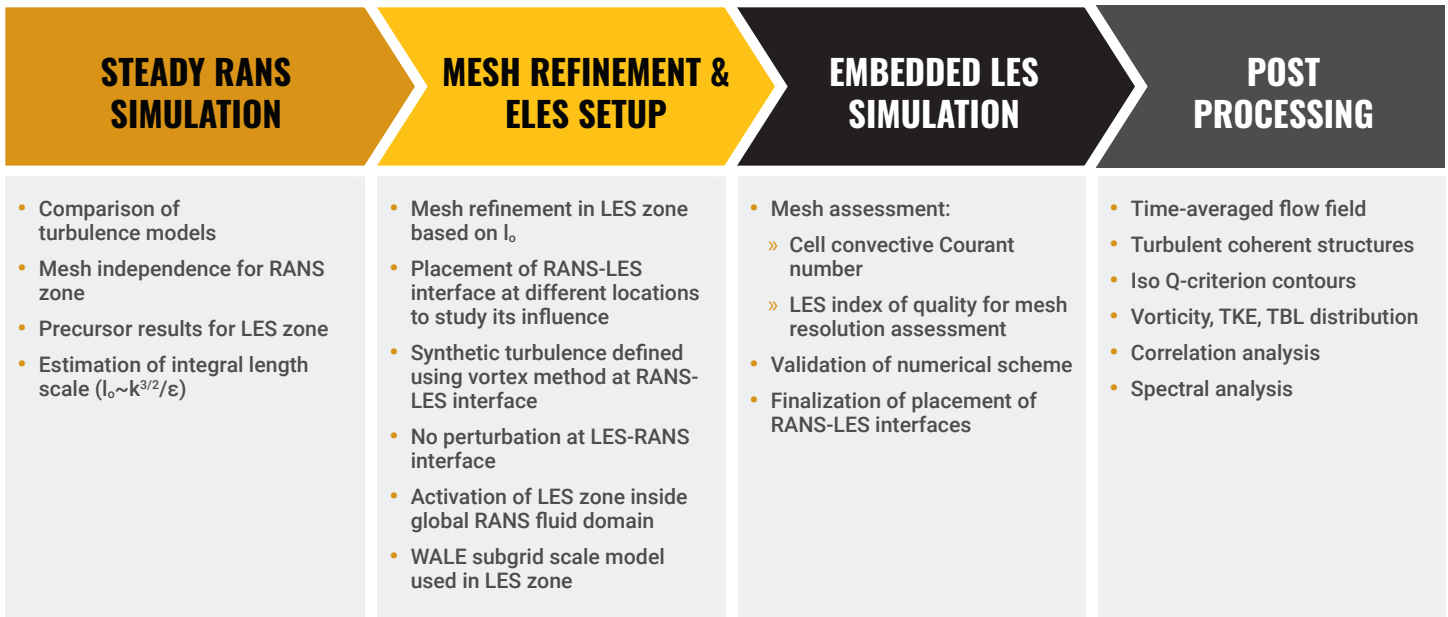


Figure 2. Flowchart of the Methodology Using the ELES Turbulence Model (Source: P. J. Disimile and S. Q. Zaheer).

starboard and port sides, and the inlet is defined as an arc having a radius of $5L$ from the bow. The outlet is placed at $6L$ from the stern, and the top boundary is located at $1L$ from the bottom surface. Velocity inlet and pressure outlet are used as boundaries. The surface of the SFS2 is defined as a wall boundary condition with a no-slip boundary condition, whereas the bottom surface of the domain is also defined as a wall with zero shear (Figure 3). The top surface is defined as a symmetric boundary condition. A structured mesh is generated on the surface of the SFS2 and then a prism layer with a maximum y^+ value of less than 40 having 25 inflation layers. A zone of higher mesh resolution, termed as the inner zone, is created around the SFS2. The rest of the outer fluid domain is coarsely meshed; therefore, nonconformal mesh interfaces are generated between the inner and

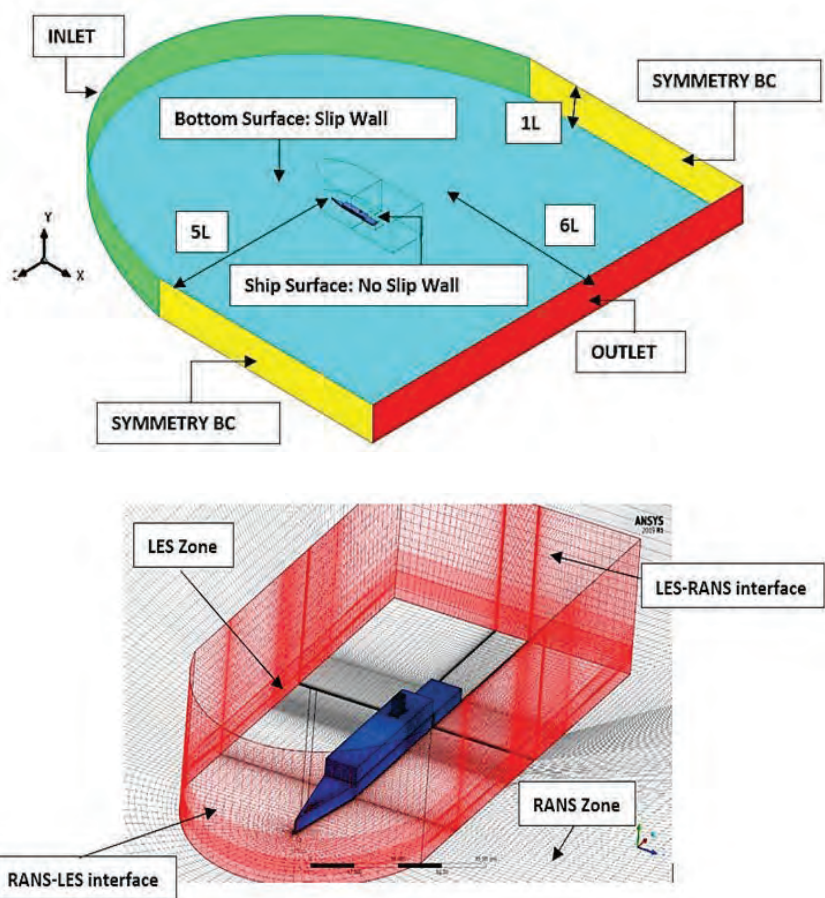


Figure 3. (Top) Meshed Fluid Domain With Boundary Conditions and (Bottom) Meshed Interfaces of the Embedded LES Fluid Domain With a Global RANS Domain (Source: P. J. Disimile and S. Q. Zaheer).

outer fluid zones. A uniform velocity of 40 kts (20.6 m/s) is defined at the inlet, which corresponds to Re_H of 2.26×10^7 . An atmospheric pressure equal to 1 atm is defined at the pressure outlet. The air is treated as incompressible fluid, and a pressure-based solver is used with a second-order accurate discretization scheme for the momentum, turbulence quantities, and time. A simple pressure velocity coupling solver is used. The viscous boundary layer on the surface of the ship model is calculated using a standard wall function since the y^+ value of the prism layer lies in the logarithmic (log) law region of the boundary layer. Given the Clean geometry of the SFS2 and the very high Re_H flow, the prism layer can take on a relatively higher value of y^+ .

After the mesh refinement in the respective LES zone and based on the precursor RANS simulation, the LES zone is activated in the defined fluid zone and the solution setup is changed from steady to transient, with a time step equal to 100 μ s. The transient ELES simulation is run for approximately two flow convective times before the unsteady flow statistics are collected for time averaging. The simulations are run for 35 seconds of physical flow time. Since the geometry of the SFS2 model is such that the separation of flow is governed by the sharp edges and steps rather than typical viscous boundary layers, the height of the viscous sublayer of the developed turbulent

boundary layer is small. At such a high Re_H , the placement of the first mesh node in the wall normal direction in the log law region is rationalized [10]. Using the $y^+ \leq 40$ in the LES zone renders the mesh unable to resolve the wall in the LES simulation, which would otherwise have required a very high computational cost. Therefore, to model the near-wall dynamics in the subsequent ELES simulations, a special subgrid scale wall model called the Werner-Wengle Model [11] is activated in Fluent 19.0 (from Ansys in Canonsburg, PA) in which the instantaneous velocity profile follows the law:

$$u^+(y) = \begin{cases} y^+ & \text{if } y^+ \leq 11.81 \\ A(y^+)^B & \text{otherwise} \end{cases},$$

where $A = 8.3$ and $B = 1/7$. This approach makes it possible to place the first layer of the mesh in the logarithmic layer (i.e., the inertial subrange). Such an approach had been adopted by different researchers in the past, especially for separated flows like the Ahmed car body [12], high-rise building dynamics [13], and prediction of flow-induced noise [14]. The results were found to be in better agreement with the experimental data at reduced computational cost compared to performing a wall-resolved LES simulation. The grid in the LES zone for ELES, after refinement, results in a mesh cell count of 8.4 million in the LES zone and 1.4 million in the RANS zone.



The resolution of the turbulence having length scales of interest is a very important contributor for accurate simulation of the flow field using the ELES turbulence model.

Validation

The resolution of the turbulence having length scales of interest is a very important contributor for accurate simulation of the flow field using the ELES turbulence model. This resolution is achieved by numerical discretization of the fluid domain, i.e., mesh size. The assessment of the mesh resolution in the LES zone of the fluid domain is carried out using the LES index of quality (LES-IQ). The LES-IQ is a nondimensional number having values from 0 to 1, where values closer to 1 indicate a mesh resolution high enough to capture flow dynamics of the large-scale turbulence. The histogram of the distribution of this index inside the LES zone is plotted in Figure 4, which clearly indicates that almost 95% of the cell count has an LES-IQ index greater than 0.85. The Courant-Friedrichs-Lewy (CFL) number distribution inside the LES zone also indicates $CFL \ll 1$ in almost the entire fluid domain, suggesting an accurate time step size is chosen for the simulation.

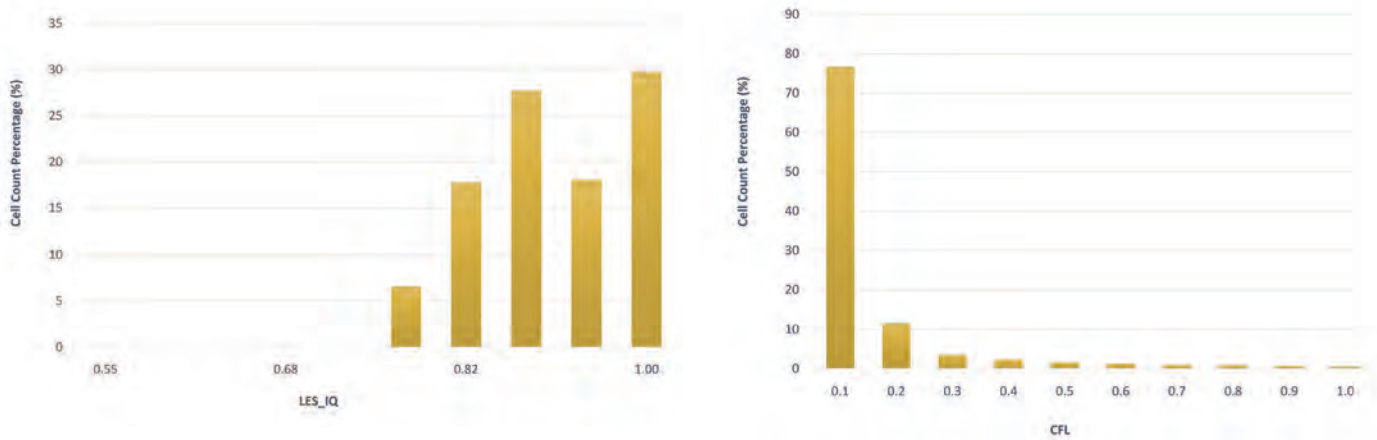


Figure 4. (Left) Histogram of the LES-IQ and (Right) CFL Distribution Within the LES Domain (Source: P. J. Disimile and S. Q. Zaheer).

To validate the numerical setup, the velocity profiles along the vertical lines at locations A–D are plotted (Figure 5). These results are compared with the experimental values obtained using fast response probes and particle image velocimetry techniques [1]. Although there is a mismatch in Re_H between the numerical and experimental setup, the qualitative assessment of the velocity profiles obtained numerically reveals very good agreement with the experimental values and provides confidence in the simulations using the ELES technique. The asymmetry in the profiles of measurement locations A and D is also captured in the present research. A slight offset in the magnitude of CFD results is attributed to the fact that an atmospheric boundary layer was incorporated in the experiment, whereas a uniform velocity profile inlet is defined in the current simulations.

To validate the flow field upstream of the flight deck, i.e., around the superstructure of the SFS2 geometry, a

widely used data set obtained from the National Research Council-Canada [2] was used as reference. The streamwise and vertical velocity components are plotted at the forward and aft lines, and the results are compared with the experimental values. The difference between the Re_H of the experiment and the current ELES simulation, i.e., $O(2)$ less than the numerical simulation, as well as the use of reduced order scaling of the SFS2 geometry in experiments, allowed qualitative comparison only. The trends of the CFD velocity profiles closely follow the experimental values, thereby validating and revealing the efficacy of the current simulations. The literature suggests that there is Re_H independence for the wake dynamics of bluff bodies above $Re_H = O(10^4)$. Hence, it is clearly visible from the plots (Figure 5a) that although there is an Re_H mismatch, the nondimensional velocity distribution follows the same trend as the experimental data. However, the dataset recorded upstream of the airwake (Figure 5b)

indicates that Re_H independence is limited to the airwake dynamics only and does not apply to the upstream flow field.

BOW FLOW FIELD ANALYSIS

Vortex Dynamics

Once the numerical methodology and turbulence models were validated against the available experimental dataset for the simplified frigate model SFS2, the bow flow field was analyzed

“

The trends of the CFD velocity profiles closely follow the experimental values, thereby validating and revealing the efficacy of the current simulations.

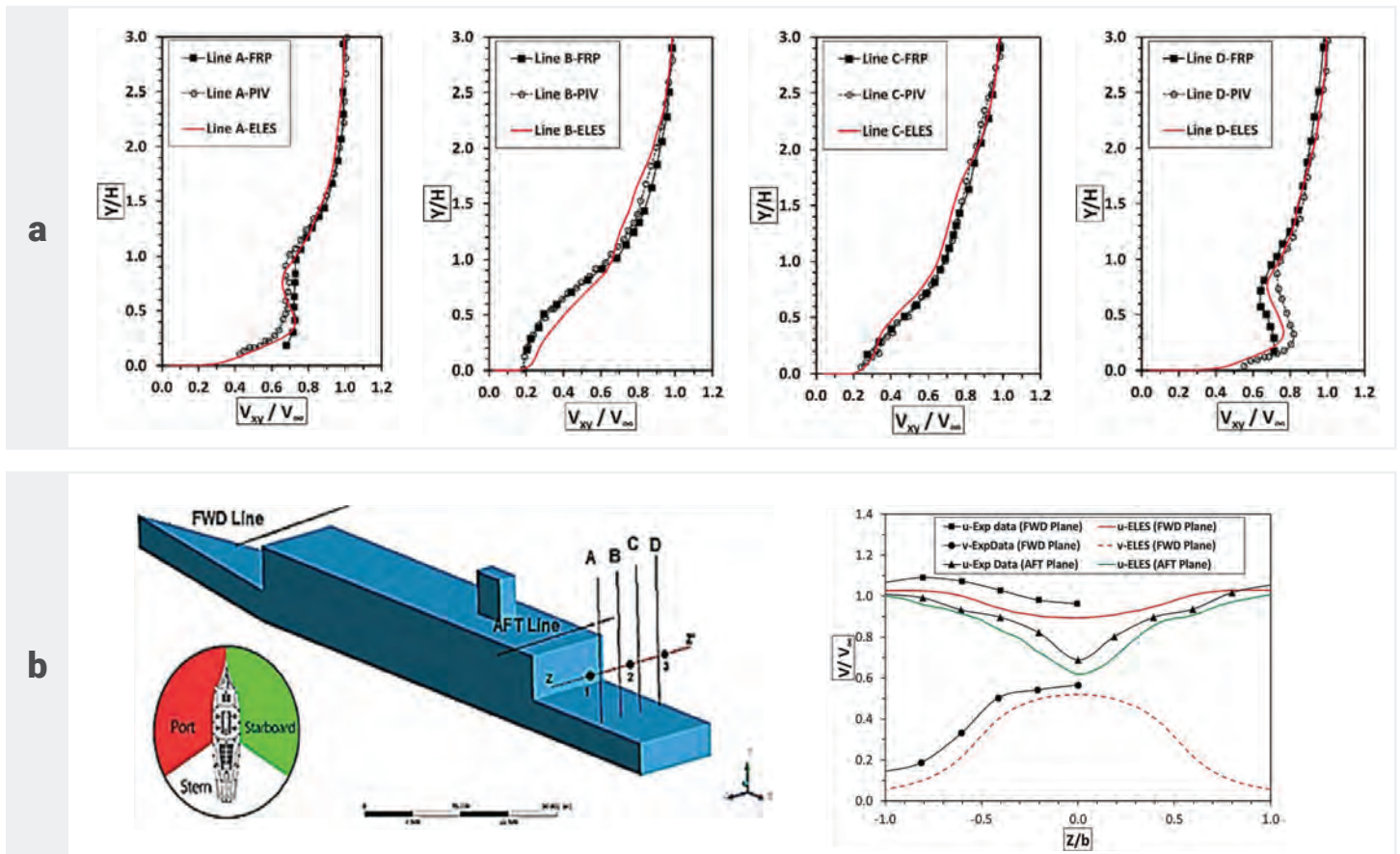


Figure 5. Comparison of Numerically Simulated Velocity Distribution at (a) Over the Flight Deck Along Vertical Lines A–D and (b) Along the Forward and Aft Lines Over the Superstructure, With the Experimental Dataset [1, 2].

extensively. To better represent the geometric features of the USS *Zumwalt*, the superstructure of the SFS2 was modified by incorporating the slanted and trifaceted forward face of the superstructure using the *Zumwalt*'s geometric ratios (Figure 6). The flow field of the Clean and Mod SS geometries of the SFS2 is compared from here onward to understand the influence of superstructure modification on the bow flow field.

The instantaneous vortices generated on the bow region are visualized using the isosurface Q-criterion surface plots (Figure 6). On the bow region are the

leading-edge vortices, attached to the top of the port and starboard sides is the bow, and a base vortex is generated at the foot of the superstructure's forward face. These vortical structures influence the bow topside flow field. A detailed investigation revealed that the coherent base vortex was much stronger for the Clean geometry than the modified superstructure (Mod SS) case. Moreover, the leading-edge vortices also interacted with the base vortex upon reaching the forward face of the superstructure. This interaction is more constructive on the starboard side than the port side; thereby, the time-averaged vorticity of the base

“

A detailed investigation revealed that the coherent base vortex was much stronger for the Clean geometry than the modified superstructure (Mod SS) case.

vortex becomes asymmetric across the midplane of the SFS2 geometry and biased toward the starboard side and can be observed by the mean swirl strength plotted along the core of

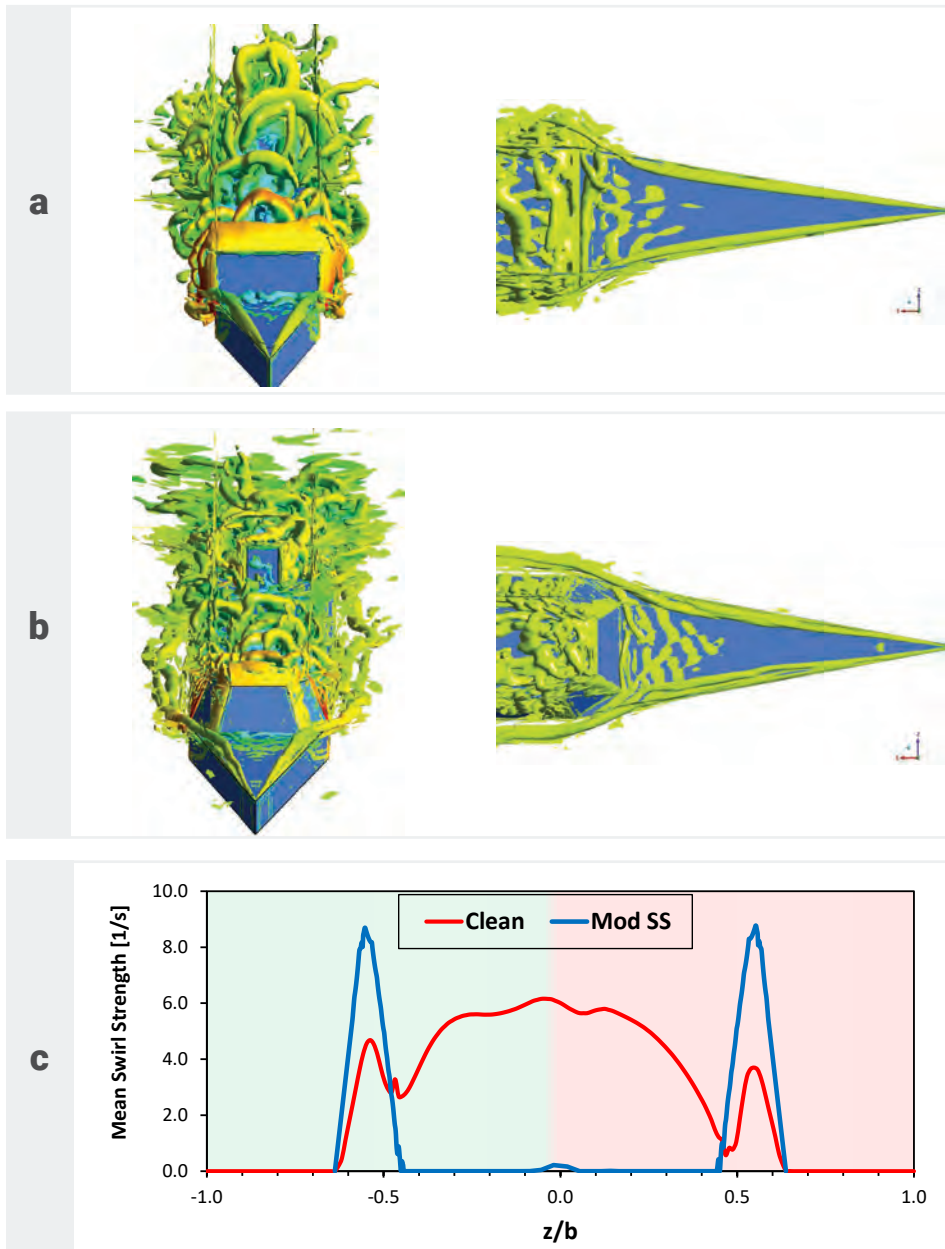


Figure 6. Isosurface Q-Criterion Plots of (a) Clean and (b) Mod SS Geometric Versions of the SFS2 and (c) Mean Swirl Strength Along the Core of Mean Base Vortex of Both Configurations (Source: P. J. Disimile and S. Q. Zaheer).

the base vortex. The biasness of the mean swirl strength of the base vortex toward the starboard side is presented in detail in Zaheer and Disimile [8]. It has been observed that more or less constructive interaction of leading vortices with the base vortex is due to the rotation direction of these vortices. The base vortex and starboard side-

edge vortex have clockwise rotation, whereas the portside-edge vortex rotates anticlockwise. It can also be observed that the mean base vortex of the Clean configuration is very strong near the midplane, as opposed to the Mod SS configuration. However, toward the edges of the bow, i.e., $z/b = \pm 0.5$, a higher swirl strength

than the Clean SFS2 geometry is observed due to coherence and strength of the leading-edge vortices for the Mod SS configuration. The Mod SS configuration also has a symmetric mean swirl distribution.

The strength of the base vortex also influences the structure and size of the leading-edge vortices. This is because the base vortex generates a suction effect by entraining the incoming fluid; hence, a stronger base vortex would entrain more fluid than a weaker, incoherent one. This entrainment of incoming fluid would generate a suction effect on the topside of the bow. Therefore, the leading-edge vortices of the Clean geometry are observed to be larger than the Mod SS configuration. Moreover, referring to the topside views of the vortical structures (Figure 6a and b), the faceted and slanted forward face of the Mod SS enables the formation of leading-edge vortices like the conventional delta wing.

A primary (large) and secondary vortex system along the leading edges is generated. The secondary vortex is found to be attached to the leading edges, whereas the primary vortex traverses inward toward the midplane, similar to a typical delta wing vortex system. However, in the Clean geometry case, there is only one strong, coherent, vortical structure along the top edges of the bow. The clear disparity between the structure of leading-edge vortices of the two configurations supports the argument

that the base vortex does influence the leading-edge vortices. These vortices in the Mod SS case remain coherent even after they travel downstream of the bow and onto the sides of the superstructure, whereas those of the Clean geometry break down once they leave the bow region.

Turbulence Characteristics

The potential installation of MACs carrying CPS hypersonic missiles on the USS *Zumwalt* would be accomplished by removing the existing two-gun mounts on the topside of the bow. These gun mounts are approximately positioned at X/L_b (L_b = length of bow) of 0.5 and 0.8 downstream distance from the front

tip of the bow at the midplane (see probe locations B12 [front gun mount] and B9 [rear gun mount] in Figure 7a). Therefore, in this section and the subsequent section, the turbulence parameters and the included integral scales of turbulence are analyzed specifically at these locations for the Clean and Mod SS cases of the SFS2. The percentage root mean square (RMS) fluctuations in the streamwise, vertical, and lateral velocity components, i.e., u_{rms} , v_{rms} , and w_{rms} , are plotted across the width of the bow at stated streamwise distances. The mean TKE is also plotted along the same lines. These measurements are carried out at $y/H = 0.25$ from the surface of the bow.

Analyzing the distribution of the RMS velocity fluctuations across the width of the bow at two different streamwise locations reveals that overall, the magnitude of fluctuations is low for both the configurations. It is also observed that in the middle or the central region of the bow at both streamwise distances, i.e., X/L_b of 0.5 and 0.8, the fluctuations in the streamwise component of the velocity are higher than the vertical and lateral components for both configurations. Moreover, the fluctuations in the central region are higher for the case of Clean geometry than the Mod SS configuration. The magnitude of U_{rms} fluctuations becomes stronger at $0.8X/L_b$ than $0.5X/L_b$. However, toward the edges of the bow, contribution from

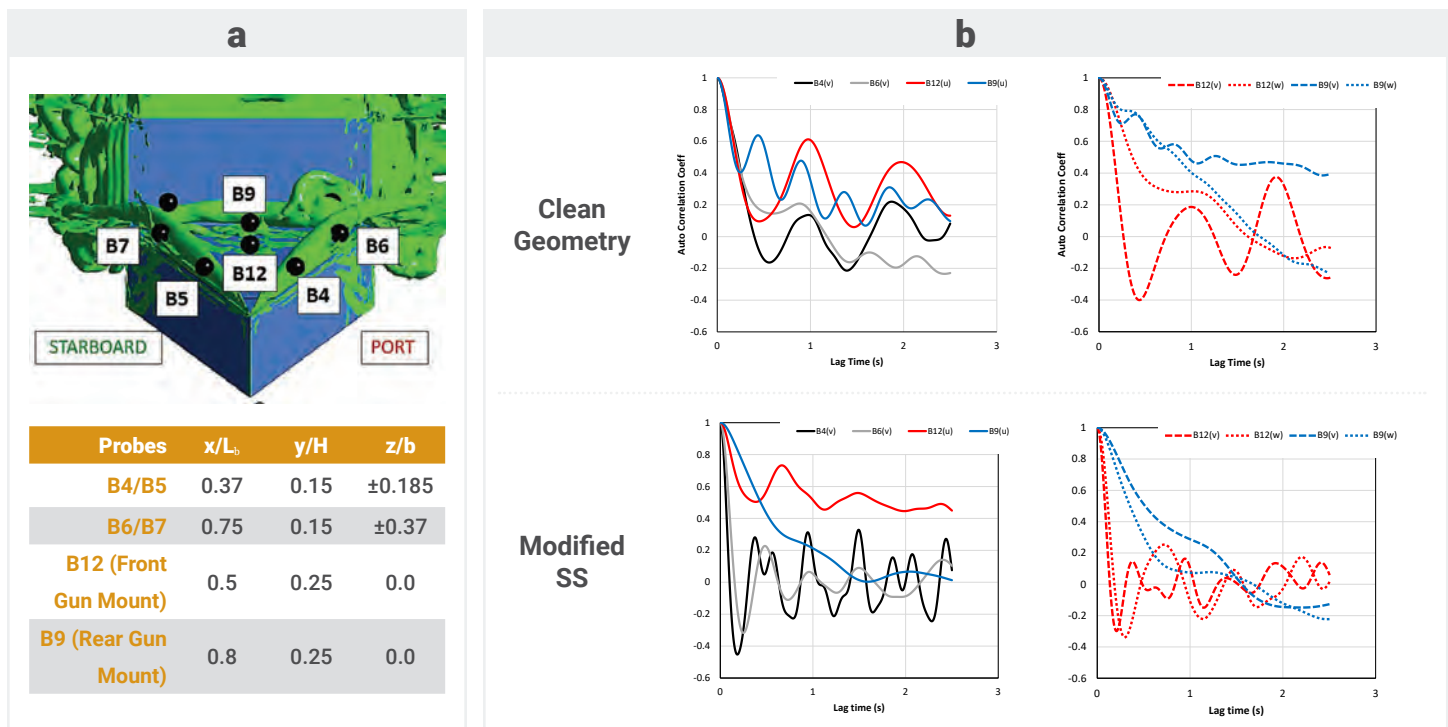


Figure 7. (a) Probe Locations for Measurement of Velocity Spectra and (b) Resultant Auto Correlation Analysis Using Different Velocity Components (Source: P. J. Disimile and S. Q. Zaheer).

the fluctuating vertical and lateral velocity components is stronger for the Mod SS than the Clean SFS2 configuration. This trend is attributed to the strong coherent leading-edge vortices of the Mod SS configuration. Likewise, the trend is duplicated in the distribution of the mean TKE across the bow region at two streamwise locations for both the configurations. From this analysis, it is suggested that the location of the rear gun mount experiences greater flow disturbances than the front gun mount location. Therefore, the front gun mount should be considered as a more favorable region for MAC installation because it experiences less turbulence.

Integral Scales of Turbulence

The autocorrelation of the velocity spectrum recorded at different locations on the bow region of the Clean and Mod SS SFS2 configurations is plotted in Figure 7 and compared to address the influence of the vortical system and configuration on the turbulent integral length scales of the eddies.

Probes B4/B5 and B6/B7 essentially capture the flow dynamics of the leading-edge vortices on the port and starboard sides of the bow. The B4/B5 probes, located upstream to the front gun mount location, influence the B12 probe, whereas B6/B7 probes predominantly influence the B9 (rear gun mount location) flow field. The vertical (v) velocity fluctuations in

the near vicinity of the leading edges are dominant for both configurations (Figure 8). Hence, the auto correlation coefficient (r_{ii}) at the B4 and B6 probes is calculated using the v-velocity component. Since the trends of r_{ii} for corresponding starboard side probes are observed to be similar, they are not included. The correlation coefficient

at the B12 and B9 probes is calculated using all three velocity components to analyze and investigate the dominant influence of leading-edge vortices. The first zero crossing of r_{ii} is taken as the criterion for assessing integral scales of turbulence at respective probe locations. For the B4 and B6 probes, the slope of the r_{ii} regarding

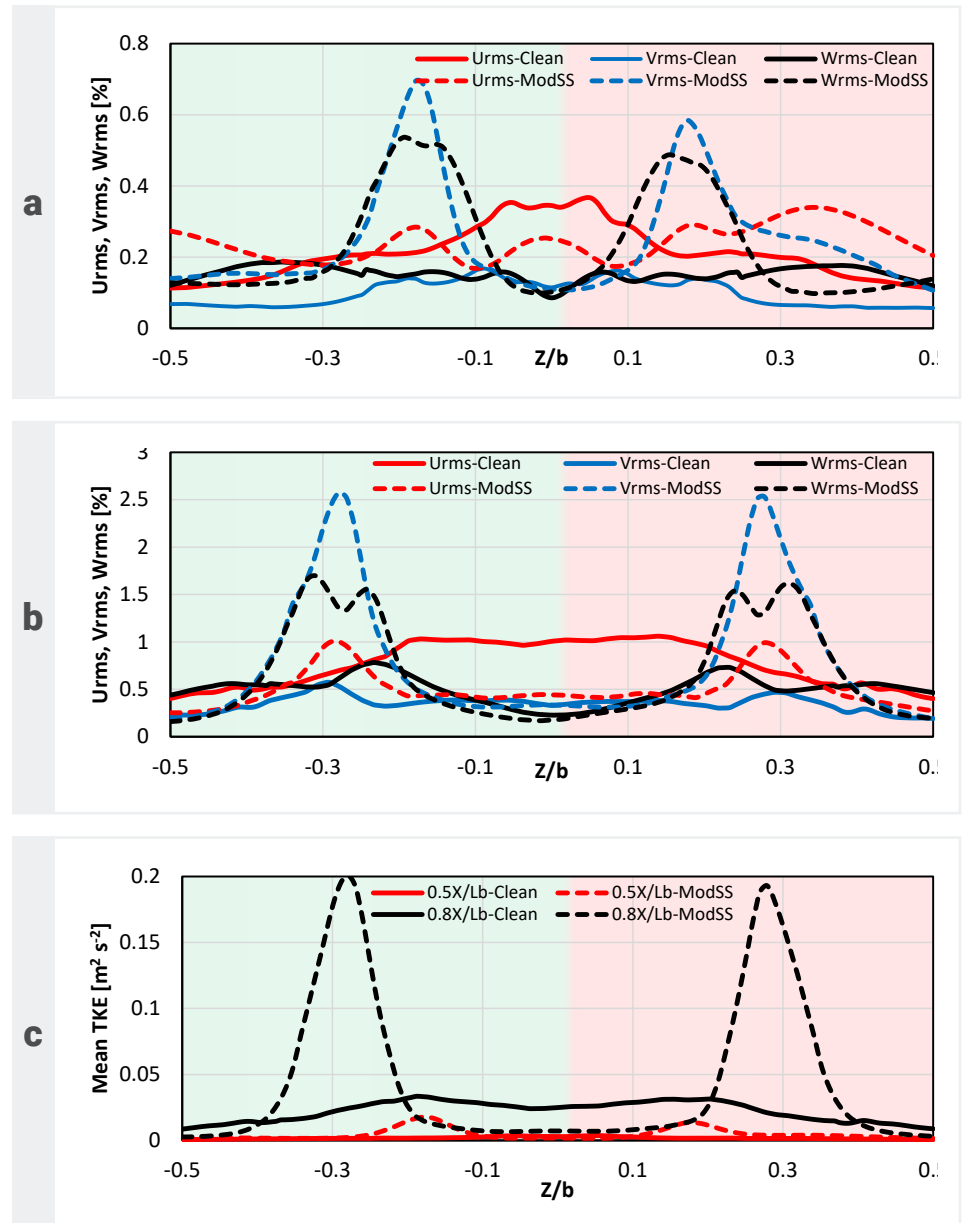


Figure 8. Distribution of Percentage RMS Values of the Turbulent Velocity Fluctuations at (a) $X/L_b = 0.5$, (b) $X/L_b = 0.8$, and (c) Mean TKE for the Clean SFS2 and Mod SS Cases (Source: P. J. Disimile and S. Q. Zaheer).

lag time is observed to be higher for the Mod SS case than the Clean geometry, signifying the existence of a significantly smaller integral scale of eddies compared to the Clean geometry. Moreover, for both the configurations, the scales of eddies are larger for the B6/B7 probes than the B4/B5.

The plot of r_{ii} for B4 probe measurement of the Mod SS configuration exhibits secondary periodic peaks that affirm the stated argument of existing secondary vortices along the leading edge of the configuration, which are missing for the Clean geometry. Owing to relatively larger-scale turbulent eddies at the leading edge of the Clean geometry configuration, their influence is pronounced in the r_{ii} spectrum of gun mount probes, as exhibited by periodic reenergization of the curve before it crosses the zero r_{ii} line. This means that the turbulent eddies at the front and rear gun mount probes of the Clean geometry configuration are periodically reenergized by the leading-edge vortices.

The input of TKE from the leading-edge vortices influences the streamwise velocity spectrum at the B12 and B9 probes. However, for the Mod SS configuration, the flow field at these probe locations is less influenced by the leading-edge vortices due to their smaller scales. The integral scales of turbulent eddies are larger for the rear gun mount probe location than

the front one for both configurations. Therefore, the front gun mount should be considered as a more favorable region for MAC installation and safe launch of CPS missiles.

CONCLUSIONS

This article explores the research gaps in the turbulent flow field and airwake characterization of the simplified model frigate/destroyers (i.e., an in-depth analysis of turbulence and associated vortical structures on the bow region of the simplified frigate model like the SFS2). The investigation of the bow topside flow field becomes pivotal for possible integration of MACs carrying CPS hypersonic missiles on the bow of the USS *Zumwalt* by replacing existing gun mounts. In this research, the bow flow field of the Clean and modified superstructure Mod SS (resembling ONRT) configurations of the SFS2 is analyzed and compared to predict the influence of superstructure modification on turbulence and vortical structures. It has been observed that the system of turbulent vortices, including the leading-edge vortices and base vortex, highly influences the bow topside flow field. Moreover, the base vortex for the Mod SS case was found to be significantly weaker than the Clean configuration. Therefore, its influence on the upstream leading-edge vortices is negligible. The analysis of turbulent

“

The front gun mount should be considered as a more favorable region for MAC installation and safe launch of CPS missiles.

intensity distribution, TKE, and the integral scales of turbulence reveals that the front gun mount is a favorable location for MAC installation as opposed to the rear one since it is located within a region of relatively higher turbulence; thereby, an adverse influence during initial launch trajectory of CPS missile is expected. ■

REFERENCES

- [1] Rosenfeld, N., K. Kimmel, and A. J. Sydney. “Investigation of Ship Topside Modeling Practices for Wind Tunnel Experiments.” In 53rd AIAA Aerospace Sciences Meeting, p. 0245, 2015.
- [2] Zhang, F., H. Xu, and N. Ball. “Numerical Simulation of Unsteady Flow Over SFS 2 Ship Model.” In 47th AIAA Aerospace Sciences Meeting Including the New Horizons Forum and Aerospace Exposition, p. 81, 2009.
- [3] Dhuree, S., J. Gordon Leishman, E. Gnanamanickam, and Z. Zhang. “Time-Resolved Ship Airwake Measurements in a Simulated Atmospheric Boundary Layer.” *Journal of Aircraft*, vol. 58, no. 3, pp. 624–649, 2021.
- [4] Zhu, N., Z. Zhang, E. Gnanamanickam, and J. G. Leishman. “Dynamics of Large-Scale Flow Structures Within Ship Airwakes.” In AIAA SCITECH 2022 Forum, p. 2532, 2022.
- [5] Forrest, J. S., and I. Owen. “An Investigation of Ship Airwakes Using Detached-Eddy Simulation.” *Computers & Fluids*, vol. 39, no. 4, pp. 656–673, 2010.
- [6] Healey, J. V. “Establishing a Database for Flight in the Wakes of Structures.” *Journal of Aircraft*, vol. 29, no. 4, pp. 559–564, 1992.

[7] Saylor, H. M. "Hypersonic Weapons: Background and Issues for Congress." Congressional Research Service, 2022.

[8] Zaheer, S. Q., and P. J. Disimile. "Simulation of SFS2 Using Embedded LES: Part-II Understanding the Asymmetry in Bistable Airwake at Zero Yaw." *Ocean Engineering*, vol. 272, p. 113838, 2023.

[9] Zaheer, S. Q., and P. J. Disimile. "Simulation of Simplified Frigate Using Embedded LES Turbulence Model: Part-I Validation and Turbulence Scales." *Ocean Engineering*, vol. 249, p. 110764, 2022.

[10] Menter, F., A. Hüppe, A. Matyushenko, and D. Kolmogorov. "An Overview of Hybrid RANS-LES Models Developed for Industrial CFD." *Applied Sciences*, vol. 11, no. 6, p. 2459, 2021.

[11] Werner, H., and H. Wengle. "Large-Eddy Simulation of Turbulent Flow Over and Around a Cube in a Plate Channel." In Eighth Symposium on Turbulent Shear Flows, Munich, Germany, 1991.

[12] Hesse, F., and A. S. Morgans. "Simulation of Wake Bimodality Behind Squareback Bluff-Bodies Using LES." *Computers & Fluids*, vol. 223, p. 104901, 2021.

[13] Masoumi-Verki, S., P. Gholamalipour, F. Haghighat, and U. Eicker. "Embedded LES of Thermal Stratification Effects on the Airflow and Concentration Fields Around an Isolated High-Rise Building: Spectral and POD Analyses." *Building and Environment*, vol. 206, p. 108388, 2021.

[14] Lane, G., P. Croaker, and Y. Ding. "Embedded Large Eddy Simulation Method for Predicting Flow-Induced Noise." In *Proceedings of Acoustics*, vol. 10, no. 13, 2019.



BIOGRAPHIES

PETER DISIMILE ("DR. D.") is an associate professor at the University of Cincinnati and a subject matter expert on fluid thermal issues involving fire/explosion events, specifically those related to aerospace and vehicle survivability. He led numerous programs for the U.S. Air Force 96th TG Aerospace Survivability and Safety Flight as a staff scientist. He was the primary investigator on several programs such as shock/blast wave generation/propagation, fuel slosh, effects of fuel inerting, hot surface and pyrotechnic ignition of jet fuels, assessment of next generation

fire suppressants, fire dynamics in a simulated aircraft environment, live fire testing, HRAM, and engine nacelle vulnerability. He has been instrumental in developing a lithium battery fire protection system with the U.S. Navy Surface Warfare Center. He has published nearly 200 papers on airflow and heat transfer phenomena, especially focusing on survivability issues, and has two fire protection system patents. Dr. D holds a B.S. and M.S. in engineering science from SUNY at Stony Brook and a Ph.D. in mechanical engineering from Michigan State University.

SYED QASIM ZAHEER is a research associate for the University of Cincinnati's Fire and Explosion Science & Technology Research Group, where he focuses on turbulence characterization of bluff bodies and ship airwakes and the aerodynamic design of a low-cost supersonic wind tunnel. He holds a B.E. in aerospace engineering from the National University of Sciences and Technology in Pakistan and an M.S. in fluid mechanics from Air University in Pakistan. Mr. Zaheer is pursuing his Ph.D. at the Department of Aerospace Engineering, University of Cincinnati.

SHARE YOUR EXPERTISE

If you are a contributing member of the defense systems community and are willing to share your expertise, you are a DSIAC subject matter expert.



Register at:
bit.ly/3sdcLhr

Photo Source: 123rf.com



Attributing Mission Performance to SUBMARINE SUBSYSTEMS

BY JONATHAN PROULE (PHOTO SOURCE: CANVA, MISSION EFFECTIVENESS DASHBOARD)

BACKGROUND AND MOTIVATION

Submarine design is a multifaceted process requiring extensive effort spanning across various disciplines and organizations. Part of this effort is deciding which missions a submarine is expected to conduct and assessing its efficacy, or mission effectiveness, in those missions via constructive simulation. This approach—characterizing a notional platform and simulating its performance in stressing tactical situations—has been and continues to be the foundation of most analytic products produced by the warfare analysts of the Undersea Warfare Mission Engineering and Analysis Department of the Naval Undersea Warfare Center Division Newport. It allows analysts to quantify the effect of different aspects of the platform, such as its acoustic profile or maneuverability, in terms of mission effectiveness. They can then answer questions such as, What sort of payloads should the submarine have to meet its mission goals, or what sensing capability is required to meet a threshold of mission effectiveness?

To ensure that a submarine concept can meet mission requirements, the conceptual submarine must first be adequately characterized, typically by defining features such as the type of sensor systems it possesses, how it maneuvers, its acoustic profile, and

its weapon composition. It can then be assessed across relevant, stressing scenarios, many of which may have competing objectives. For instance, a conceptual submarine may favor the use of torpedoes in one mission while preferring the use of missiles for another. Stowage aboard the platform is limited due to spacing, so the decision must be made as to how to balance both the number and type of weapon to meet competing mission requirements. By simulating submarine performance across various missions, analysts can quantify the trade-offs associated with each design decision.

While much is to be gained from this approach, stakeholders may find themselves limited when attempting to gauge the mission effectiveness of a platform at input levels that were not originally run as part of the constructive simulation. For example, if three levels of submarine speeds—5 knots, 15 knots, and 25 knots—were simulated as part of a study and the customer was interested in what the associated mission effectiveness at 10 knots would be, the customer is relegated to mental means of interpolation to estimate the quantity. While this is achievable in lower dimensional space, it quickly grows difficult in the presence of additional attributes (such as submarine acoustic profile, maneuverability, and sensing capability), as does the visualization of these estimates. Furthermore, that customer may not have the operational

“

By simulating submarine performance across various missions, analysts can quantify the trade-offs associated with each design decision.

context and assumptions (threat capability or environmental conditions) readily available to make informed design decisions.

It is through the Undersea Warfare Mission Engineering and Analysis Department’s Mission Effectiveness (ME) Dashboard that analysts and customers can rectify these shortcomings and facilitate the concept assessment process. This article will review the capabilities of the Dashboard, the mapping models that translate architectural design components into Dashboard inputs, and its application in evaluating a notional submarine concept with the goal of attributing mission performance to the submarine concept’s subsystems.

INTRODUCTION

The ME Dashboard is a browser-based tool designed to allow users to understand and study background and assumptions, quantify relationships between performance attributes,

generate new data, make predictions, conduct constrained optimization, and visualize outputs as part of the process of making informed submarine design decisions. The Dashboard's landing page is shown in Figure 1, where all attributes and their values with the surrogate models are arbitrarily chosen and meant to illustrate the Dashboard's capabilities.

architects want to know the designs are worth additional study by assessing how well they would perform in several mission contexts and learn more about the impact of different design components on mission effectiveness. Furthermore, they wish to determine if improvements can be made to the design and, if so, what sensitivities exist, and what

review mapping models and see how it can be employed to address the idea of attributing mission performance to submarine subsystems.

THE ME DASHBOARD

Prediction

The foundational competency of the ME Dashboard is its predictive capabilities. Derived from the ideas of response surface methods associated with classical experimental design techniques, the Dashboard houses a collection of statistical and machine-learning models that act as fast-running surrogates to slower running, higher fidelity models. These higher fidelity models are used to simulate submarine performance for each mission it is expected to conduct. The inputs and outputs from these simulations are captured as the covariates and response variable used in the training/fitting of the surrogate models in a supervised fashion.

These surrogates provide estimates of what the higher fidelity models would produce if they were used to simulate over inputs of interest. The Dashboard houses the following types of surrogate models:

- Elastic net regularized regression
- Generalized additive models
- Binary logistic regression
- Beta regression
- Binary Gaussian processes
- Treed Gaussian processes



Figure 1. The ME Dashboard Landing Page (Source: J. Proule).

By quantifying the military utility of submarine subsystems, the Dashboard can be used as a scoping mechanism to identify those technologies that require further study and analysis. The scoping process begins with naval architects who develop conceptual submarine designs, each consisting of thousands of descriptive parameters such as displacement, weight, length, diameter, and sensor configuration. Conceptual submarines may have unique features that do not easily align with existing submarine classes. The

are the minimal amount of changes that can be made to yield the largest improvement in mission effectiveness? Answering these questions comes with several challenges, as there is a translation required that maps the design components of the submarine to mission inputs. This scenario is typical of the questions warfare analysts face and can answer via mapping models in conjunction with the Dashboard. After briefly reviewing the different aspects of the Dashboard, we will return to this scenario to

- Gradient-boosted trees
- Multiadaptive regression splines
- Feed-forward neural networks

Which surrogate model is applied to which mission depends on the type of input data that is under consideration. Lower dimensional, all-numeric data tend to be represented well by Gaussian processes; this class of surrogate models can capture the predictive variance of numeric data that does not exhibit any step function-like behavior. Conversely, data with many categorical features may be better fit with tree-based models. These surrogate models may be stacked or combined/extended via boosting, bagging (bootstrap aggregation), or other ensemble methods and may require additional feature engineering on the original data produced from the simulation run with the higher fidelity model. The only constraints on the surrogates are that they are relatively quick to load and operate (does not exceed five seconds) and they generate predictions with low (<3%) generalizable error (a measure of how accurately an algorithm can predict outcome values for previously unseen data). This generalizable error is assessed via different kinds of nested cross-validation or other forms of out-of-sample assessments such as train-test-validation sets and bootstrapping. To help reduce this generalizable error and foster the creation of highly predictive surrogate models, the higher fidelity models typically simulate

over specialized experimental designs that allow nonlinear effects to be realized. These experimental designs are often space-filling designs that offer exceptionally strong coverage over the tradespace of interest or they may be a hybrid between space-filling and classical experimental designs (fractional factorial or D-optimal designs).

Through its user interface, the Dashboard offers users the ability to upload data or manually enter it within the browser and then generate predictions with the click of a few buttons (Figure 2). There are no command-line interactions or coding requirements, and users can download predictions for further analysis.

Inference and Visualization

In addition to downloading the predictions generated from the surrogate models within the ME

“

The Dashboard offers users the ability to upload data or manually enter it within the browser and then generate predictions with the click of a few buttons.

Dashboard, users have the option to investigate the predictions via various visualizations and inference methods. They can employ any of the following to graphically depict their predictions or the example datasets that come with each housed mission:

- Heatmaps
- Treemaps
- Scatterplots and scatterplot matrices
- Sunburst plots
- Parallel coordinate plots
- Correlation matrices/plots

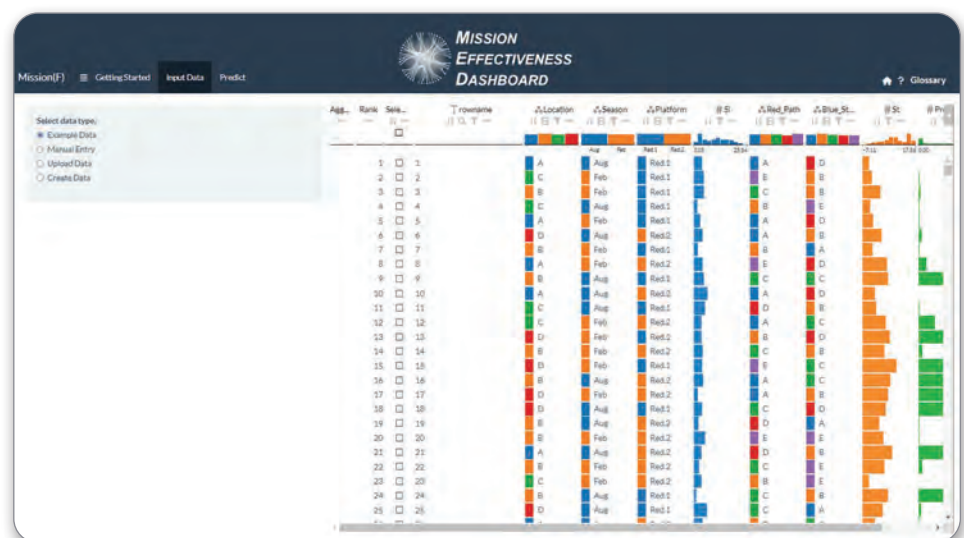


Figure 2. Data Upload Window Screenshot for a Single Mission in the ME Dashboard (Source: J. Proule).

- Histograms
- Density plots
- Boxplots

While these techniques are useful means to quickly identify and plot trends and gradients within the data, users are also supplied with options to quantify these trends via more rigorous means like the following:

- Individual conditional expectation plots
- Partial dependency plots
- Beeswarm and waterfall plots to visualize SHapley Additive exPlanations (SHAP)
- Breakdown plots
- Variable importance plots
- Sobol indices plots
- Friedman’s H-statistic plots
- Plots to visualize t-distributed stochastic neighbor embedding and principal component analysis
- Plots to visualize anomalies quantified via autoencoders

All these visualization and inference approaches are model agnostic; they can be applied to any of the surrogate models listed in the subsection titled “Prediction.” Many of the more computationally intensive techniques have already been applied to the example datasets for each mission and come preloaded within the Dashboard to provide a starting intuition about the data. For instance, by examining the precomputed variable importance plots, users may learn that the speed of the submarine was the most

influential factor within the context of a specific simulated mission. They may use the partial dependency plots to identify the general trends speed has across different missions and what minimal average speed is required to meet a threshold of mission success. A submarine design can be tailored to meet that speed while then being modified with other considered influential attributes. This modification can happen using counterfactual analysis, which is a process by which users can identify the minimal changes in inputs that yield a desired output via multiobjective optimization. It can be done in a constrained fashion wherein some of the inputs are not permitted to change. Within the context of the Dashboard, this technique allows analysts to determine if major improvements in mission success can be achieved within

the local tradespace and, if so, what changes need to be made to the inputs’ variables. It can help guide analysts on how to reach a desired threshold measure of effectiveness given a specified starting point.

Figure 3 shows an outlier investigation window of the Dashboard, where outliers are highlighted in the histogram of autoencoder reconstruction errors for a mission. The selected points are described in a summary table and automatically highlighted in a scatter plot and SHAP plot.

Operational Context

The ability to generate and visualize predictions can be an incredibly powerful capability, but it can also prove damaging and lead to faulty conclusions if lacking the requisite



Figure 3. Outlier Investigation Window Screenshot of the ME Dashboard (Source: J. Proule).

“

The ability to generate and visualize predictions can be an incredibly powerful capability, but it can also prove damaging and lead to faulty conclusions if lacking the requisite background knowledge.



Figure 4. Screenshot of the ME Dashboard Landing Page (Source: J. Proule).

background knowledge. Without a strong understanding of the underlying assumptions of the simulation inputs that generated the data in the first place or how a measure of effectiveness is calculated, the user has the potential to misunderstand or misrepresent the outputs to decision-makers.

To help remedy this issue, the ME Dashboard comes with briefs for each of the corresponding missions (Figure 4). Partial dependency plots are drawn for a selected attribute that is categorical in one mission and continuous in another mission. Study briefs detailing the development and results of a constructive simulation for each mission are hyperlinked in a table that also shows correlations of attributes shared between missions. These briefs are generated by analysts as part of their customer deliverables and typically provided as a static analysis in PDF format

upon the study’s completion. They detail how the higher fidelity model was constructed, what intelligence sources and environmental inputs were used, what tactics were employed, what third-party dependencies and collaborations existed, and what insights were gained from running the simulation. Complementing the briefs are graphics associated with each mission mapped on a globe to provide a less intensive but faster review of the operational context of the mission. By incorporating these elements into the Dashboard, users can understand the underlying implications of the predictions they are generating.

Application and Mapping Models

Returning to the scenario in the Introduction, suppose there are three missions that can be used to assess the efficacy of a submarine design—

Mission A, Mission B, and Mission C. Each of these requires a unique set of tactics stressing different aspects of the submarine’s build (information that is detailed in the briefs housed in the ME Dashboard). For each mission, a high-fidelity model is used to simulate combinations of relevant inputs and generate a metric of interest (i.e., some form of probability of success). We see this represented in Figure 5, where the authoritative model (high-fidelity model) ingests measures of performance (relevant inputs to the high-fidelity model) as well as contextual information to produce a measure of effectiveness. Once the simulations in the high-fidelity model are complete, the outputs are used to generate three briefs and three separate surrogate models (one for each mission) to comprise the surrogate model set housed within the Dashboard. The predictions resulting from the surrogate models are used to

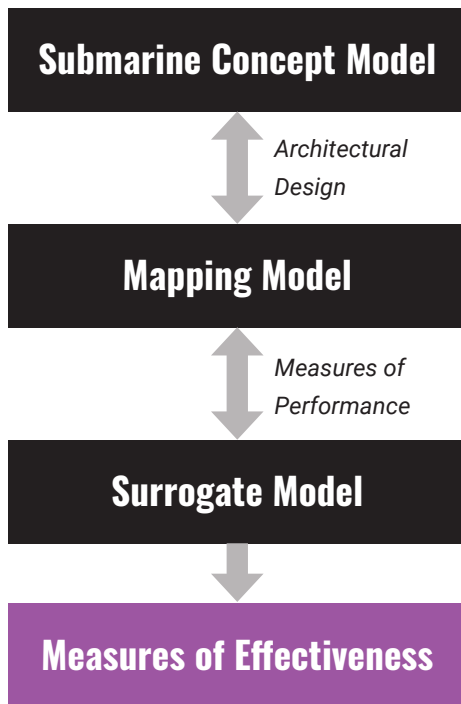


Figure 5. Submarine Concept Evaluation Flowchart (Source: J. Proule).

explore the tradespace by generating various explanatory visualizations that highlight the sensitivities present in each mission and quantify the marginal impact of each attribute. The platforms with many torpedoes and higher speeds tended to do well in Mission A, whereas platforms with lower radiated noise and lower speeds did better in Mission B. While these insights help guide the architects in their conceptual submarine design, more information is required to help establish a concrete link between their designs and the impact on mission effectiveness.

To establish this link, one first must recognize that many of the simulation inputs are measures of performance rather than architectural design

decisions and do not map directly back to the architect’s plans. For instance, the speed of a submarine is not an architectural component but rather a calculated byproduct of its design. Submarine propulsion, along with diameter and other drag-related features, combine to produce a speed. Similarly, the number of weapon tubes in conjunction with storage and launching systems dictates the submarine’s weapon salvo rate. These features require mapping models to translate the effect of design decisions on measures of performance, which can then be ingested by the surrogate models to generate measures of effectiveness (or mission success).

Figures 5 and 6 depict the process of how a third party is required to convert architectural components into surrogate model inputs. In the previous example, a payload’s working group may act as the mapping model needed to convert the number of torpedo tubes and launching systems (which fall within the architectural design components of Figure 6) into a salvo rate that can be used

“

The speed of a submarine is not an architectural component but rather a calculated byproduct of its design.

by the simulation. This salvo rate is a measure of performance that can be used to generate a prediction of mission effectiveness with the surrogate model.

These mapping models are often exceedingly complex, physics-based models that have been developed for years and maintained and improved by highly trained domain experts. The subject matter expertise of these domain experts is leveraged to convert architectural design components into inputs that can then generate the measures of performance used by the surrogate models.

To further illustrate the importance of a mapping model, we consider a submarine’s methods of communications with external entities. While getting more information can be beneficial in directing a search for a threat platform, it also puts the submarine at risk of being detected by surface/air assets and can reduce its search rate due to slowed speeds and changing acoustic profiles in the water column. There is both a cost and benefit to increasing and decreasing the frequency of communications. In the context of a high-fidelity constructive model that simulates the submarine in a mission requiring communications between platforms, the frequency is simply represented as a scalar value dictating how often the submarine receives information; there is no direct link to its architectural components. A mapping model

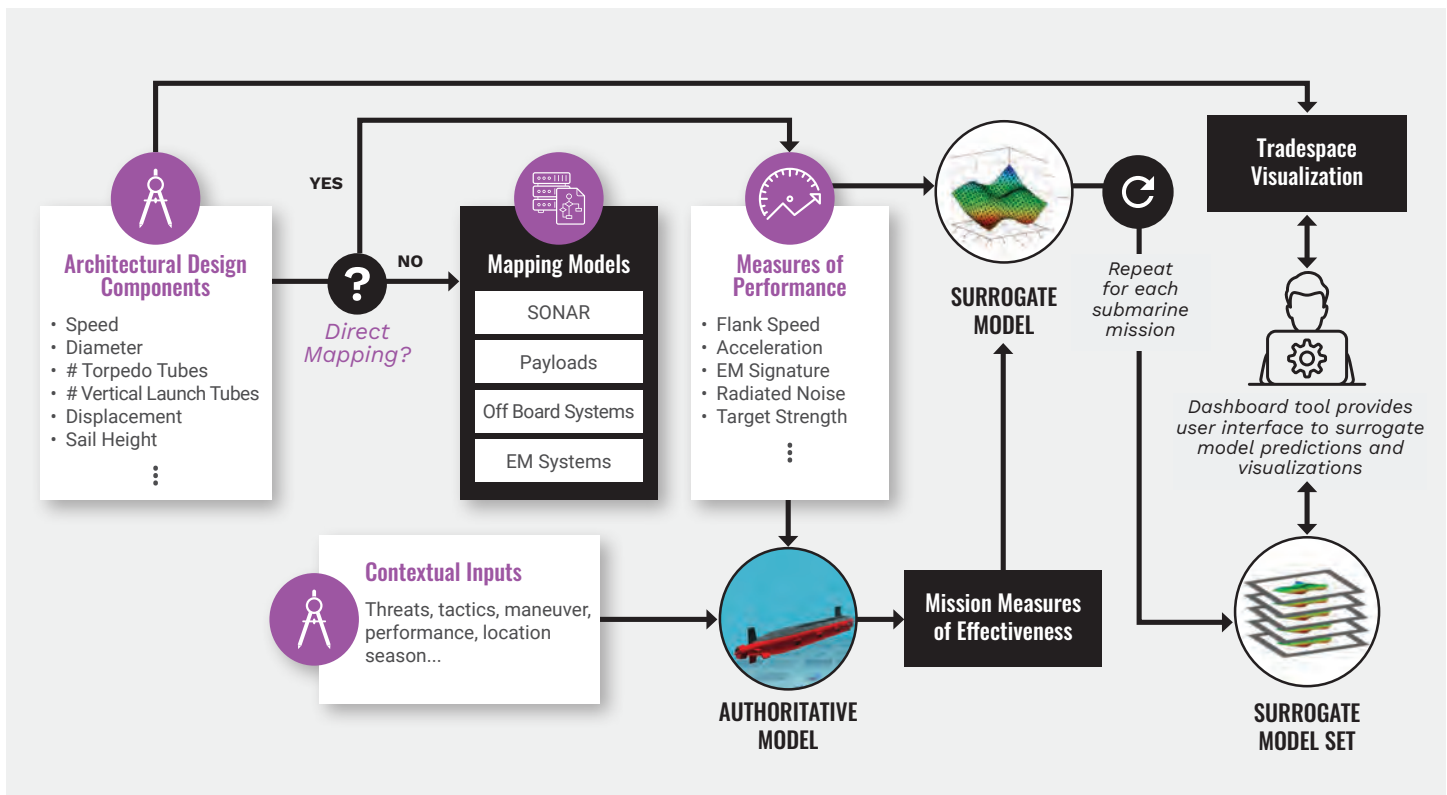


Figure 6. Information Flow From Architect to Analyst (Source: J. Proule).

is required to translate this scalar value to communication subsystems, such as different types of masts. Different masts can have major design implications and force the architect to include different technologies into the conceptual submarine. It is through these mapping models that a submarine subsystem defined by architectural means can be linked to measures of performance (a communications cycle) that can then be ingested by the surrogate models to produce a measure of effectiveness.

After generating the predicted measures of performance through this translation process, analysts can assess how well a design can complete the three different missions by uploading its characterization into the Dashboard

and generating predicted measures of effectiveness. How well a conceptual submarine does in each mission is largely contextually dependent—all nondesign attributes like location, season, or threat speed vary to yield a spectrum of mission effectiveness for each mission. Analysts can visualize how a single design fares against competing designs that have previously gone through this process if it can be considered an outlier and improvements can be made. Furthermore, they can use the optimization tools present in the Dashboard to find counterfactuals. For example, if a specific design was expected to have a 63% probability of success in Mission B and the threshold architects were attempting to meet was 75%, they can identify the minimal

amount of change necessary to characterize the design that will yield a 75% success rate.

Given this information, the analyst must then coordinate with the architects and subsystem experts to translate these measures of performance *back* to architectural features of the conceptual submarine design (see Figure 1). It is in these translations (the mapping models) where much of the difficulty lies and conflicting assumptions across organizations operating these tools are possible. Much of the success of the mission-effectiveness attribution process depends on this translation process and is still in the development process.

CONCLUSIONS

By relying on surrogate models to quickly evaluate thousands of possible conceptual submarine designs while bypassing the slow revisitation of the authoritative model, analysts can eliminate low-performing designs and, with the aid of mapping models, attribute varying levels of mission success to different subsystems. A vital step in this process, the mapping models necessitate a communicative, iterative pipeline between architect and domain experts to produce the measures of performances required by the ME Dashboard, where analysts can perform the following:

1. Conduct sensitivity analysis to identify high-gradient areas in the tradespace or areas that meet minimum thresholds of performance across different missions.
2. Identify what attributes are common to succeed in multiple missions.
3. Identify the highest performing scenarios to see if/when specialization matters.

All three aspects help the architect and analyst identify the locally optimal submarine design that yields the highest military utility given cost and building constraints. Of course, this approach is not limited to submarine design. Such benefits are transferable across industry, as these techniques

are germane to applications that rely on high-fidelity, slow-running models or physical, real-world tests that are expensive and difficult to coordinate. Using these techniques, organizations can make the intelligent choice on how to focus their efforts for further analysis and investment. ■

BIOGRAPHY

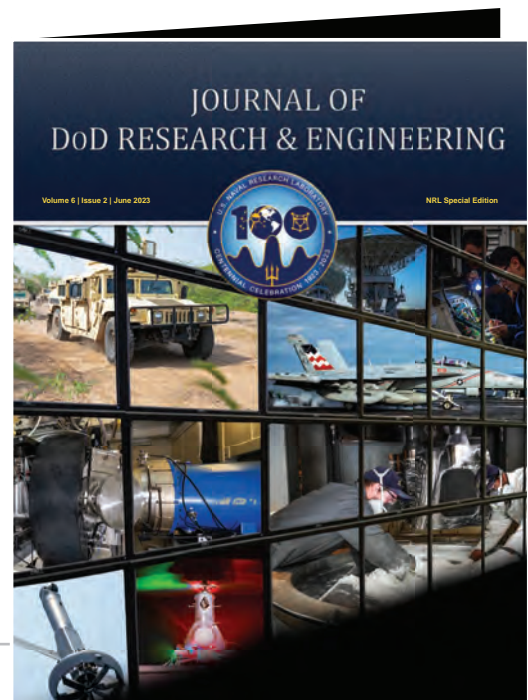
JONATHAN PROULE is a senior warfare analyst at the Naval Undersea Warfare (NUWC) Division Newport. After spending three years in the Sensors and Sonar Department at NUWC, he moved to the Undersea Warfare Mission Engineering and Analysis Department as a warfare analyst. Mr. Proule holds a B.S. in industrial engineering and systems engineering and an M.Eng. in technology management from Rensselaer Polytechnic Institute and an M.S. in operations research from the Georgia Institute of Technology.

DTIC'S JOURNAL OF DoD RESEARCH & ENGINEERING

AVAILABLE NOW. NRL SPECIAL EDITION

A peer-reviewed journal for controlled-unclassified and classified papers by DoD researchers, scientists, and engineers.

<https://discover.dtic.mil/products-services>



TECHNICAL INQUIRY SERVICES

FOUR FREE HOURS

Research within our 10 focus areas available to academia, industry, and other government agencies. Log in to dsiac.org to submit your inquiry today.

TECHNICAL AREAS

Survivability & Vulnerability
Advanced Materials
Autonomous Systems
Non-Lethal Weapons
Weapons Systems
Military Sensing
Directed Energy
Energetics
RMQSI
C4ISR



DS IAC JOURNAL

The Defense Systems Information Analysis Center (DSIAC) is a component of the U.S. Department of Defense's (DoD's) Information Analysis Center (IAC) enterprise, serving the defense enterprise of DoD and federal government users and their supporting academia and industry partners.

WWW.DSIAC.ORG

CONNECT WITH US ON SOCIAL MEDIA

